THE HYDROTHERMAL SYNTHESIS OF ALUMINOSILICATES

by

David John Marshall.

A Thesis submitted for the
degree of Doctor of Philosophy
in the University of London

Department of Chemistry,
Imperial College,
London, S. W. 7.

October, 1962.

ABSTRACT

In this work factors affecting the hydrothermal synthesis of aluminosilicates are discussed and the results of an investigation of the hydrothermal synthesis of some aluminosilicates of strontium and barium are presented. Hydrous gels with the general composition $MO.Al_2O_3.nSiO_2$ + water in which M = Sr or Ba, and n ranges from 1 to 9, were made up from highly reactive reagents and subjected to hydrothermal treatment in stainless steel bombs at temperatures between 110°C and 455°C.

In the case of strontium the major products were two polymorphs of the felspar (one hexagonal and the other probably orthorhombic), a mica, an unidentified hydroxylated tetragonal mineral, and three zeolites, one a near-chabazite and the other two not identified with any natural mineral. There were also isolated and irreproducible occurrences of analcite, mordenite, gmelinite, heulandite, and two minor unidentified products. One other unidentified product was obtained in moderate yield and the excess silica crystallised as α-cristobalite at the higher temperatures.

In the case of barium the major products, which occurred in good and reproducible yield, were celsian and its hexagonal polymorph, and a product with a structure apparently similar to that of celsian but containing hydroxyl groups. Harmotome and three zeolites without natural counterparts, one with a low silica:alumina ratio and two with a high ratio, were obtained in good yield. In addition one unidentified product was obtained in moderate yield. Excess alumina crystallised as boehmite

at low temperatures and excess silica crystallised as α-cristobalite at high temperatures.

The products were studied and characterised by optical and electron microscopy, X-ray powder diffraction, differential thermal and thermogravimetric analysis, infra-red spectroscopy and sorption studies. The products are compared with their natural and synthetic homologues and the possible effects of cation size and basicity on their formation and crystallisation fields are discussed.

ACKNOWLEDGEMENTS

The author wishes to express his sincere thanks to Professor R. M. Barrer for his help and encouragement throughout the course of this work.

Thanks are also due to Dr. I. S. Kerr of the Chemistry Department, Imperial College, for work on the electron microscope; and also to the technical staff of the Chemistry Department for their assistance in the construction and maintenance of apparatus.

The author wishes to thank his colleagues in these laboratories, and in particular Dr. R. M. Carr, for many helpful discussions; and the award of a bursary from the Ministry of Aviation is gratefully acknowledged.

TABLE OF CONTENTS

1.	INTRODUCTION.		1
2.	STRUCTURES OF SILICATES AND ALUMINOSILICATES.		4
	2.1.	General principles.	4
	2.2.	Classification of structures.	5
	2.3.	Some particular aluminosilicates:	
		2.3.1. Micas.	8
		2.3.2. Felspars.	11
		2.3.3. Zeolites.	17
3.	CRYSTALLISATION.		24
	3.1.	Nucleation.	24
	3.2.	Crystal growth.	29
	3.3.	Spherulitic growth.	32
4.	METHODS OF MINERAL SYNTHESIS		36
	4.1.	Vapour phase crystallisation.	36
	4.2.	Reactions at low temperatures and pressures.	37
	4.3.	Sintering reactions.	37
	4.4.	Pyrolytic crystallisations.	38
	4.5.	High pressure crystallisation.	39
	4.6.	Hydrothermal crystallisation.	40

5. THEORETICAL ASPECTS OF HYDROTHERMAL SYNTHESIS. 41

5.1. Thermodynamic considerations. 41
5.2. Kinetic considerations. 44
5.2.1. Solvent action of water. 44
5.2.2. Diffusion in water. 45
5.2.3. Complex ion formation. 46
5.3. Phase equilibria. 47

6. SOME PREVIOUS SYNTHESES. 52

7. EXPERIMENTAL APPARATUS AND METHODS. 57

7.1. Hydrothermal crystallisations. 57
7.1.1. Chemicals. 57
7.1.2. Preparation of gels. 58
7.1.3. Reaction vessels. 59
7.1.4. Ovens and furnaces. 59
7.2. Recovery of products. 62
7.3. Examination of products. 64
7.3.1. Optical microscopy. 64
7.3.2. Electron microscopy. 64
7.3.3. X-ray diffraction. 65
7.4. Interpretation of X-ray photographs. 66
7.4.1. Cubic system. 67
7.4.2. Tetragonal system. 67
7.4.3. Hexagonal system. 70
7.4.4. Orthorhombic system. 70
7.4.5. Monoclinic and triclinic systems. 72

	7.5.	Differential thermal analysis.	73
		7.5.1. General principles.	73
		7.5.2. Apparatus used.	74
		7.5.3. Thermogravimetry.	77
	7.6.	Infra-red spectroscopy.	78
	7.7.	Sorption experiments.	78
8.	EXPERIMENTAL RESULTS.		82
	8.1.	The strontium aluminosilicates.	82
		Tabulated results.	84
		8.1.1. General remarks.	104
		8.1.2. Particular species.	106
	8.2.	The barium aluminosilicates.	139
		Tabulated results.	140
		8.2.1. General remarks.	139
		8.2.2. Particular species.	155
9.	GENERAL DISCUSSION.		174
		Summary.	188
10.	REFERENCES.		190
	APPENDIX.		200

1. INTRODUCTION

The silicates and aluminosilicates are the major constituents of the earth's crust, and hence have always attracted great interest both from the point of view of economic exploitation and from a purely scientific desire for a greater understanding of the environment we live in. For many years the synthesis of numerous materials similar to the rock forming minerals has been attempted, using the methods outlined in a later section. Several different methods of synthesis have been developed, among them the hydrothermal method, which each have their own range of applicability. One or another method may be used according to the nature of the problem which it is desired to investigate.

There are at least two basically different approaches open to a worker in the field of mineral synthesis. On the one hand there is the theoretical petrological approach. A simplified system is used as an approximation for the relations in a complex natural assemblage and an attempt is made to determine the true stability fields of the various minerals and mineral assemblages of the system. It is often very difficult to be certain of attaining equilibrium under laboratory conditions, and also this method does not give any information on the

effect which the many impurities found in natural minerals may have on their stabilities. However, the amount of work along these lines is increasing and has had some success. On the other hand there is the chemical approach. The object here is to achieve the satisfactory synthesis of a particular species, which may or may not have a natural counterpart. Chemical systems which are unlikely to have occurred in nature can be investigated in the laboratory. These include high purity of the reactants, high concentrations of rare elements, high reactivity of starting materials and control over the pH of the solutions. In such experiments the formation of metastable compounds may be welcomed and interesting structures not found in nature can be produced.

Work in these laboratories has been concerned with the hydrothermal synthesis of the aluminosilicates of the alkali metals, and also those of thallium, calcium and some substituted alkyl ammonium bases. For the most part highly reactive starting materials have been used and a number of synthetic minerals have been produced, some of them without known natural counterparts. The strongly alkaline low temperature hydrothermal conditions used have favoured the production of zeolites and the study of the ion-exchange and sorptive properties of these products has formed an important part of the work.

The present work is a continuation of these studies in an investigation of the synthesis of aluminosilicates of strontium and barium, and is a partial study of the systems $SrO-Al_2O_3-SiO_2-H_2O$ and $BaO-Al_2O_3-SiO_2-H_2O$. Reactive starting materials have again been used and the systems have been studied between 100°C and 450°C. The object of the work has been to investigate the crystallisation fields of the various species produced in the region studied. It was also to determine the optimum conditions for the reproducible synthesis of the major species and to study some of their properties. The work was not concerned with the delimitation of thermodynamic stability fields for the species obtained, nor with relating the conditions of formation to their petrological occurrence.

Before the experimental results are presented a number of topics of general relevance to the work will be discussed.

2. STRUCTURES OF SILICATES AND ALUMINOSILICATES

2.1. General Principles

The chief characteristic of silicate structures is the way in which complex structures are built up by linking together in various ways the simple basic units formed by the coordination of large anions around small cations. Goldschmidt's rules[1], deduced from a study of a wide variety of mineral types, state that the coordination number of any ion is governed by the ratio of the radius of the central cation to the radius of the anion surrounding it. For fourfold coordination of the central ion this ratio must lie between 0.22 and 0.41, and for sixfold coordination between 0.41 and 0.73. The radius ratio of silicon to oxygen is 0.37 and so silicon is always found in tetrahedral coordination with oxygen, whereas the aluminium:oxygen radius ratio is 0.40 and as a consequence aluminium may form either tetrahedral or octahedral groups with oxygen. The size of the $[AlO_4]$ tetrahedron is close to that of the $[SiO_4]$ tetrahedron and isomorphous replacement of $[AlO_4]$ for $[SiO_4]$ may take place provided that an additional cation can be introduced into the structure to neutralise the additional negative charge produced by such a substitution.

This type of isomorphous replacement cannot occur indefinitely however since the third of Pauling's rules[2] states a further requirement if a stable structure is to be achieved. This is that shared edges or shared faces of groups in a coordinated structure decrease the stability, and this effect is particularly great in a case where the radius ratio approaches the lower limit of stability for that coordination number. This rule may be applied to the aluminosilicates in the form:- when two similar atoms are both neighbours of a given atom, the most stable configuration is achieved when one of them is in its highest coordination state. Hence no two adjoining tetrahedra in a silicate structure may both contain aluminium as the central atom. From this Lowenstein[3] has deduced that in an aluminosilicate the ratio of aluminium to silicon can never be greater than 1:1, and that in structures which do have this maximum substitution the $[SiO_4]$ and $[AlO_4]$ tetrahedra must occur alternately in an ordered fashion throughout the structure.

2.2. Classification of Structures

The most satisfactory general classification of silicate structures is that first formulated by Bragg[4] and based on the way in which the $[SiO_4]^{4-}$ tetrahedra are linked. The silicon-oxygen bonds are so strong that the

tetrahedra themselves are found to be of nearly constant shape and dimension whatever the rest of the structure may be.

The orthosilicates. The four oxygen ions surrounding each silicon are not bound to any other silicon atom and so the structure is built up of units each having four negative charges which are neutralised by the cations in the structure. An example of this type of structure is the olivine group, $(MgFe)_2SiO_4$, where for example in forsterite every O^{2-} anion is situated at the apices of a $[SiO_4]$ tetrahedron and a $[MgO_6]$ octahedron. Minerals of the garnet group are also built up from isolated $[SiO_4]$ tetrahedra with the charge neutralised by iron or aluminium ions in six-fold coordination.

The sorosilicates. The $[SiO_4]$ tetrahedra may be linked together in a number of ways to form finite groups from which the structure is built. For instance, two tetrahedra may be linked together through a common apex to give an $[Si_2O_7]^{6-}$ group as in thortveitite, $Sc_2[Si_2O_7]$. Tetrahedra can also link together to form rings of three tetrahedra as in benitoite, $BaTi(Si_3O_9)$, and a well known example of rings composed of six tetrahedra is beryl, $Be_3Al_2Si_6O_{18}$. An unusual example in this class of structures composed of finite groups is zunyite, $Al_{13}Si_5O_{20}(OH,F)_{18}Cl$, where the unit $[Si_5O_{16}]^{12-}$ consists of a central $[SiO_4]$ tetrahedra linked to another tetrahedron at each apex.

The inosilicates. Structures composed of infinite chains of $[SiO_4]$ tetrahedra are typical of such common minerals as the pyroxene group, for example diopside, $CaMg(Si_2O_6)$, where the chains are held together by the calcium and magnesium ions which satisfy the free valencies of the oxygen anion in the chains. The closely related mineral group, the amphiboles, are built up from double chains since alternate tetrahedra in a pair of adjacent chains point towards each other and share the apical oxygen. An example of this type is tremolite, $Ca_2Mg_5(Si_8O_{22})(OH)_2$.

The phyllosilicates. If the process described for the conversion of a pyroxene to an amphibole is continued indefinitely in two dimensions then sheet structures will be built up. In these sheets three corners of each tetrahedron will be linked to a neighbouring tetrahedron and this can be represented by the formula $n(Si_2O_5)^{2-}$. The simplest example of this type of structure is hexagonal barium feldspar, which will be discussed later, but double sheets built on this principle are the basis of the structures of all the clay minerals. As an example we may take pyrophyllite $Al_2(Si_4O_{10})(OH)_2$. This is built up from parallel layers of two $n(Si_2O_5)$ hexagonal networks, between which there are octahedral groups of aluminium cations surrounded by oxygen and hydroxyl anions.

In the micaceous minerals additional aluminium replaces some of the silicon and the resultant charge is neutralised by interposing cations having a high coordination number between the double layers.

The tectosilicates. When all four corners of each tetrahedron are shared by neighbouring tetrahedra a three dimensional framework is produced and this is the basis of the structures of the crystal varieties of silica, and of the felspars, felspathoids and zeolites. In the felspars cations are accommodated in the interstices of the structure to neutralise the charge produced by the replacement of some of the silicon by aluminium. This replacement also takes place in the felspathoids and zeolites but the very much more open structures of these types often enable them to contain in addition to the cations considerable quantities of inorganic salts, e.g. cancrinite $Na_6Ca_2(SiAlO_4)_6(CO_3)_2$ or water, e.g. chabazite $(Ca,Na_2)Al_2Si_4O_{12}.6H_2O$.

2.3. Some Particular Aluminosilicates

2.3.1. Micas. The chemical constitution of the structural units in micas was determined by Mauguin[5] in 1928 and in 1930 Pauling[6] deduced the basic principles of its layer lattice structure which were confirmed by Jackson and West[7,8]. Later Hendricks and Jefferson[9]

showed the existence of a complex polymorphism among the micas based on the relative orientations of successive layers. A portion of the structure of muscovite is shown in Fig. 1. In this structure one in every four of the silicon atoms in the tetrahedral layer is replaced by aluminium, but in the brittle micas such as margarite, $CaAl_2(Al_2Si_2O_{10})(OH)_2$, every other silicon is replaced by aluminium and so the charge on the sheets is twice as great and is balanced by the replacement of monovalent potassium by divalent calcium. Yoder[10] points out that polymorphism in the micas arises because the atomic arrangement of the fundamental sub-cell is monoclinic but the surface of the sub-cell is hexagonal or pseudohexagonal. Hence rotation of the sub-cell by 60° does not affect the packing of the surfaces but does affect the position of the sub-cell. Smith and Yoder[11] have developed this concept and enumerated the simpler combinations of regular packing which can be expected to occur. Many of these possible polymorphs have been shown to occur in various natural and synthetic micas[12,13] and methods of distinguishing them by means of slight differences in the X-ray powder pattern have been developed.

Dehydration studies and differential thermal analyses on mica show some variation in the literature (14,15,16,17,18) and cannot be used for identification

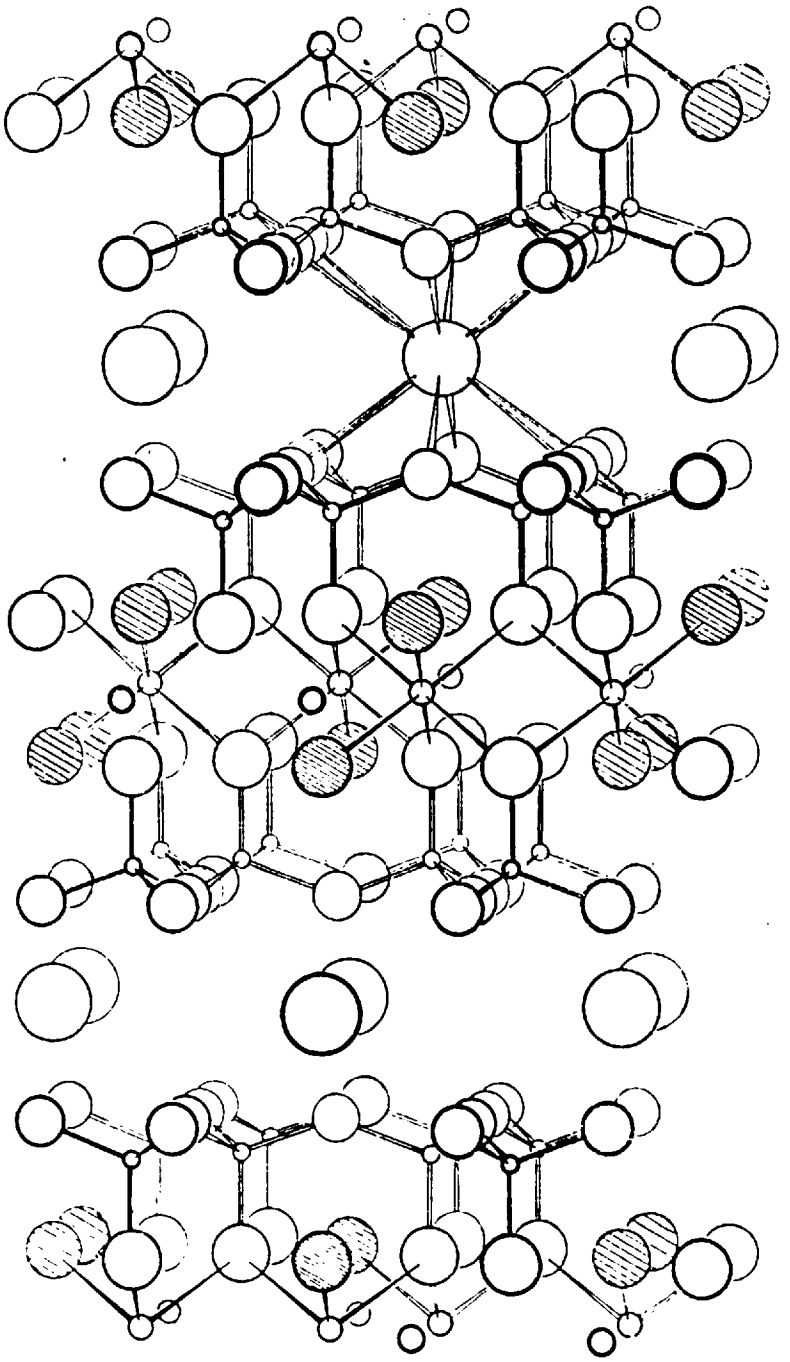


Fig. 1 The muscovite structure, viewed along the *a* axis. Approximately one-half of the unit cell is shown. Open circles in increasing size indicate, respectively, silicon, aluminium, tetrahedral oxygen, octahedral oxygen, and potassium. Hatched circles are hydroxyls (from Brindley and MacEwan 1953).

purposes with much certainty. Apart from differences in the actual structures of different micas, the temperature at which the hydroxyl groups are lost appears to depend upon the particle size and the rate of heating. The general features of the dehydration curve of micas which can be deduced from the various authors , are that the curve starts off fairly level with little loss for the first few hundred degrees, but then rises, often quite sharply, to a maximum steady value of around 6% loss anywhere between 600°C and 900°C. Likewise the d.t.a. trace always shows an endothermic peak due to the volatilisation of the hydroxyl groups, and this occurs between 550°C and 950°C but may be either a broad ill-defined peak covering a 200-300°C temperature range, or it may be a sharp peak only occupying a range of 50°C. Roy[16] has found that a number of micas when heated to a temperature sufficient to drive off the hydroxyl groups but not destroy the lattice, undergo a slight permanent expansion. He also found that with most micas the structure was lost around 950°-1050°C often with subsequent recrystallisation to a spinel.

2.3.2. Felspars. The felspars are the most common of the rock-building minerals and are all closely similar in structure and physical properties. They may however be divided into two main groups, the monoclinic

felspars consisting of those containing potassium or barium as the predominant cation, and the triclinic or plagioclase felspars, which have sodium or calcium as the predominant cation, either alone or mixed together. The basic work on the structure of the felspars was done by Taylor and his co-workers in the 1930's[19,20] and showed that all the felspars were based on the same three-dimensional network of $[SiO_4]$ and $[AlO_4]$ tetrahedra. A convenient way to visualise the structure of the felspars is shown in Fig. 2. The chains, composed of pairs of tetrahedra facing in opposite directions, are crosslinked with neighbouring similar chains to form a rigid framework with interstices of suitable size to contain the potassium or barium cations. In the plagioclase felspars the framework is collapsed a little to give a closer fit around the smaller cation and this reduces the monoclinic symmetry to triclinic. However when the X-ray and optical properties are considered in more detail the felspars are found to exhibit complex polymorphic variations. For instance, the potash-felspar $KAlSi_3O_8$ is known to mineralogists in four varieties - sanidine, orthoclase, microcline, and adularia. Similarly pure $NaAlSi_3O_8$ occurs as low albite and high albite, besides its solid solution with anorthite. The suggestion was first made by Barth[21] that this polymorphism might be the result of different degrees of

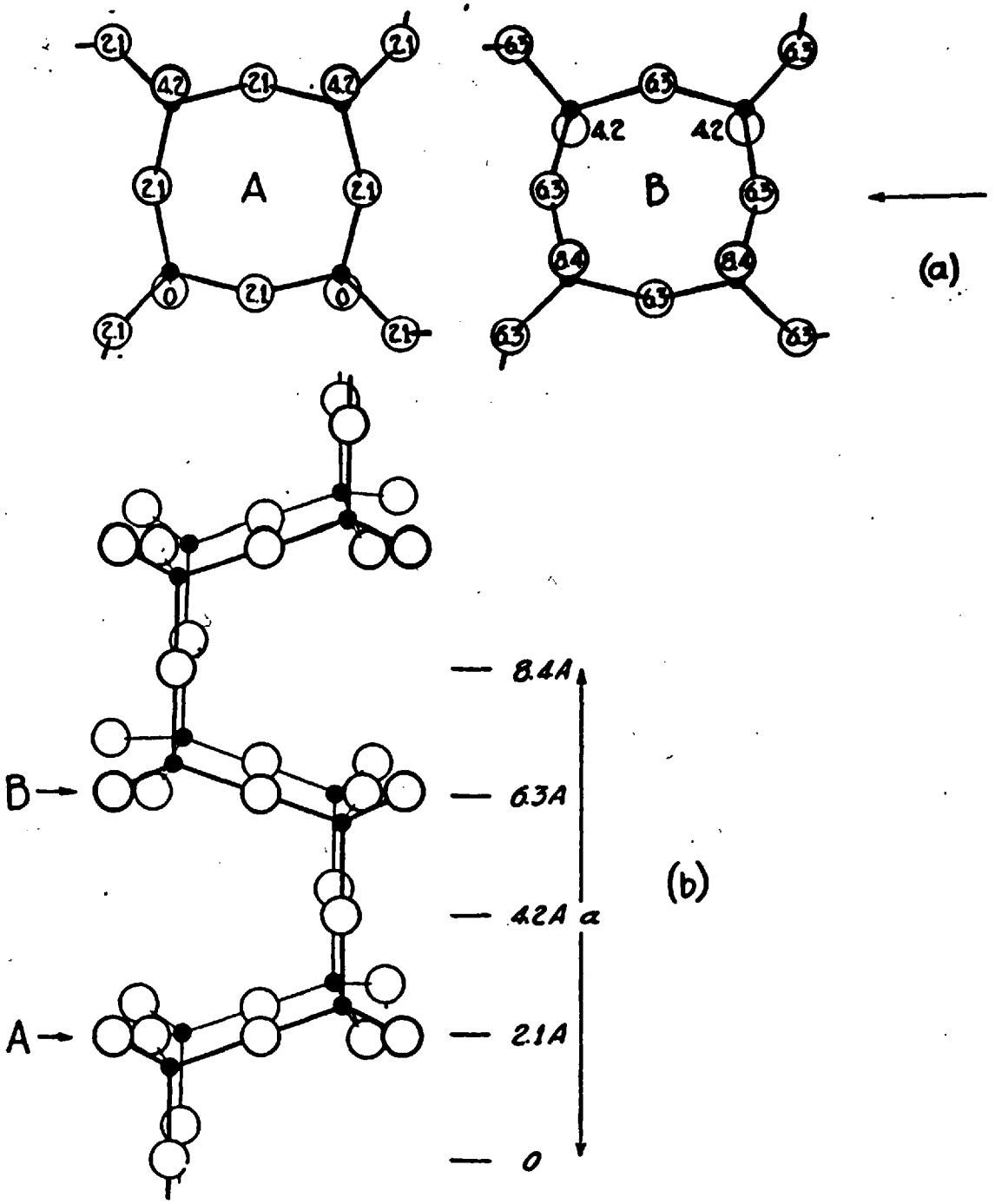


Fig.2—The essential structural feature of all felspars. (a) Rings of four tetrahedral groups, with two *adjacent* vertices pointing up and two down. (b) The same rings joined to form a chain by placing B over A. The oxygen atoms projecting to right and left form the means of linking this chain to its neighbours (after Taylor).

order among the $[SiO_4]$ and $[AlO_4]$ tetrahedra, and later workers[22,23,24,25] have shown this view to be substantially correct. Thus sanidine and high albite are both high temperature forms which have a completely random distribution of the two types of tetrahedra, whereas the respective low temperature forms, orthoclase and low albite exhibit a considerable degree of ordered substitution of aluminium for silicon. The ordering does not appear to be perfect, but it has been shown[26] that the degree of order observed in low albite gives a structure of greater electrostatic stability than complete order would achieve. In the cases of celsian and anorthite the ratio of aluminium to silicon is 1:1 and so we would expect from Lowenstein's rules that the structure would not be stable unless there was a considerable degree of order. Such has been found to be the case[27,28] and as a result the c-axis of the unit cell is doubled in the case of these two felspars.

Although the felspars containing divalent cations do not show polymorphism of the ordered/disordered type they can exist in polymorphic variations which have not been reported for the felspars of monovalent cations. Two further polymorphs of $BaAl_2Si_2O_8$ are known, besides natural monoclinic celsian. In 1915 Ginzberg[29] produced a hexagonal modification by sintering a mixture

of oxides and this was repeated by Dittler and Lasch[30] in 1931 and Thomas[31] in 1950, although the latter worker did not identify his product correctly. This hexagonal modification was later made in kilogram quantities of large flaky hexagonal crystals by electrofusion of kaolin and barium carbonate[32,33] and Ito[34] was able to carry out X-ray studies on this sample to determine its structure, shown in Figure 3. He was able to show how this structure could be simply derived from the monoclinic felspar framework by the twisting and crosslinking of tetrahedra about a reflection plane. Later Takeuchi [35] showed that the transition at about 300°C was of the $\alpha \rightleftarrows \beta$ type and that the structure was in fact orthorhombic below the transition point and only became truly hexagonal above 300°C. No definite occurrence in nature has been established for this polymorph but the mineral cymrite[36] has an X-ray powder pattern very close to that of the hexagonal polymorph, although the authors assign to it the formula $BaAlSi_3O_8(OH)$.

The other polymorph of $BaAl_2Si_2O_8$ is well known in nature, though rare, and is called paracelsian. It is in fact just monoclinic ($\beta = 90\pm10'$) but is usually regarded as orthorhombic and is isostructural with danburite $CaB_2Si_2O_8$[37] whose structure is also closely related to that of the monoclinic felspars[38].

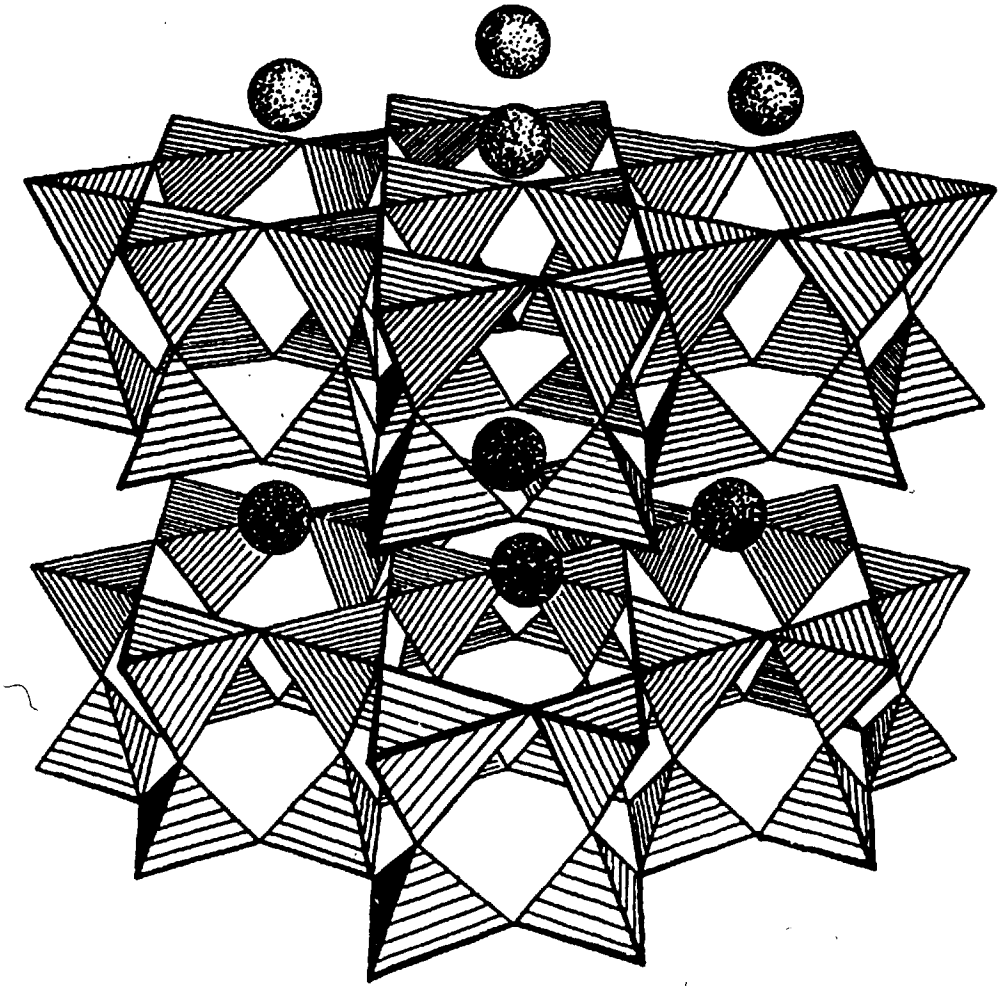


Fig. 3 —Structure of α-$BaAl_2Si_2O_8$ (Ito); shaded spheres represent barium cations, the silicon and aluminum cations are in the centers of the oxygen anion tetrahedra. (Courtesy of the American Ceramic Society.)

Similar synthetic orthorhombic and hexagonal [39,40,41,42] modifications have been reported for $CaAl_2Si_2O_8$ although some of the workers state that these analogous compounds are not isostructural with those of barium. It will be shown later that there are grounds for believing that a similar series of analogous modifications exists for $SrAl_2Si_2O_8$.

2.3.3. Zeolites. The zeolites are also aluminosilicates based on a three-dimensional framework of $[SiO_4]$ and $[AlO_4]$ tetrahedra. Their composition may be expressed by the general formula $(R_1^{++}, R_2^{+})O.Al_2O_3.nSiO_2.mH_2O$, where m and n are variable and may also vary to some extent within the fixed structure of a particular species of zeolite. Also the ratio base : alumina is 1:1 and (Al+Si):O is 1:2. However the frameworks formed are much more open than in the case of the felspars and so the crystal is traversed by channels and cavities, which give rise to the special properties of zeolites. Although all zeolites are truly three-dimensional frameworks, the total bond strength in particular directions depends on the way the tetrahedra are linked in each structure, and on this basis it is possible to divide the zeolites into three classes.

(a) Fibrous zeolites: These may be considered as composed of infinite chains which are strongly bonded along

the c-axis, but only relatively weakly bonded to the neighbouring chains. The common unit of five tetrahedra is repeated at intervals of 6.6Å which gives this characteristic dimension to the unit cell of the fibrous zeolites. Four of the five tetrahedra are linked into a ring with their apices pointing alternately up and down and the fifth tetrahedra links the two upper apices whilst the lower two are linked by the equivalent tetrahedra of the unit below, turned through 90°. The remaining projecting apices link up with their equivalents in the adjacent chains, but this means that the total bonds in these directions are weak compared with those along the chain. This is the explanation of the fibrous habit of these zeolites, of which scolecite and thomsonite are examples.

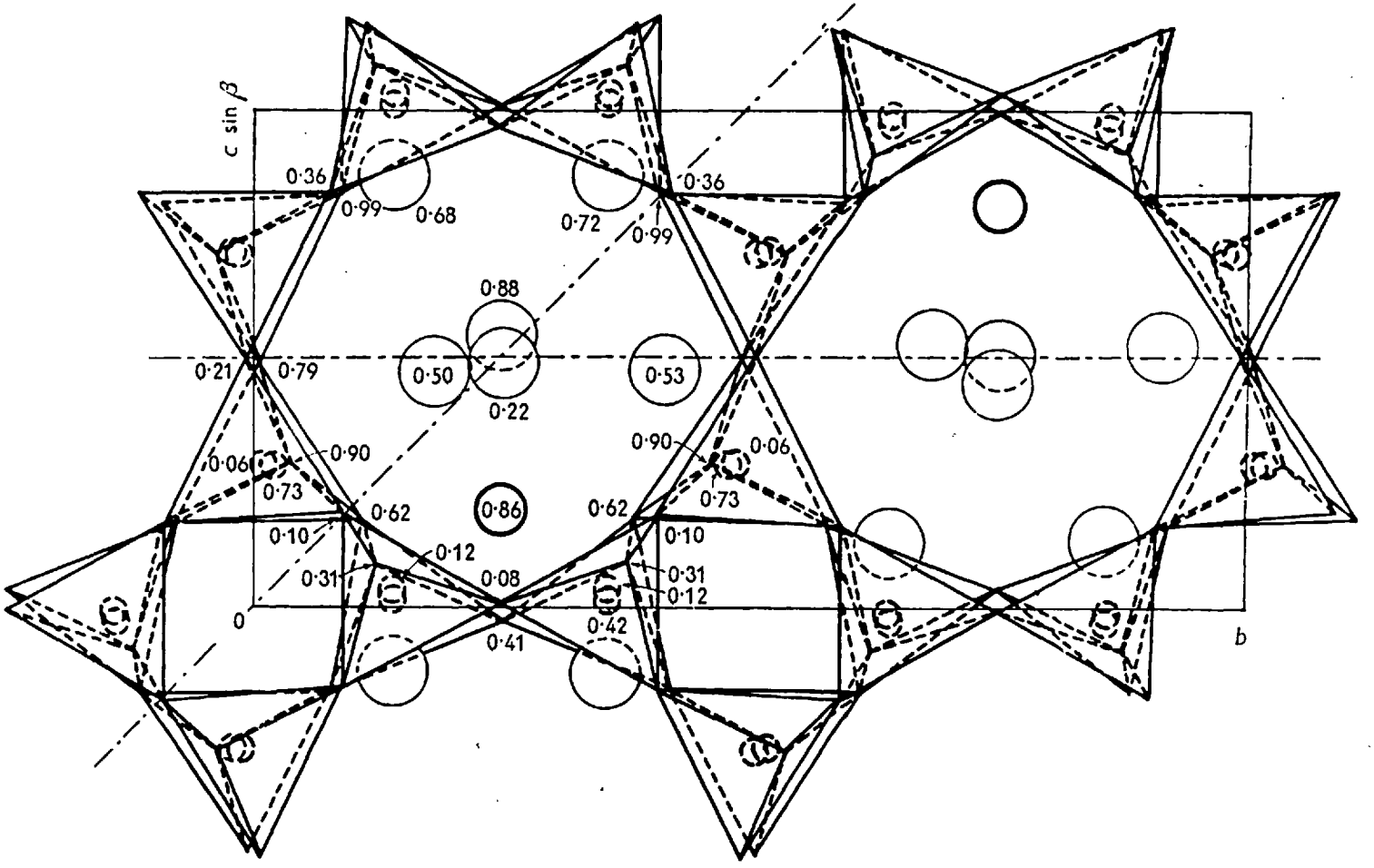
(b) Lamellar zeolites: The best studied of these zeolites showing a platy cleavage is heulandite, the structure of which has been studied by Ventriglia[43]. He shows that the section parallel to [001] consists of a strongly bonded network of five-membered and eight-membered rings. These sheets are linked together by the apices of tetrahedra projecting alternately above and below the plane. The whole structure has alternate pentagonal and octagonal channels perpendicular to [001] and hexagonal channels perpendicular to [100], giving a very open framework.

(c) Robust zeolites: The bonding in these zeolites is strong in all directions and there is no pronounced preferred cleavage. Typical of this group are such zeolites as analcite, chabazite and faujasite, which have a very open structure and do not collapse on dehydration. The structure of harmotome, a barium zeolite of this class, has recently been described[44]. The framework consists essentially of four- and eight-membered rings of tetrahedra, similar to those found in the felspars but linked together in a much more open pattern (Figure 4). Thus two sets of open channels traverse the framework along the a- and b-axes respectively and in them are situated the barium atoms and water molecules. Eight of the twelve water molecules per unit cell are bound to barium atoms, and the remaining four have fixed positions in the cages. The minimum width of the channels along the a-axis is about 4Å and the cross-section of those along the b-axis is $3 \times 4 Å^2$. These sets of channels intersect at right angles, forming spacious cavities.

The nature of the water in zeolites has been the subject of many investigations. All naturally occurring and freshly synthesised zeolites contain considerable quantities of water, but this can be driven off by gentle heating with only slight change of the lattice parameters, particularly in the case of the robust three-

Fig. 4

THE CRYSTAL STRUCTURE OF HARMOTOME, $Ba_2Al_4Si_{12}O_{32}.12H_2O$



dimensional zeolites. When zeolites are subjected to isobaric dehydration three types of dehydration curve may be obtained. In general the fibrous zeolites give a stepped curve similar to that obtained with inorganic salt hydrates and the structure tends to break down readily, but the details reported in the literature show some variation[45,46]. The lamellar zeolites display a smoother curve with one or more discontinuities. Often, as for instance in the case of heulandite[46,47], the loss of the final one or two molecules of water per unit cell is irreversible, and leads to the breakdown of the lattice. In the case of the robust three-dimensional zeolites a smooth dehydration curve is obtained which is completely reversible on exposing the dehydrated product to water vapour once more, provided that the zeolite has not been heated to such a high temperature, usually greater than about 450°C, that the lattice is completely destroyed.

As a result of these dehydration studies combined with results from workers on dielectric studies[48,49] and X-ray structure determinations[44,50] the state of the water in zeolites is considered to be intermediate between normal inorganic water of crystallisation and merely physically adsorbed water. Most, and probably all, of the water molecules occupy definite sites in the crystals, either coordinated to the alkali cations or weakly bonded

to sites in the framework. However, although the presence of water molecules appears to be necessary as a 'space-filler' during the growth of the zeolite, their bonding is relatively weak, and in the case of the robust zeolites at least they have no part in the rigid structure of the framework.

A further consequence of the open channels extending through the zeolite framework is their capacity for ion exchange[51,52] and selective sorption[53]. The freedom of movement of ions into and out of the crystals is governed by the minimum dimensions of the channels, that is, the diameters of the 'windows' through which the ions have to pass to enter the cages. For instance, in chabazite these values are 4.2Å and 2.2Å for the two principal channels, and hence the sodium form will undergo extensive exchange with such ions as K^+, Ag^+, NH_4^+, Ca^{++}, Sr^{++}, Ba^{++} and Zn^{++}, and considerable exchange with Cs^+, Mg^{++}, Cu^{++} and $MeNH_3^+$. In these exchanges the change produced in the unit cell dimensions is less than 1%. Similar considerations can explain the molecular sieve action of zeolites, although the minimum "free" diameters determined in this way are usually a little larger than those determined by X-ray methods[54]. For instance, outgassed chabazite will not sorb aromatics or iso-paraffins, but will take up straight chain paraffins from C_3H_8 to

C_7H_{16} slowly, and C_2H_6, CH_4 and smaller molecules rapidly, whereas faujasite, with a greater pore diameter, will take up such isoparaffins as neopentane.

3. CRYSTALLISATION

The process of crystallisation can be divided into two distinct parts, firstly the nucleation of the crystalline phase, and secondly the subsequent growth to a well-defined visible crystal.

3.1. Nucleation

In a pure metastable phase, free from foreign particles which can often act as nucleating agents, the formation of nuclei is regarded as being due to local fluctuations leading to small changes in concentration resulting in the formation of aggregates of molecules[55]. The rate of nucleation is greatly dependent on such factors as the degree of supercooling and agitation. A certain amount of theoretical work has been carried out for the simple case of nucleation from vapours[56,57]. During the process of crystallisation the new phase, although thermodynamically stable, usually only appears in the form of nuclei under conditions of considerable supersaturation or supercooling. Although the particles in question are extremely small, thermodynamic methods have been applied, and the stability of the nucleus determined from the difference between the decrease in the Gibbs free energy on forming the stable phase from the metastable phase, and

the increase in the surface free energy of the nucleus. If this process is carried out for the formation of drops from the vapour phase, it is found that there is a critical size for the nucleus, and the graph of the free energy of formation of the nucleus against the radius of the nucleus, passes through a maximum. Below the critical size the fluctuation will give rise to unstable embryonic nuclei, which can be regarded as forming and breaking up continuously until they reach a critical size, when a favourable fluctuation will cause them to grow[59]. The formation of actual crystals introduces a further complication in that there will be additional specific free energies due to edges and corners, and these are difficult to calculate. Becker and Doring[57] developed a kinetic approach and deduced an equation for the rate of formation of nuclei which showed reasonable agreement with experimental values in the simple case of the formation of drops by adiabatic expansion of air containing water vapour[60]. The equation showed that the rate of formation was very sensitive to the degree of supersaturation and that this must reach a quasi-critical value if nucleation is to be observed within a reasonable time. In considering the formation of nuclei in supersaturated solutions the matter is complicated by the possible effects of such further factors as diffusion, surface adsorption

and double layer formation. Stauff[61] was able to count the actual nucleation rate for supersaturated potassium chlorate and obtained results which were in reasonable agreement with the formula $\log I = k_1 - k_2/\left[T^3(\log {}^{s}/_{s_\infty})^2\right]$ where I = rate in nuclei per cm^3 per second;

k_1 and k_2 are constants;

s = the supersaturation;

s_∞ = the saturation concentration.

Other approximate equations have been derived[87,88] but it is very difficult to apply these considerations to a hydrothermal system where we have a multicomponent inhomogeneous phase, and little knowledge of the solubility or supersaturation of the species present. The formation of metastable products, for instance, is very common in hydrothermal systems, and these do not readily break down to give the stable phase. Goldsmith[62] has attempted a qualitative explanation of nucleation in such complex systems by means of the concept of simplexity. This is defined by saying that the compound with the highest degree of randomness in its structure, irrespective of space group symmetry, is the compound of greatest simplexity. Thus he postulates on kinetic grounds that the structures of greatest simplexity should be those most readily nucleated in a complex random system such as we have in hydrothermal syntheses, since the greater the

disorder or entropy which can be tolerated and yet produce a nucleus which can grow, the greater is the chance of this occurring by means of random fluctuations in the solution. He suggests that the observed fact that synthetic alkali felspars are obtained in the high-temperature, that is, disordered form supports this view, although it could also be explained if the principle of simplexity applied only to the rapid growth of the felspar subsequent to nucleation. In the case of alternative polymorphic forms the more disordered form, or the more structurally simple form, often has a smaller unit cell than the more ordered or more complex form and so it may be that the form with the greatest simplexity can be nucleated by a smaller embryo than the more complex form. That the high simplexity form would continue to grow and persist is probably due to the high energy barrier to transformation, which is illustrated by many natural minerals, notably the felspars. It is clear that this principle cannot be used to predict possible products with much certainty since other thermodynamic properties may overrule these essentially kinetic considerations. Nor does it imply that a particular structure of low simplexity cannot be synthesised, although it may provide a possible explanation for failure to do so up till now.

Some efforts have been made to determine the species present in solution when quartz[63,64] or felspars[65,66] are dissolved under hydrothermal conditions, but without conclusive results. Barrer et al[67] have suggested that it is difficult to visualise complex open structures such as zeolites being built up by the single addition of $[SiO_4]$ or $[AlO_4]$ tetrahedra. A study of the zeolites with known structures suggests that they can be regarded as built up from simple rings or polyhedral units of tetrahedra. It was therefore postulated that such secondary building units exist in anionic form in solution, and these stack together in various co-ordinations to form the different zeolitic structures. For example, six four-membered rings can pack together to give the cubo-octahedral unit typical of the nosean-sodalite family, whilst structures such as faujasite and Linde Sieve A can be formed by packing together the cubic units formed by linking together a pair of four-membered rings. Such a unit of eight $[SiO_4]$ tetrahedra, up to four of which could be substituted for by $[AlO_4]$, would have a negative charge of from 8 to 12 units. This might be rather excessive, but it seems quite likely that at least some of the free oxygen bonds would be converted to hydroxyl groups, and that these large anions could link up into frameworks by means of a condensation reaction. If such

anions exist it seems quite probable that marginal variations in the condition of synthesis may cause them to link together in some particular way and so nucleate one of several possible zeolitic products, since the free energy balance between the species must often be very delicate.

3.2. Crystal Growth

Once nucleation has taken place there are still many factors which can affect the subsequent growth of the crystal, such as degree of supersaturation, agitation, and the presence of dissolved impurities[55,68]. Much theoretical and practical work has been put into attempts to elucidate the mechanism whereby large polyhedral crystals develop from the invisible nuclei[69,70,71]. The older or 'classical' theory was developed by Volmer, Kossel, Stranski, Becker and Doring, Frenkel, and Burton and Cabrera. This theory deals with the growth of perfect crystals from the vapour or solution and assumes that low index faces in equilibrium with their surroundings are fundamentally flat. Thus Kossel[72] has shown that in crystals of the sodium chloride type the (100) faces will be true planes whilst the (110) faces will be composed of vicinal steps formed by the junction of (100) faces. Stranski[73] has shown that from energy

considerations nucleation is most likely to take place at corners and more likely to take place at edges than on flat surfaces. Therefore high index faces will grow rapidly until they disappear, and faces with ridges or incomplete layers will grow until the face is completed. Before further growth can take place a two-dimensional nucleus must be formed on one of the faces, providing an edge at which further growth can take place. This nucleus must be formed as a result of fluctuations in the number of molecules adsorbed on the surface and it has a critical minimum size below which it will not grow. Becker and Doring[57] deduced an expression for the activation energy of surface nucleation and hence for the rate of formation of nuclei. This theory predicted that growth should be very sensitive to the degree of supersaturation and that at quite a high value of the supersaturation (25-50% for normal cases of growth from the vapour) the nucleation rate should suddenly change from a negligible value to a high value which offers no barrier to growth. The theory has been further developed by Burton and Cabrera[74,80] who calculated the shape of the nucleus, and also suggested that for every rational face of a crystal there is a critical temperature, which they called the surface melting temperature, above which the surface roughness on an atomic scale increases rapidly, and can promote

rapid growth. It seems that this theory provides a mechanism for crystal growth at high supersaturations, and experimental evidence has been claimed by Bunn and Emmett[75] for simple salts and Seager[76] for natural minerals, but many of these results could also be explained on the dislocation theory. However when a direct attempt was made to test the theory of surface nucleated layer growth, Volmer and Schultze found that iodine crystals grew from the vapour at 0°C when the supersaturation was less than 1%[77].

The alternative theory deals with the growth of imperfect crystals and is largely due to Frank[78,79]. He bases the theory on the fact that nearly all real crystals are imperfect and will contain dislocations. Except in very special cases these dislocations will have screw terminations in the crystal face. If such features are present the crystal face will always have edges of molecular terraces exposed on which growth can readily occur. For example, if just one such screw dislocation emerges at the centre of the face then the crystal can grow round and round up a spiral, and the need for two dimensional nucleation never arises. Frank also shows that growth would occur in a very similar manner if there were many dislocations emerging in a crystal face, but that where there are only few,

these would tend to emerge in the centre of the face. He also shows that a pair of disclocations can co-operate to give the effect of spreading layers and vicinal pyramids. Photographs of growth spirals had already been obtained by Heck[81] on paraffin crystals, and were shortly afterwards photographed on beryl by Griffin[82]. Further evidence has been provided by subsequent workers (83,84,85,86).

Also rough calculations based on the theory gave good agreement with Volmer's experimental results for the growth of iodine crystals. It is now generally accepted that the growth of crystals, particularly at lower degrees of supersaturation, can be explained on the basis of the dislocation model.

3.3. Spherulitic Growth

When substances are grown rapidly from highly supersaturated solutions the crystals produced are very often dendritic, that is composed of feathery crystals or branching needles[69]. A particular form of dendritic growth, which is very common in the hydrothermal synthesis of minerals, occurs when the individual crystallites are radially organised in some way, producing spherulites. This form of growth is also common in the crystallisation

of high polymers[71], but has not been studied in much detail in other fields. Morse et al[89] carried out a series of studies on the spherulitic growth of many inorganic salts, in particular the carbonates and sulphates of heavy metals. These he grew by allowing a concentrated solution of one salt to diffuse into a dilute gel of another, the desired product being produced by double-decomposition. In a summary of his results[90] he describes common characteristic forms which he observed (Figure 5). All these have been

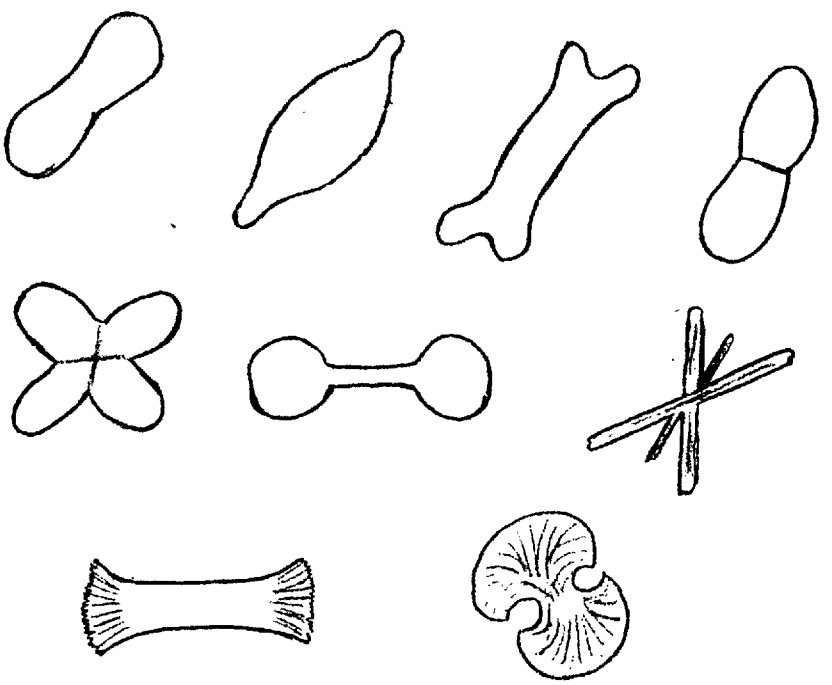


Fig. 5. Typical spherulitic growth forms (after Morse and Donnay).

observed in the present work, together with other obviously related forms. Morse and Donnay claim that almost all these shapes may be explained on the basis of radiating crystallisation from an initial nucleus, subject to the limitation that crystallisation can only take place within a certain solid angle at a point already reached, each point being able to act as a fresh source. Shubnikov(91) has suggested that spherulites may originate from a cluster of nuclei, or from a single nucleus by splitting. Assuming the first case to be true, he shows that each nucleus can only develop outwards along a radius and that surviving crystals will be orientated with their direction of greatest growth velocity along the radius of the sphere. He deduced a mathematical expression for the two-dimensional case which leads to a shape similar to that experimentally observed. Barrer and Kerr(92) have studied the crystal forms of a number of hydrothermally grown synthetic analcites, some of which grew as spherulites. Each of the single crystals composing the spherulite had the same crystallographic direction orientated parallel to the radius, and was regarded as a single cone with its vertex towards the centre of the spherulite and terminating with the facets visible on the surface. By making a number of simple assumptions they showed that the concentration of nuclei is high near the centre of the spherulite and

diminishes asymptotically outwards.

Recently an interesting explanation of the origin of spherulites has been advanced by Sears[93], based on the Cahn-Hilliard theory of non-classical nucleation[94]. It is pointed out that the classical theory of nucleation, derived from Gibbs' theory of phase stability, is not valid at high degrees of supersaturation, or supercooling. An approximation for the critical value of the supercooling above which non-classical nucleation will result can be obtained. Rigid non-classical nuclei may be either: (a) of a polycrystalline or spherulitic nature, or (b) an extremely defective single crystal or glassy nucleus. Sears gives experimental evidence for the formation of both these types of nuclei. Non-classical nucleation, and hence spherulitic growth, will be favoured when the supersaturation is high, the unit cell is large, and there is a large anisotropy of the specific surface free energy together with small grain boundary energies. In some cases however spherulite growth may occur under conditions the same as, or less supersaturated than, those which produce single crystals[92,95]. These observations indicate that spherulites can in some cases be formed by classical nucleation.

4. METHODS OF MINERAL SYNTHESIS

The experimental methods employed in the synthesis of minerals are largely imitative of natural processes. In the laboratory it is possible to control such factors as the purity and nature of the starting materials and the conditions of pH, temperature and pressure under which they react. However it is not possible to match the great periods of time taken for the formation of most natural minerals, and it is only in recent years that extremes of temperature and pressure, such as those required to form diamond, have become available.

The principal methods employed in the synthesis of silicates and aluminosilicates have been summarised by Barrer[96].

4.1. Vapour Phase Crystallisation

The commonest example of this process in nature is the formation of snowflakes, but it may take place at higher temperatures in active volcanic regions. Frankel has produced cassiterite (SnO_2) by volatilization[97] and in glass making furnaces the ceramic linings react with the alkali metal oxide vapours produced[98]. Also gaseous SiF_4 is reported to react with superheated water vapour to give quartz crystals[99].

4.2. Reactions at Low Temperatures and Pressures.

Mineral reactions which take place under the ambient conditions of temperature and pressure take extremely long times. In nature this is exemplified by the atmospheric weathering of rocks to produce clay minerals, and the reported formation of phillipsite in submerged sediments at about 10°C. The formation of montmorillonite from dilute solutions kept at room temperature for several years has been reported by Sedletsky[100] and other workers.

4.3. Sintering Reactions.

This basically simple process involves reactions in the solid state by the diffusion of the reacting species at temperatures below the melting points of the solids concerned. Such reactions are nearly always very structure sensitive and the rate of reaction depends very much on such factors as the grain size of the reactants, the intimacy of mixing and the compacting pressure, and on the previous thermal and chemical histories of the reactants, including the presence of small amounts of impurity. The crystals produced by such solid state reactions are normally very small and sintering studies are usually aimed at the elucidation of reaction mechanisms and the kinetics of reaction. Since chemical reaction is only possible at the phase boundaries, reactions in the solid state can be considered

as consisting of reactions between two components only, irrespective of the number of reactants in the mixture. Many minerals have been synthesised in sintering reactions, but since the nature of the product is usually governed by rate phenomena and the presence of catalysts, metastable products may result. It has been shown for example that when amorphous silicic acid is heated to about 1150°C the product is cristobalite, although the conditions lie in the stability range of tridymite. However, in the presence of calcium oxide, the primary reaction product is quartz[101]. Care must therefore be exercised when drawing conclusions from the products formed by the ignition of the hydrothermally produced species reported later in this work.

4.4. Pyrolytic Crystallisation

In this method the crystalline product is obtained by cooling a homogeneous melt of the desired composition. Several techniques have been devised to grow large good quality single crystals by the use of a temperature gradient, as in the methods of Stockbarger and Kyropoulos which have proved very successful in the case of the alkali halides[102, 103]. In the case of silicates, however, the method is complicated by the high viscosity of the melt and its very ready solidification to a glass if cooled too rapidly.

When the melting point of the desired compound is very high, the flame-fusion technique of Verneuil may be used. In the production of single crystals of corundum, for instance, a fine powder of alumina is fed through the oxygen jet of an oxy-hydrogen burner. It melts as it passes through the flame and is deposited on the molten surface of the growing crystal beneath. In this way good single crystals of several refractory materials have been produced. A summary of the requirements for the successful operation of this technique has been given by White[104].

When the desired product is an incongruently melting compound it can sometimes be grown successfully from a mixed flux with a relatively low-melting salt, but the resultant crystals are usually small and of poor quality.

4.5. High Pressure Crystallisation

In nature deep seated igneous rocks have cooled very slowly from about 1400°C at pressures up to 10 tons per square inch. Michel-Lévy has obtained small crystals of felspar by detonating explosive charges in bombs up to temperatures of 850°C[105]. An authentic synthesis of diamond was first established by workers at the General Electric Company of America[106] using apparatus capable

of maintaining pressures up to 100,000 atms. at temperatures between 1200 and 2400°C[107]. Other high pressure minerals such as borazon and coesite[108,109] have also been synthesised by these methods.

4.6. Hydrothermal Synthesis

Since water is by far the most common solvent in geological systems, it is perhaps not surprising that the methods of hydrothermal synthesis have proved very successful in producing a very wide range of synthetic minerals. The method involves heating the desired reactants, which may be very diverse, in a sealed vessel with a large amount of water, thus generating considerable pressures of water vapour. Temperatures used in hydrothermal crystallisations are normally below 600°C and the pressures involved may range up to at least 60,000 p.s.i. The products may be either hydrated or anhydrous, but in general the degree of hydration decreases as the temperature is raised. In most hydrothermal syntheses the size of the crystals produced is very small, but by careful control of the conditions and the application of a temperature gradient, large good quality crystals of many species can be produced. In particular, much attention has been given to the production of quartz, and very pure, high quality crystals weighing several hundred grams are readily produced on a commercial scale[104,110].

5. THEORETICAL ASPECTS OF HYDROTHERMAL SYNTHESIS

The basis of hydrothermal synthesis is the crystallisation of mineral species from aqueous solutions at elevated temperatures and pressures. Apart from temperature and pressure, the composition and nature of the starting materials are the dominant factors in determining the synthetic products. The complicated situation produced by these variables can be partly resolved in terms of simple thermodynamic and kinetic considerations.

5.1. Thermodynamic Considerations

If it is desired to relate the results of hydrothermal syntheses to petrological conditions then great care must be taken to ensure the attainment of equilibrium. Fyfe[111] has pointed out a number of factors which cast doubt on the stability of many reported "equilibrium" synthetic assemblages. A stable product is here regarded as the species which has the minimum free energy in the given physical and chemical environment. Fyfe and Verhoogen[112] have pointed out that the free energy of polymorphic transitions or of reactions between silicates is, in general, only of the order of a few hundred or a few thousand calories per mole. Consequently, in laboratory experiments where highly reactive amorphous reactants are

used metastable assemblages may form and persist. Slight impurities, surface effects, and methods of preparing reagents may have a very marked effect on the final products.

The free energies of reaction have only been determined with accuracy for relatively few systems, and thermodynamic data for aluminosilicates is sparse and often too inaccurate to be used quantitatively. However, the above authors have suggested an approximate method for calculating the entropies of compounds encountered in hydrothermal work, which is based on the addition of conventional entropy values for the component elements, subject to certain corrections.

Entropy changes may be a major factor affecting the production of metastable species, that is, species which have a free energy higher than the minimum for the system, but whose rate of reaction to form the stable species is extremely slow. Ostwald's step rule, or law of stages, states that the phase which is most likely to appear is not necessarily the most stable one. Two different, but not contradictory explanations have been proposed. One suggestion is that the nucleation of the form with the least surface energy will be favoured, resulting in the preferential growth of a metastable phase, which may then persist[113]. In the other approach Fyfe and Verhoogen

show that the rate of nucleation for a polymorphic transformation includes a term with the form $\exp(-\Delta S_{\Delta}T/2RT)$. This indicates that the greatest rate of nucleation is obtained for the transformation involving the least decrease in entropy. Therefore there is a strong tendency for a phase with a crystalline structure close to that of the reactant, or a previously formed species, to nucleate. For example, there may be several possible polymorphs between the starting materials of high free energy and entropy and the stable product with minimum free energy and low entropy. In such a case a metastable polymorph, whose formation involved a smaller change in entropy, will often be produced in experiments of normal laboratory duration. It is therefore expected that the very reactive hydrous gels used in the present work will tend to produce metastable species.

A further application of thermodynamics to hydrothermal systems has been pointed out by Barrer[58] based on the method of solution thermodynamics. He has shown how the changes in chemical potential, enthalpy and entropy caused by the occlusion of guest molecules, as in the case of the zeolites or members of the nosean-sodalite family of minerals, may be determined. From his work it is clear that open framework lattices may be greatly stabilised by the presence of some space filling mineraliser, such as water.

Consequently it is probable that such minerals could only be formed by hydrothermal methods.

5.2. Kinetic Considerations

When examining the role of water in hydrothermal reactions several different aspects can be considered.

5.2.1. Solvent action of water. The solubility of most silicates and aluminosilicates in water is low, and in solubility determinations difficulties may arise on account of preferential leaching of one of the components. The rate of solution of the solid reactants may exercise considerable influence on the species produced as it normally requires high degrees of supersaturation to nucleate a crystalline phase. If one of the reactants dissolves very much faster than the others then the composition of the solution will be greatly different from that intended and unexpected products may result. The solubilities of many substances increase with increase in temperature, and there is no discontinuity at the critical point, showing that the solvent properties of the supercritical fluid are similar to those of the liquid phase. The solubility isobars of quartz at pressures up to 600 bars, for example, are smooth curves which show a maximum between 375° and 420°C[114]. When a reactant is metastable there will be no true value for the solubility. It should

continue to dissolve and the stable phase will be precipitated when the solution becomes sufficiently supersaturated. The rate controlling step in such a process may be either the solution of the reactant, the diffusion of the dissolved species, or the nucleation and growth of the stable phase.

5.2.2. Diffusion in water. The diffusion coefficients of the relevant species have not been determined but there is no doubt that the rates of diffusion in water are very much greater than in solids. The activation energy of diffusion in liquids is normally rather small, being around 5 kcals, and so diffusion rates will not depend greatly on temperature[112].

The viscosity of water may be important when considering diffusion rates. The data available in 1950 have been summarised by Keyes[115] and Franck has extrapolated these values by calculation[116]. The viscosity decreases sharply over the first 200°C compared with subsequent changes as the temperature is raised. This can be attributed to the decreased association of the water molecules. The viscosity rises again as the pressure increases, and would have reached a maximum of about 0.6 centipoise in the present work. Under the conditions used there would be effective mixing by thermal agitation and diffusion

would be rapid. It is therefore unlikely that diffusion would be the rate controlling step of the crystallisation process.

5.2.3. Complex ion formation. Many complex minerals are known to form very rapidly from their component oxides in water (e.g. 117). If the formation of a complex mineral depended on the chance collisions of ions in solution in the appropriate proportions, then the rate of formation would be extremely slow. Since it is known that complex ions can exist in other inorganic solutions, it seems likely that hydrothermal solutions could contain such complicated anions as $[AlSiO_4]^-$, $[AlSi_2O_6]^{--}$, $[AlSi_3O_8]^{--}$ or even perhaps $[Al_2.AlSi_3O_{10}.(OH)_2]^-$ together with their hydrolysis products[112]. Wood[118] and others[63,120] have concluded that dissolved silica probably exists in solution as $Si(OH)_4$ under moderate conditions, but that it forms polymeric ions or molecules at higher pressures. The suggestion by Barrer et al[67] that complex anions are formed by linking together $[AlO_4]$ and $[SiO_4]$ tetrahedra into rings and polyhedra has already been mentioned (p.28).

The kinetics of ionic reactions have been discussed by Glassstone, Laidler and Eyring[121], who show that the entropy of activation for such a reaction will contain a term ΔS_ϵ arising from the dielectric constant

of the solution. This term is proportional to $(1/\epsilon^2)(\partial\epsilon/\partial T)$ and also to the product of the ionic charges on the two ions reacting. In ordinary water it is found that the reaction rate will, in general, increase ten to one hundred times for each unit increase in the product $(-Z_A Z_B)$, where Z_A and Z_B are the respective charges on the reacting ions. Under the hydrothermal conditions used in this work the dielectric constant falls to as little as 9 in the extreme case and $\partial\epsilon/\partial T$ increases[122]. The effect of the ΔS_ϵ term will therefore be even more marked and highly charged ions of opposite sign will react very readily, whereas the association of ions of the same sign will be slow.

5.3. Phase Equilibria.

The treatment of phase relationships in a theoretical hydrothermal system has been outlined by Morey and Niggli[123] and Morey and Ingerson[124]. Although in practice hydrothermal systems will contain three or four components at least, some general principles may be deduced from a consideration of the simpler binary case.

In the temperature-concentration projection of the phase equilibrium diagram for a binary system, the solubility or fusion curve joins the triple points of the two components. This gives the composition of the liquid

co-existing in equilibrium with the vapour. The critical points of the two components will also be joined by a critical curve, which is the locus of all points where the critical phenomena ~~view~~ occur for mixtures intermediate between the two pure components. In each case part of the curve may lie outside the stable region if transformation, decomposition, or limited miscibility occurs. There are therefore two possibilities to consider. Firstly, ~~that~~ the solubility curve does not intersect the critical curve, and secondly ~~that~~ the solubility curve does intersect the critical curve.

In the first case (Fig. 6), since the critical point of each component will lie at much higher values of temperature and pressure than its melting point, and the curves do not intersect, then the solubility curve must always lie below the critical curve. Also, the two-phase line in co-existence with the solid will be below the critical curve. Therefore only unsaturated solutions will show critical phenomena, and the two-phase line equilibrium with the solid phase can be studied without the appearance of critical phenomena. Under these conditions the critical point of the more volatile component does not influence the solubility relations of the solid-liquid or solid-vapour systems. For example, in a water-silicate system of this type there would be a

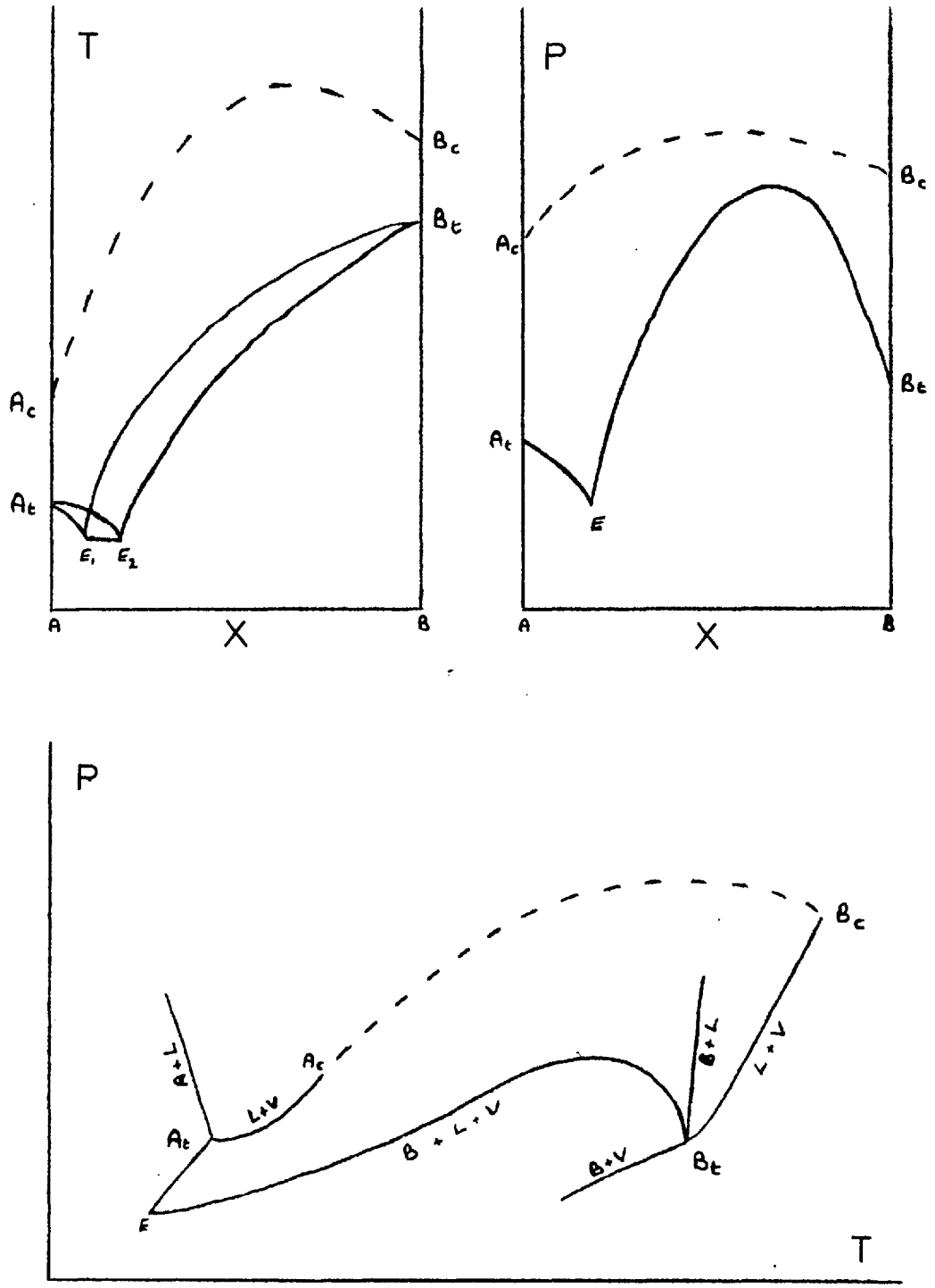

T
B_c
B_t
A_c
A_t
E_1
E_2
A
X
B
P
B_c
A_c
B_t
A_t
E
A
X
B
P
B_c
A+L
A_c
L+V
A_t
B + L + V
B+L
L+V
B+V
B_t
E
T

Fig. 6. Case 1.

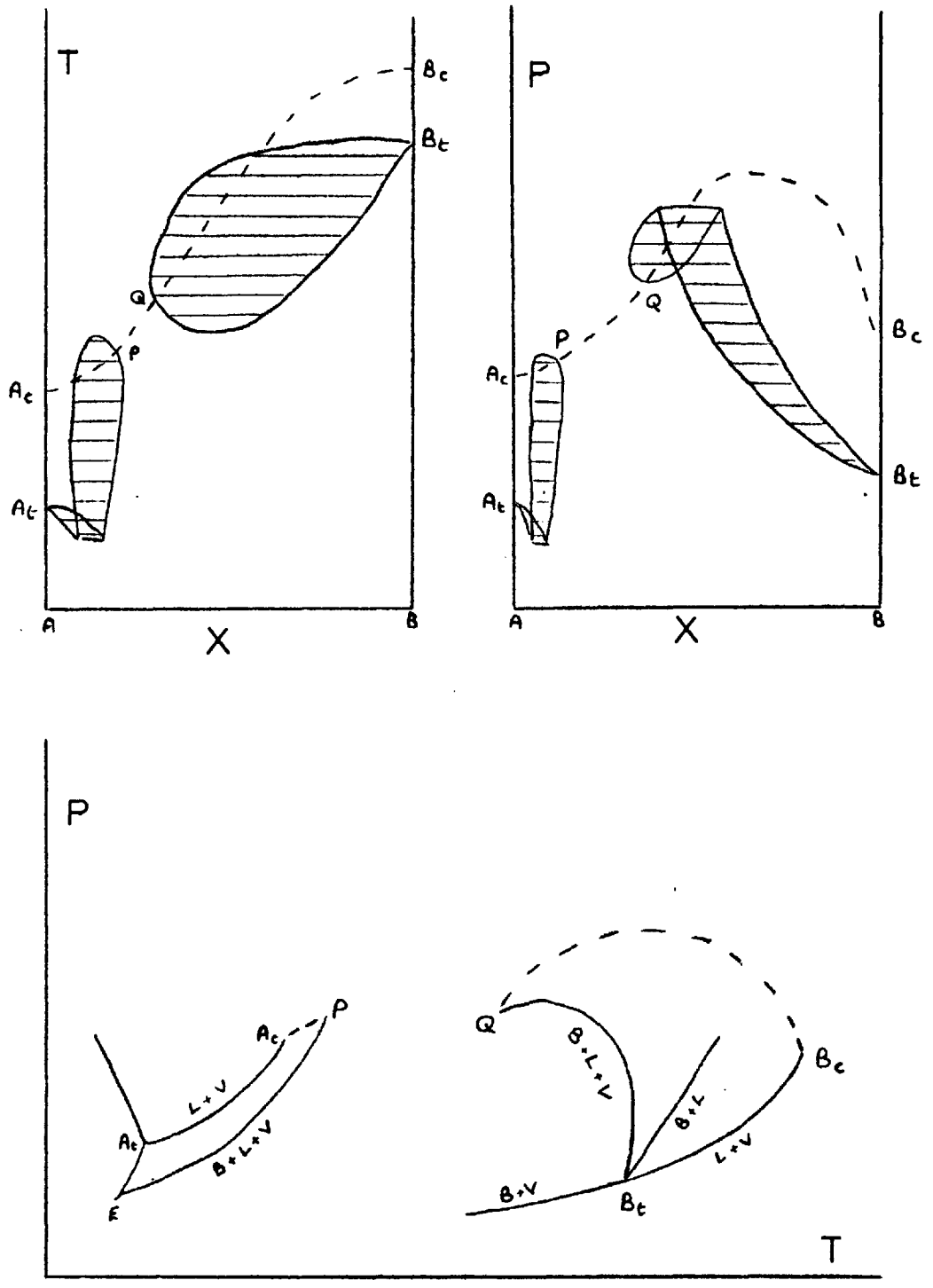

T
B_c
B_t
Q
P
A_c
A_t
A
B
X
P
Q
P
A_c
A_t
B_c
B_t
A
B
X
P
A_c
P
L+V
A_t
B+L+V
E
Q
B+L+V
B+L
B_c
L+V
B+V
B_t
T

Fig. 7. Case 2.

continuous two-phase line in co-existence with the solid connecting the melting point of ice with the melting point of the silicate. The systems K_2SiO_3-H_2O and $K_2Si_2O_5$-H_2O are found experimentally to behave in this way[125].

When considering the second case (Fig. 7) it is clear that when the composition of a mixture is close to that of a pure component then the two-phase line co-existing with the solid must lie below the critical curve. Therefore if this line intersects the critical curve it must do so at two points. There will be an upper and a lower critical point at which the saturated solution will show critical phenomena. Above the upper and below the lower of these intersection points the three phases, solid liquid and vapour may co-exist, whilst in the intermediate region solid and gaseous solutions will be the only stable phases. There is not a continuous line representing two-phase equilibria in the presence of the solid phase. This has the following consequences. For a moderate amount of water and a given volume, in the region below the lower critical end point the state of the system will be determined by the temperature alone. At a constant temperature reasonable variations in the amount of water are without effect on the concentration of either the saturated vapour or saturated solution. Provided that the total volume remains the same, such variations only affect the relative

amounts of vapour and liquid solution.

In the region between the two critical end points the two-component system will be divariant and for a given temperature and volume, a small change in the amount of water will change the pressure, and therefore the concentration, of the vapour phase. As a result variations in the degree of filling of a closed vessel may influence the product produced. A given system is likely to follow this second type of behaviour if it satisfies the following conditions. The volatility of one component must be very much less than that of the other, and the solubility of the less volatile component in the more volatile component must be very small near the critical point of the latter. This is the case in most silicate or aluminosilicate and water systems. When this is so then the saturated solution will show critical phenomena at a temperature and pressure very little above those for pure water. Above this point there is a region where solid and supercritical fluid are the only stable phases, but the gaseous phase is as much a solvent as the ordinary aqueous solution in contact with vapour. Hence in this case also the critical point is without direct influence on the solubility.

6. SOME PREVIOUS SYNTHESES

The methods of hydrothermal synthesis have been widely employed to produce a very wide range of synthetic minerals. The work done up to 1937 has been surveyed by Morey and Ingerson[124]. Many of the identifications proposed in much early work are doubtful as the products were characterised by optical measurements on extremely small crystals.

Workers in these laboratories using the methods followed in the present investigations have studied the hydrothermal crystallisation of aluminosilicates using gels with the general composition $M_2O.Al_2O_3.nSiO_2$ + water. The silica:alumina ratio has been varied between 1 and 9 or 12, and the cations studied have been lithium[126], sodium[67,127], potassium[128], rubidium and caesium[129]. Other cations which have been studied by similar methods include thallium[130], calcium[42], and substituted methyl ammonium bases[119]. The experiments have been carried out between 60°C and 450°C, and very often excess alkali has been added, which in many cases caused a different product to be obtained.

Under these conditions aluminosilicates with framework structures have been by far the most common product. Many zeolites have been synthesised, some are

exact or close analogues of species found in nature, and others have structures which have no parallel in nature.

Felspars have also been produced, usually in the high temperature disordered form. Examples are sanidine, albite, anorthite and its hexagonal polymorph, and rubidium felspar. A number of felspathoids have also been produced, among them leucite and basic sodalite.

There has been little hydrothermal work on the systems $SrO-Al_2O_3-SiO_2-H_2O$ and $BaO-Al_2O_3-SiO_2-H_2O$. Carlson and Wells[131] have investigated the hydrothermal reaction of silica gel with strontium hydroxide solutions at temperatures up to 300°C. In addition to the two anhydrous silicates, $SrSiO_3$ and Sr_2SiO_4, which were formed at temperatures down to 124° and 142°C respectively, seven ~~other~~ hydrated strontium silicates were produced and identified by means of X-ray powder patterns. The hydrates found were $SrO.2SiO_2.H_2O$, $SrO.SiO_2.H_2O$, $2SrO.2SiO_2.3H_2O$, $3SrO.2SiO_2.3H_2O$, $3SrO.SiO_2.2H_2O$, $3SrO.2SiO_2.4H_2O$, and $2SrO.SiO_2.H_2O$. Most of these hydrates decomposed below 150°C. It was also observed that different forms of silica gel used as starting materials gave different products. In all cases save one the excess silica was converted into cristobalite. Corwin et al[132] have studied the attack of strontium hydroxide solutions on vitreous silica under supercritical hydrothermal conditions.

They found that the reaction proceeds quite rapidly at first with the formation of strontium silicate ($SrSiO_3$) and amorphous silica. The rate of reaction decreases to a minimum after 65 hours after which it increases once more with the formation of β-cristobalite which very rapidly transforms to α-cristobalite. The rate then falls to a second minimum after 96 hours. Similar investigations into the attack of barium hydroxide solutions on vitreous silica showed that a tightly adherent layer of insoluble barium silicate forms on the surface of the silica, preventing any further reaction[133].

Barrer et al[134] have studied the hydrothermal attack of barium chloride and barium bromide solutions on synthetic analcite. With concentrated salt solutions around 200°C the analcite recrystallised to a new mineral species with the formula $BaO.Al_2O_3.4SiO_2.0.66BaCl_2.2\text{-}3H_2O$. The occluded barium salt could be removed by hydrothermal extraction leaving a zeolitic structure with sorptive properties[135]. This mineral tended to recrystallise to barium felspar or another unidentified mineral if the extraction process was too prolonged or vigorous.

<u>High-temperature dry crystallisation</u>. The phase equilibria of the strontium aluminosilicates have been studied by Dear[136] and Sorrel[137]. Dear studied the subliquidus

equilibria of the system $SrO-Al_2O_3-SiO_2$ by a sintering method. Besides three strontium silicates and four strontium aluminates he found three ternary compounds. One was a felspar of the anorthite type, $SrO.Al_2O_3.2SiO_2$, and the others had the compositions $2SrO.Al_2O_3.SiO_2$ and $6SrO.9Al_2O_3.2SiO_2$. Eskola claimed to have produced strontium anorthite by heating the component oxides in a strontium vanadate flux at 1400°C. The product had a fibrous habit, and was obtained as very small poorly formed crystals, which were identified by their refractive indices[138]. Sorrel investigated the reaction between kaolinite and strontium sulphate at temperatures up to 1400°C. He produced both strontium anorthite and its hexagonal polymorph, but the evidence pointed to the probability that the hexagonal form was a metastable phase.

The same author carried out similar experiments with kaolinite and barium sulphate and produced celsian and its hexagonal polymorph. The barium hexagonal felspar was also believed to be metastable but it was much more persistent than the strontium form. As outlined earlier (p. 15) this modification has been produced by many workers under the same general conditions. The system $BaO-Al_2O_3-SiO_2$ has been studied by Toropov et al[139] using a quenching method. No X-ray data were given but two silicates

$2BaO.3SiO_2$ and $BaO.2SiO_2$ were reported in addition to celsian ($BaO.Al_2O_3.2SiO_2$) and a new aluminosilicate ($3BaO.3Al_2O_3.2SiO_2$.).

7. EXPERIMENTAL APPARATUS AND METHODS

7.1. Hydrothermal crystallisations.

7.1.1. Chemicals.

(a) Silica. The silica used in all the experiments was in the form of a stable suspension of amorphous silica in water, supplied by Monsanto Chemicals Ltd. under the trade name "Syton-2X". This contained 29.7% by weight of silica and had a specific gravity of 1.2, a pH ~10, and contained a trace of chloride.

(b) Alumina. The aluminium hydroxide used was prepared by the method of Wislicenus[140]. Aluminium foil was divided into small pieces and amalgamated lightly by contact with a 2% solution of mercuric chloride for about 15 seconds. It was then well washed and allowed to stand overnight in a large volume of distilled water maintained at 0°C. The precipitated gel was separated from any unreacted foil by washing through a fine gauze and filtered off, washed with water, alcohol and ether and sucked dry. It was then sieved through an 85-mesh sieve and allowed to stand overnight in an open vessel. The light grey powder was then analysed by igniting a sample to constant weight, and kept in a closed bottle. It was normally found to contain between 50 and 58% Al_2O_3, and when freshly prepared was amorphous to X-rays. The gel

was not used more than about three weeks from its preparation because of its tendency to age and crystallise.

(c) Alkalis. The strontium used was in the form of the strontium hydroxide octahydrate (recrystallised) supplied by Messrs. Hopkins and Williams. The barium used was B.D.H. AnalaR grade barium hydroxide octahydrate.

7.1.2. Preparation of the gels.

From the chosen formula of the gel the quantities of the above reagents required to give a dry weight of 0.5g. oxides in 7 ml. of water were calculated. The barium or strontium hydroxide octahydrate was weighed out, transferred to a mortar and ground up with a little water added from a burette. The weighed amount of aluminium hydroxide gel was added and mixed to a smooth paste with a little more water, then the calculated amount of Syton 2X was added from a graduated pipette, and carefully mixed in. The resultant gel was transferred to a conical flask with the remainder of the water, and stirred vigorously for about two hours, taking precautions to exclude carbon dioxide from the air which reacted with the hydroxides. Sufficient gel for from 5 to 15 experiments was prepared in one batch and 7 ml. of suspension were added to each autoclave, using a small measuring cylinder.

7.1.3. Reaction vessels.

For the runs carried out at 110°C sealed Pyrex tubes with an internal diameter of about 1.5 cm and a capacity of 20 ml were used. They were charged with 10 ml of suspension containing 0.7 g of dry oxides.

In all the other experiments at temperatures from 150°C to 455°C stainless steel tube autoclaves supplied by Messrs. Baskerville and Lindsey were used. These had a capacity of 14 ml and were sealed with silver washers (Figure 8), which flowed slightly on closing the autoclave and also expanded more than the steel on heating. This form of seal was very satisfactory provided that the washers were renewed from time to time, and only two cases of leakage occurred. A molybdenum sulphide anti-scuffing paste was used on the threads so that they would not seize up at high temperatures.

7.1.4. Ovens and furnaces.

Electrically heated air ovens, thermostatically controlled to ± 3°C, were used for runs at temperatures between 100°C and 300°C inclusive. For runs at temperatures above 300°C a specially constructed furnace was used (Figure 9). This consisted of a large copper block having nine holes drilled in it to closely fit the autoclave, and packed

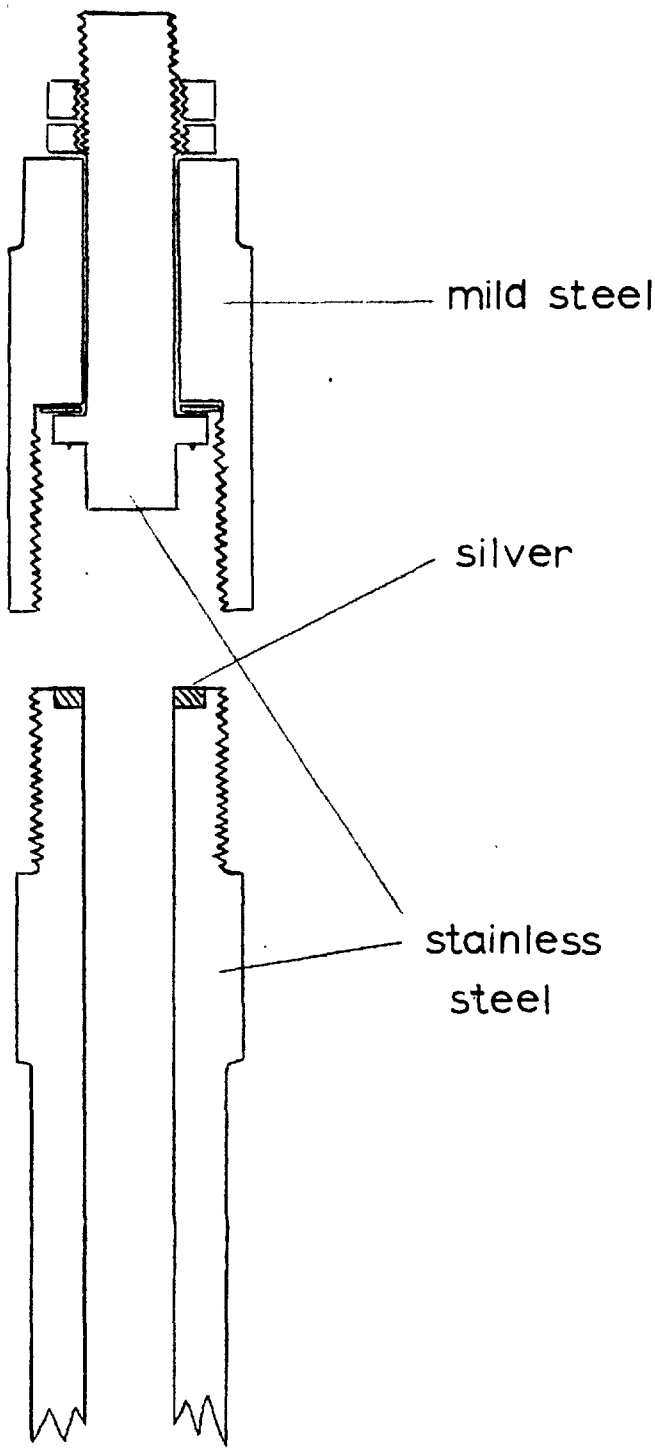
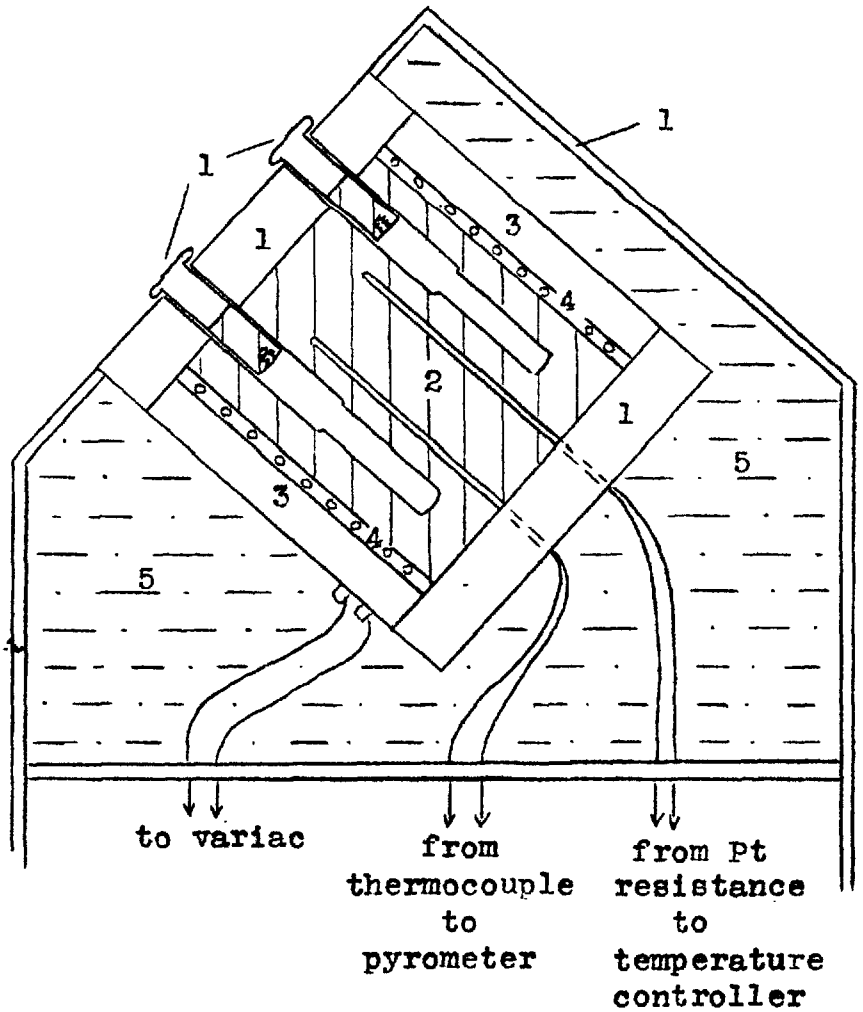


Fig. 8. Autoclave Closure.



1. Sindanyo.
2. Copper.
3. Alumina Cement.
4. Nichrome Windings.
5. Asbestos.

FIG. 9. The Large Furnace.

around with asbestos wool inside a Sindanyo case. The electrical circuit was as shown in Figure 10. The control relay was operated by the amplified out of balance signal from a Wheatstone bridge, one arm of which was a platinum resistance inserted into the copper block of the furnace. This could maintain a given temperature $\pm 1^{\circ}C$ over a long period. The temperature was measured directly with a pyrometer, using chromel/alumel thermocouples also inserted into the copper block, but each time that the furnace was adjusted to a fresh steady state the temperature was checked using a Pt/Pt-13%Rh thermocouple placed in one of the autoclave sockets and a Cambridge potentiometer, with the cold junctions at $0^{\circ}C$.

7.2. Recovery of Products

On completion of the desired period of treatment the autoclaves were removed from the oven or furnace and normally quenched in cold water. However this was sometimes not convenient so the autoclaves were allowed to cool down in air at room temperature, since preliminary tests had revealed no difference in the products whether the autoclaves were quenched or not. When cold, the autoclaves were opened, the mother liquor decanted, and its pH measured to the nearest 0.5 unit with Universal indicator paper. The product was washed out of the autoclave,

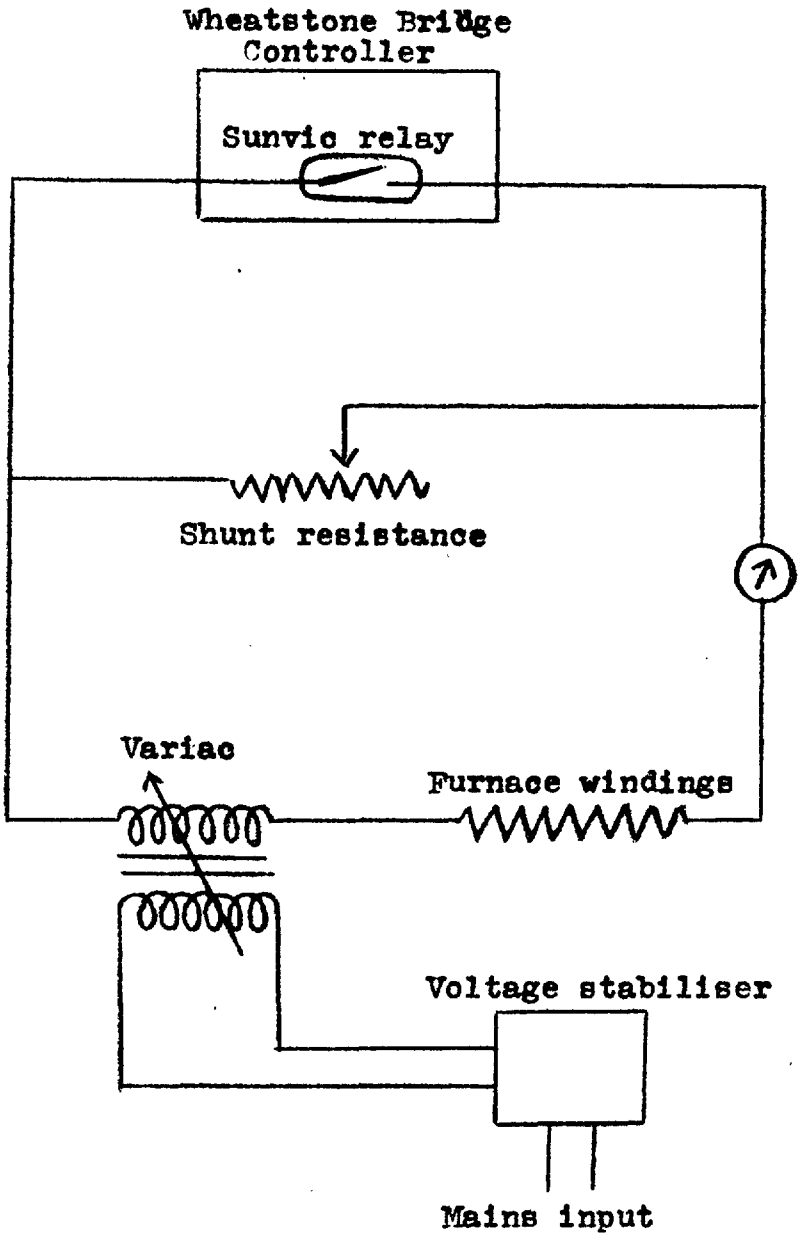


FIG. 10. Circuit of large furnace.

filtered off, washed with cold water and dried at 105°C.

7.3. Examination of Products

7.3.1. Optical microscopy. A drop of a water suspension of each product was taken, dried out on a microscope slide and examined under a Leitz IIIC polarising microscope. A Vickers projection microscope capable of magnification up to 2000x was used for further examination and for taking photomicrographs. In this way the crystal habit of the product could be studied and the purity of the preparation estimated. In a few cases the mean refractive index of a well crystallised species was determined using immersion liquids and the Becke line test, but the crystals were too small to determine the true refractive indices in known crystallographic directions.

7.3.2. Electron microscopy. Samples yielding crystals too small for study with the optical microscope, or otherwise of interest were examined on a Phillips 100 desk model electron microscope with the help of Dr. I. S. Kerr of this department. It was often possible to obtain electron diffraction patterns from some of the crystals so that minor species could be identified and unit cells determined.

7.3.3. X-ray diffraction.

Copper Kα X-radiation was generated by means of either a Newton Victor Raymax 60 or a Hilger and Watts Microfocus X-ray set, operating at 40 kv with a water or oil cooled copper target. No filter was used since in all the investigation a Guinier camera[141], supplied by Nonius of Delft, was used with a quartz monchromator. Because of the self-focusing action of this camera which causes the $K\alpha_1$ and $K\alpha_2$ copper radiation to be coincident for a wide angle around 15°, no doublets were observed and so the weighted mean value of 1.542Å for the two wavelengths was used. The camera was designed to record the diffraction patterns of four samples simultaneously. The specimens were mounted in a flat plate with four apertures, each containing a thin layer of powder held in place with 'sellotape'. This plate could be given a translatory motion in its own plane, but this was very seldom used as the size of the grains produced in the syntheses was such that smooth diffraction lines were obtained without it.

The dispersion factor of this camera was 4 mm per degree and it was thus equivalent to a Debye-Scherrer camera of 22.9 cm diameter. However, because of the shrinkage of the film on processing and storage it was necessary to calibrate the camera in some way and this was

done by putting a dusting of synthetic quartz in one of the apertures. The spacings thus obtained were compared with those for quartz in the A.S.T.M. file[142] and the apparent dispersion factor calculated. The camera also printed the image of two fixed notches at the bottom of each film, and once these had been calibrated with a quartz pattern it was possible to use this method also to calculate the apparent dispersion factor for any film.

The distance of the diffraction lines from the zero mark was measured to 0.005 cm using a film measuring rule with a Vernier scale, supplied by Hilger and Watts Ltd. These distances were converted into values of θ and looked up in graphical tables of θ vs. d [143]. The intensities of the lines were estimated visually. For preliminary investigation the d spacings could be measured directly with an accuracy of about 1% on a perspex ruler supplied by Solus-Schall. Also it was often found to be very helpful to compare the X-ray photograph visually with those from a library of X-ray photographs of natural and synthetic minerals built up in these laboratories.

7.4. Interpretation of X-ray photographs.

Once a list of observed d spacings had been drawn up attempts were made to index these lines and so deduce the unit cell of the compound. For cubic, tetragonal and

hexagonal crystals this can be done by quite simple graphical and analytical procedures using the equations

$$Q_{hkl} = \frac{1}{a^2}(h^2+k^2+l^2) \qquad \text{Cubic}$$

$$Q_{hkl} = \frac{1}{a^2}(h^2+k^2)+{}^{l^2}/_{c^2} \qquad \text{Tetragonal}$$

$$Q_{hkl} = \frac{4}{3a^2}(h^2+hk+k^2)+{}^{l^2}/_{c^2} \qquad \text{Hexagonal}$$

where $Q_{hkl} = {}^{1}/_{d^2{}_{hkl}}$. If the compound was known to fall into one of these systems, or was suspected to do so on account of its crystal habit then the d spacings were converted to Q values from tables[144] and one of the following procedures was adopted.

7.4.1. Cubic.

It can be seen that all the Q values will be integral multiples of ${}^{1}/_{a^2}$ which can therefore be determined by inspection. Indices can be assigned to all the lines and the most accurate value of the unit cell parameter computed from a series of carefully measured higher lines.

7.4.2. Tetragonal.

In this case all the Q_{hk0} values will be integral multiples of ${}^{1}/_{a^2}$ and it should be possible to find a set of Q values which satisfy this requirement and so deduce a. However it was often more profitable to use a graphical

method to determine the indices first, the chart used for this purpose being that devised by Harrington(145). The principle of this chart can be derived from the tetragonal equation as follows. Two special cases of this equation are

$$Q_{hk0} = \frac{h^2+k^2}{a^2}$$

and $$Q_{001} = {}^{l^2}/_{c^2}$$

by addition $$Q_{hk0}+Q_{001} = \frac{h^2+k^2}{a^2} + {}^{l^2}/_{c^2}$$

$$Q_{hkl} = Q_{hk0} + Q_{001} .$$

From this we see that the interplanar spacing of an hkl plane is asymtotic to the interplanar spacing of the corresponding hk0 or 001 plane as either a^2 or c^2 becomes very large. Therefore if the hk0 and 001 curves are drawn as families of parallel straight lines, the hkl curves, being asymptotic to them, have the same shape and the chart is easy to construct from a single template. This condition was realised by plotting the axial ratio ${}^{c}/_{a}$ on a logarithmic scale, when all hk0 curves have a slope of -2 and all 001 curves a slope of +2. An example of the resultant chart is shown in Figure 11. To use this method the observed d spacings were plotted on a slip of paper using a logarithmic scale, and this strip of paper was

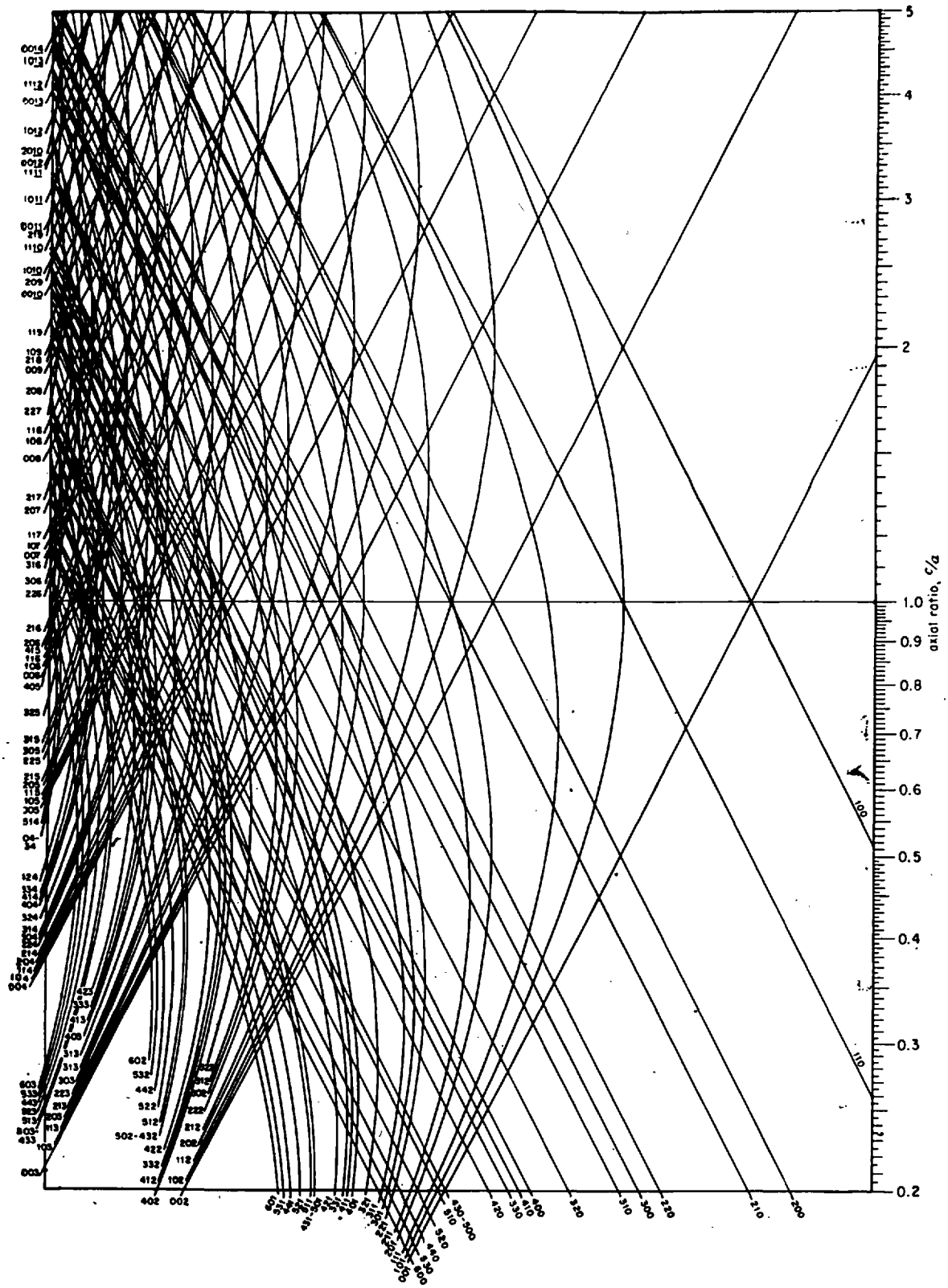


Fig. 11 **Harrington chart for tetragonal crystals.**

moved up and down the chart parallel to the horizontal axis until a satisfactory fit of at least all the lower angle lines was obtained. The axial ratio and the indices of the lines were noted and these values used to compute the unit cell which gave the best fit to the experimental data.

7.4.3. Hexagonal.

It can be seen from the hexagonal equation that there is a very close similarity between this system and the tetragonal one, and hence the same methods are applicable. Thus, although analytical methods are possible in theory, whenever hexagonal symmetry was known or suspected an attempt was made to index the lines using a large scale Harrington chart. If consistent indices were obtained these were used to compute the unit cell which gave the best fit to the observed data.

7.4.4. Orthorhombic.

The corresponding equation for the orthorhombic system is

$$Q = {}^{h^2}/_{a^2} + {}^{k^2}/_{b^2} + {}^{l^2}/_{c^2} ;$$

and graphical methods similar to those above can be used if one of the axial ratios is known. However when it was possible that the species being studied was orthorhombic

analytic methods were attempted, but without success in the present work. The two approaches attempted were the Hesse-Lipson procedure and Ito's method. The Hesse-Lipson procedure[146,147] is based on the assumption that if all possible combinations of the observed values of $\sin^2\theta$ are used to form equations of the type

$$\sin^2\theta_{0k_10} = \sin^2\theta_{h_1k_10} - \sin^2\theta_{h_100}$$

$$\sin^2\theta_{00l_1} = \sin^2\theta_{h_1k_1l_1} - \sin^2\theta_{h_1k_10}$$

$$\sin^2\theta_{00l_1} = \sin^2\theta_{h_2k_2l_1} - \sin^2\theta_{h_2k_20}$$

then the $\sin^2\theta$ values which will be obtained most frequently from such equations will be those of the pinacoid reflections h00, 0k0, and 00l. Thus if the observed $\sin^2\theta$ values are calculated and the difference between each possible pair is tabulated, then the differences which occur most often, within the limits of experimental error, can be tested as possible values for the pinacoid reflections by attempting to index all the observed reflections by means of them.

Ito's method can be applied regardless of the symmetry of the crystal and is based on the fact that each reflection on the powder photograph corresponds to a vector in reciprocal space[148]. If six appropriate lines can be chosen from the powder pattern then a reciprocal unit cell can be obtained and it will be possible to index all the

lines observed. The two chief difficulties with this method are that reciprocal lattice points which correspond to weak or absent reflections will not be available, and hence the reflections selected to represent Q_{100}, Q_{010}, Q_{001} may not account for all the observed reflections. This can be overcome by trial and error but the other requirement of this method is that in order that it may be applied with reasonable success it is necessary to know the value of Q accurately to at least three and preferably four figures. This requires that the d spacings must be known to at least three places to the right of the decimal point, and this was not always possible with the samples studied.

7.4.5. Monoclinic and Triclinic.

Ito's method is also applicable to these crystal systems but is very lengthy, and in this work if previous tests had failed and the species was known or believed to be in either of these systems no attempt was made to index the pattern. A programme to test trial structures on a computer was investigated but was not available in time.

7.5. Differential Thermal Analysis

7.5.1. General principles.

The method of d.t.a. is widely used in the investigation of minerals, particularly of clays, and a good review on this subject has been edited by Mackenzie[149]. The principle of d.t.a. is to heat the sample at a steady heating rate under conditions identical to those of an inert reference material, and to measure the difference in temperature between the two samples. Thus if any reaction involving a heat change takes place in the sample under study, such as chemical reaction, dehydration or phase change, then the temperature of the sample will change with respect to that of the inert reference. Ideally a plot of ΔT vs T will show a horizontal base line with peaks corresponding to those temperature ranges over which some reaction takes place, and the direction, shape and position of these peaks will be characteristic of that particular substance and also provide information on its thermal stability or the occurrence of phase transformations. In practice however a number of factors may operate to cause considerable base line drift. There may be a variation of the specific heat or thermal conductivity with temperature, or a variation in packing density or thermal contact which may result from such reactions as gas evolution, or shrinkage

on dehydration. Such effects are most serious when quantitative data is sought from the d.t.a. record since it makes it very difficult to draw a base line so as to calculate the area under a peak, but in severe cases these effects may sometimes make the qualitative interpretation of the record uncertain. Sewell[150] has developed a method for calculating a more accurate base line when the drift is due to differences in s pecific heats and thermal conductivity. However the method is complicated and requires knowledge of the thermal properties of the materials which was not available in this work. In order to get reproducible and consistent results with different samples the rate of heating must be constant and the thermocouples must be carefully centered in each sample.

7.5.2. Apparatus used.

The apparatus used was based on the design of Mackenzie[151] and was fully described by Langley[160]. Ceramic cell holders and cells were used, of the Roberts and Grimshaw type. The cell was a block about 19x9x8 mm in size with two cylindrical wells 7 mm in diameter, one for the sample and one for the reference material. Chromel/alumel thermocouples were used, and the temperature measuring thermocouple was situated in the inert sample. The furnace consisted of a metal and Sindanyo

case packed with alumina insulating powder and having the heating element wound on a central horizontal porcelain tube into which the cell holder just fitted. This tube was lined with an earthed sheet of nickel foil to screen the thermocouples from the furnace windings. A temperature controlling thermocouple, also chromel/alumel, was brought through the back of the furnace case and rested closely against the wall. The thermocouple wires were connected to the recorder leads through thermostatted mercury connections.

The temperature and differential temperature were recorded on Kent "Multilec Moving Chart Potentiometers". These recorders balance the signal received by means of a mechanically driven sliding contact on a potentiometer wire which is automatically standardised against a standard cell at regular intervals. The sensitivity of the differential temperature recorder could be adjusted by a simple potential divider to give a full scale deflection ranging from $\pm$2mV to $\pm$10μV.

The furnace temperature was recorded on a similar Kent Multilec recorder fitted with a programming cam which had been cut by trial and error to give a rate of heating of 10°C/min. The heating element of the furnace was fed from a pair of concentrically mounted Variacs set about 10 volts apart whose output was slowly raised by a suitably

geared motor. The programming cam operated a relay which switched the output to the furnace from the higher to the lower setting when the temperature rose above the programmed value, and vice versa. The slight change in heating rate which was thus caused could be picked up by the differential temperature recorder on its more sensitive settings, and so gave rise to "hunting" which at higher temperatures could obscure or distort the true curve. This could be minimised by adjusting the starting voltage of the variacs, but only at the expense of loss of linearity in the rate of heating.

All the recorders were situated in an air thermostat maintained at 25°C. The switches for all the parts of the apparatus were mounted on a control panel and subject to a single master switch, so that all the recorders and the furnace could be started simultaneously. From the automatically recorded curves of differential e.m.f. vs. time and temperature vs. time the graphs of differential temperature vs. temperature could be plotted by converting the thermocouple e.m.f. to temperature (40 μV=1°C) and making allowance for the small but definite difference in the speeds of the two charts.

The inert reference material used in all the experiments was ignited kaolin. The cells were filled with equal volumes of reference material and sample, and

tightly packed down by hand using as nearly as possible identical conditions each time. All the samples were pretreated by being allowed to stand for several days over a saturated solution of magnesium nitrate (84% relative humidity).

7.5.3. Thermogravimetry.

In order to provide further information on those samples which showed peaks on the d.t.a. curves, thermogravimetric studies were carried out, which made it possible to distinguish between peaks due to phase changes and those due to dehydration or dehydroxylation by plotting graphs of percentage weight loss vs. temperature. In order that the comparison with the d.t.a. results might be as close as possible an identical furnace was used, mounted vertically, and controlled by the same programming recorder. The bucket used was half a d.t.a. cell, suspended on 55 cm of platinum wire from an air-damped Stanton balance so that it hung freely in the centre of the furnace. A series of baffle plates and screens minimised the effects of draughts and hot air currents on the suspension and the balance.

The temperature was measured with a chromel/alumel thermocouple mounted in the furnace and previously calibrated by comparison with another thermocouple fixed

in a cell containing ignited kaolin and held at the position which would be occupied by the suspended bucket. A dummy run was also carried out with a bucket of ignited kaolin to determine the bouyancy correction. All the samples were pretreated as for the d.t.a. experiments.

7.6. Infra-Red Spectrophotometry.

The infra-red spectra of some samples were obtained on a Perkin-Elmer Infracord 137E, using sodium chloride optics. The samples were ground up with a little Nujol (liquid paraffin) forming a mull which was squeezed between two sodium chloride plates and placed in the beam of the spectrophotometer. The instrument drew a graph directly of transmittance vs. linear wavelength, from 2.5 to 15 microns.

7.7. Sorption Experiments.

The sorption capacities of most of the hydrated samples which were believed to be zeolitic were investigated with oxygen at 90°K in the standard volumetric sorption apparatus shown in Figure 12. In order to calculate the volume of oxygen sorbed by the samples the following volumes were determined.

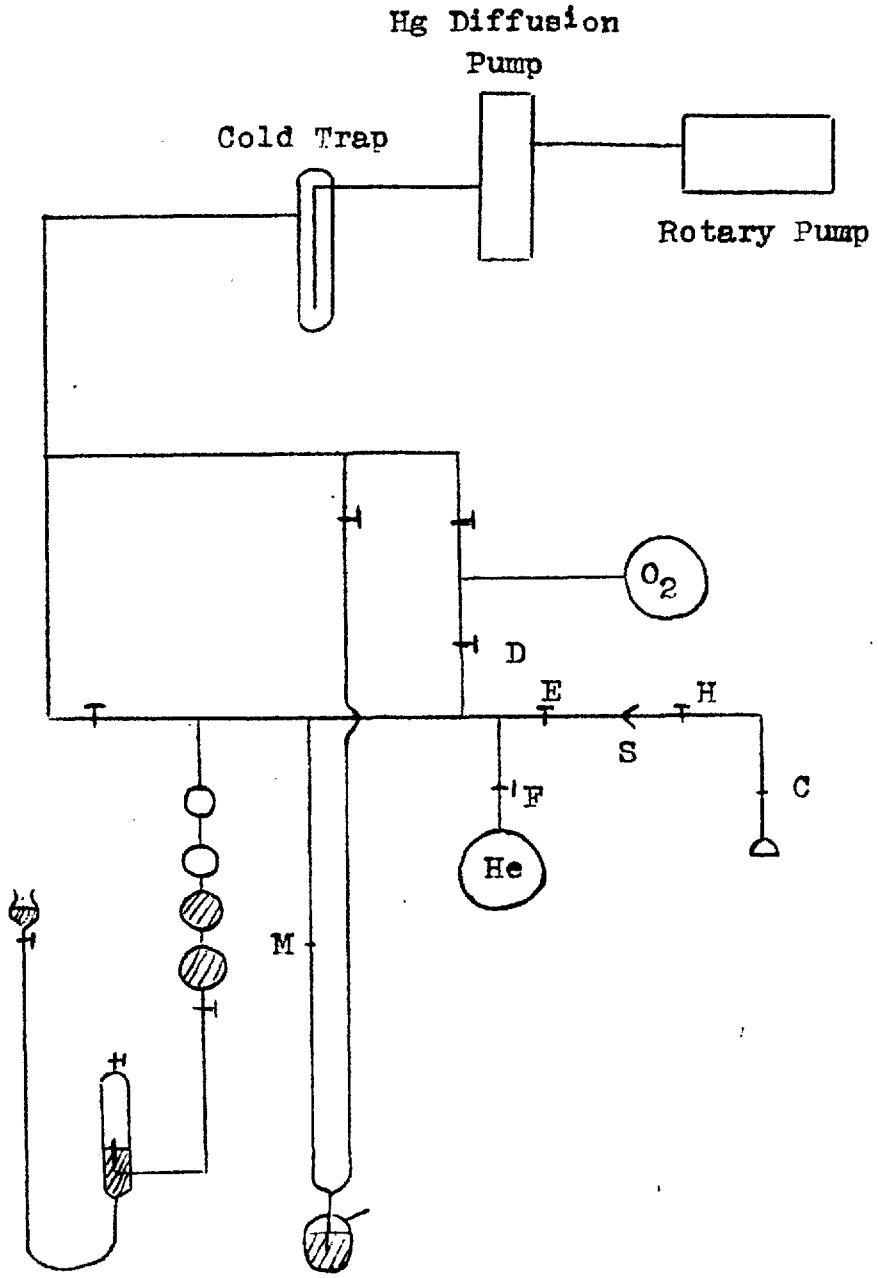


FIG. 12. The Sorption Apparatus.

(a) The gas burette volumes were found by filling the burette to each mark in turn and weighing.

(b) Even bore tubing was used for the manometer and the volume per cm was found by weighing the amount of mercury required to fill a measured length.

(c) The doser volume is the volume between the taps A, D, E, F, and the marks B and M on the gas burette and the manometer respectively. This volume was calculated by admitting a dose of helium into this system and measuring the pressure as it was expanded into each bulb of the gas burette in turn and then applying the ideal gas laws.

(d) The cold volume is the volume of the sorption bulb below the etch mark C and was determined by weighing the bulb, filled to the mark with mercury, before sealing it into the tap and socket assembly S-H. The volume of the sorbent was afterwards deducted.

(e) The volume between the tap E and the mark C is also required and this was obtained by addmitting a dose of helium to the whole system and then calculating the total volume from which the doser volume and the cold volume were subtracted.

The rest of the experimental procedure was as follows. A sample of about 0.5 g of the species to be studied was equilibrated over a saturated magnesium nitrate solution and then weighed into the calibrated sorption bulb

which was sealed on to the tap H and connected to the system by means of the ground glass cone and socket joint S. It was evacuated for several hours, and then surrounded by a suitable furnace and the temperature was raised slowly to 340°C, held there for about twelve hours, and then allowed to cool under high vacuum.

With tap E closed a dose of oxygen was admitted to the system and the volume, pressure and ambient temperature were measured, the height of the manometer being read to $\pm$0.001 cm with a cathetometer. The bulb was surrounded with liquid oxygen to the mark C and tap E opened. After allowing time for the system to come to equilibrium, the pressure was again read, then tap E was closed and the process repeated. The volumes of oxygen present with the tap E shut and open could be calculated and reduced to N.T.P. The difference between them was a measure of the amount of gas sorbed by the sample. An isotherm could be obtained by plotting the amount sorbed against the equilibrium pressure. The saturation capacity was obtained from the slope of the straight line obtained by plotting $P/_X$ vs. P.

8. EXPERIMENTAL RESULTS

8.1. The Strontium Aluminosilicates.

The crystallisation fields of the strontium aluminosilicates were investigated using hydrous gels of the oxide composition $SrO.Al_2O_3.nSiO_2$ where n was varied from 1 to 9 inclusive. A few experiments were also carried out with excess strontium hydroxide added to the gels, and also with a few gels of composition $SrO.2Al_2O_3.2SiO_2$. The conditions used and the products obtained are tabulated in tables 1-16 and the crystallisation fields of the major species are indicated in figure 13. For ease of reference each species has been given a code letter, and a list of these letters showing the species and the yield is given in table 17.

When a species is said to occur in major yield, this indicates that, in the best specimen obtained, it was well crystallised and formed more than 60% of the total product, as estimated from optical examination and the intensities of the X-ray powder pattern. A minor species is one which occurred only in small quantities even in the best synthesis and often was only deduced to be present from the occurrence of weak lines on the X-ray powder photograph, additional to those of the major product. When a species is said to occur in 100% yield this indicates

that under the optimum conditions of formation, the species could be formed reproducibly and with no significant impurity revealed by X-ray or microscopic examination.

TABLE 1 Products from gels of composition $SrO.Al_2O_3.0.87SiO_2$

435°C	20 hours	3 days	7 days
	mod C	mod C	some C
	good N	good N	fair N
	$SrCO_3$	$SrCO_3$	(10.0)
	(>10,5)	(10.0)	

TABLE 2 Products from gels of composition $0.77SrO.Al_2O_3.SiO_2$

410°C	25 hours	5 days
	mod C	mod C
	fair N	good N
	(>10.5)	$SrCO_3$
		(>10.5)

TABLE 3 Products from gels of composition $SrO.2Al_2O_3.2SiO_2$

455°C	17 hours	20 hours	63 hours	4 days	4 days
	good C	good C	good P	good P	good C
	good L	good L	good L	trace L	good L
	(5.0)	(6.0)	(5.5)	(7.0)	(7.0)

250°C	6 days
	good P
	(7,0)

TABLE 4. Products from gels of composition $SrO.Al_2O_3.SiO_2$

435°C	24 hours	3 days	7 days		
	good C	mod C	good C		
	mod N	mod N	$SrCO_3$		
	$SrCO_3$	(10.0)	(7.0)		
	(>10.5)				
380°C	17 hours	24 hours	36 hours	41 hours	3 days
	good C	mod L	good C	good C	mod C
	good P	(7.0)	$SrCO_3$	good P	good L
	mod S		(10.0)	mod S	$SrCO_3$
	$SrCO_3$			(7.5)	(7.0)
	(7.5)				
	3 days	7 days	7 days	8 days	13 days(2)
	mod C	good C	good C	mod C	mod C
	good L	fair L	mod S	good N	mod N
	(7.0)	(7.0)	trace P	$SrCO_3$	$SrCO_3$
			(7.5)	(10.5)	(10.5)
340°C	21 hours	3 days	7 days		
	fair C	fair C	fair C		
	(10.5)	(10.5)	$SrCO_3$		
			(10.5)		
295°C	44 hours	6 days	20 days		
	good C	good C	good C		
	trace T	some N	trace N		
	$SrCO_3$	$SrCO_3$	$SrCO_3$		
	(10.0)	(10.0)	(10.5)		

continued

TABLE 4 (continued)

250°C	3 days	8 days	22 days
	good P	good P	v. good C
	mod C	mod C	trace P
	trace T	$SrCO_3$	$SrCO_3$
	(7.5)	(8.0)	(9.0)
205°C	44 hours	6 days	20 days
	mod C	good C	good C
	trace P	trace P	mod T
	(>10.5)	(10.5)	(10.5)
150°C	3 days	8 days	22 days
	good P	good P	good P
	mod E	good C	good C
	(>10.5)	$SrCO_3$	$SrCO_3$
		(>10.5)	(>10.5)

TABLE 5 Products from gels of composition $SrO.Al_2O_3.2SiO_2$

435°C	24 hours	3 days	7 days	
	v.good C	good C	good C	
	(7.0)	$SrCO_3$	(7.0)	
		(7.0)		
430°C	6 hours	7 hours(2)	18 hours(4)	
	good C	good C	good C	
	$SrCO_3$	$SrCO_3$	$SrCO_3$	
	(8.0)	(10.0)	(8.0)	
	19 hours	4 days	7 days	
	good P	good C	good C	
	(7.0)	(7.0)	(7.0)	
380°C	24 hours	3 days	5 days	5 days(9)
	good C	good C	good C	good C
	(8.0)	$SrCO_3$	(7.0)	$SrCO_3$
		(7.0)		(8.0)
	5 days	5 days	7 days	8 days
	good C	good P	v.good C	good C
	good L	trace C	(7.0)	$SrCO_3$
	(7.0)	$SrCO_3$		(8.0)
		(8.0)		
340°C	20 hours	3 days	6 days	
	good P	good C	good P	
	(7.5)	$SrCO_3$	$SrCO_3$	
		(9.0)	(8.0)	

continued

TABLE 5 (continued)

300°C	3 days mod P some C $SrCO_3$ (7.0)	7 days fair P fair C (7.0)	15 days v.good C (7.0)
250°C	3 days v.good P (7.0)	7 days good P good C (7.0)	
200°C	7 days good P $SrCO_3$ (7.0)	15 days good P $SrCO_3$ (7.0)	25 days good P $SrCO_3$ (7.5)
150°C	7 days mod G poor P $SrCO_3$ (8.0)	15 days good G mod P $SrCO_3$ (8.0)	
110°C	39 days good G $SrCO_3$ (8.0)		

TABLE 6 Products from gels of composition $SrO.Al_2O_3.3SiO_2$

435°C	24 hours	3 days	7 days		
	good P	good P	good C		
	trace C	some C	trace H		
	(7.0)	(7.0)	(7.0)		
405°C	26 hours	65 hours	6 days	9 days	
	good P	good C	good C	good C	
	some B	$SrCO_3$	$SrCO_3$	$SrCO_3$	
	(7.5)	(9.0)	(10.0)	(7.5)	
380°C	23 hours	2 days	3 days	3 days	
	fair P	good P	good C	good P	
	trace C	some C	good I	some C	
	(7.0)	(7.5)	(8.0)	(7.0)	
	4 days	7 days	8 days	15 days	
	good P	fair P	good C	v.good C	
	some C	some C	trace H	trace H	
	(6.5)	(7.0)	(7.5)	(7.0)	
340°C	16hrs(2)	18hrs(2)	3 days	7 days	8 days
	good P	good P	good P	fair C	mod P
	trace C	$SrCO_3$	(6.0)	(8.0)	poor C
	(6.0)	(5.0)			(5.0)
300°C	7 days	16 days	26days		
	mod C	fair C	good C		
	fair P	some P	(7.0)		
	(7.5)	(7.0)			

continued

TABLE 6 (continued)

265°C	24 hours X (7.5)	3 days mod C some P (8.5)	11 days mod C (8.5)	13 days poor C (7.5)	20 days poor C (7.0)
250°C	5 days fair P trace C (7.0)	12 days mod P some C (7.0)	26 days mod P mod C (7.0)		
200°C	5 days mod P (7.0)	12 days poor P (7.5)	17 days mod P $SrCO_3$ (7.0)	26 days mod P trace G $SrCO_3$ (7.0)	
150°C	5 days some P mod G (9.5)	12 days fair G $SrCO_3$ (8.0)	17 days good G $SrCO_3$ (7.0)	21 days good G $SrCO_3$ (7.0)	
	26 days(2) good G $SrCO_3$ (7.5)	33 days good G $SrCO_3$ (7.0)	35 days good G $SrCO_3$ (7.0)	35 days good G (7.0)	
115°C	12 days X (7.5)				

TABLE 7 Products from gels of composition $SrO.Al_2O_3.4SiO_2$

435°C	22 hours poor C some P trace H (7.0)	3 days good C some H (7.0)	7 days good C good H (7.0)		
410°C	24 hours some P some C some H (7.0)	3 days good C good H (7.0)	5 days good C good H (7.0)		
380°C	23 hours fair P trace C (7.0)	3 days good P good H (7.0)	5 days good C trace H (7.5)	7 days good P trace C some H (7.0)	12 days good C trace H (7.0)
340°C	16 hours mod P (4.0)	3 days poor P (7.0)	7 days mod P trace Q (6.0)		
300°C	3 days mod P (7.0)	8 days mod P (7.0)	13 days mod C (7.5)		
250°C	3 days mod P (7.5)	8 days mod P (7.0)	13 days poor P (8.5)		
200°C	3 days poor P (8.0)	8 days poor P (7.0)	13 days trace P (8;5)		
150°C	3 days poor P trace G (9.5)	8 days poor P some G (7.0)	13 days trace P (7.0)	15 days X (10.0)	32 days X (9.0)
110°C	61 days trace G (>10.-)				

TABLE 8 Products from gels of composition $SrO.Al_2O_3.4.5SiO_2$

300°C	4½ days	8 days		
	poor C	fair C		
	poor P	(7.0)		
	(7.0)			
295°C	2 days	6 days	12 days	
	mod P	mod P	good C	
	(8.5)	mod C	(6.5)	
		(8.0)		
250°C	4½ days	8 days		
	poor C	poor C		
	(7.0)	some P		
		(7.0)		
205°C	2 days	6 days	12 days	15 days
	X	good F	X	X
	(5.5)	(10.0)	(6.5)	(7.0)
200°C	4½ days	6½ days	8 days	
	X	X	X	
	(7.0)	(6.5)	(7.0)	
	8½ days	9 days	22 days	
	X	X	X	
	(7.0)	(7.0)	(7.0)	
110°C	40 days			
	X			
	(7.0)			

TABLE 9 Products from gels of composition $SrO.Al_2O_3.5SiO_2$

435°C	22 hours	3 days	7 days		
	mod C	good C	fair C		
	some P	good H	good H		
	some H	(7.0)	(7.5)		
	(2.0)				
380°C	24 hours	2½ days	5 days	7 days	12 days
	poor P	good P	good C	good P	good C
	(7.0)	good K	good H	good K	good H
		(7.0)	(7.5)	(7.0)	(7.0)
340°C	20 hours	3 days	7 days		
	trace P	poor P	mod Q		
	(6.0)	(7.0)	(7.0)		
295°C	2 days	5 days	21 days		
	poor C	good C	good C		
	(7.0)	(5.5)	(7.0)		
250°C	3 days	8 days	15 days		
	X	mod P	mod P		
	(-)	(-)	(7.0)		
205°C	2 days	5 days	21 days		
	X	X	X		
	(8.5)	(7.0)	(7.0)		
200°C	3 days	8 days	22 days		
	X	X	X		
	(-)	(-)	(10.5)		
110°C	48 days				
	some G				
	(10.0)				

TABLE 10 Products from gels of composition $SrO.Al_2O_3.6SiO_2$

435°C	22 hours	3 days	7 days		
	mod P	good C	fair C		
	good H	good H	good H		
	(7.0)	(7.0)	(7.5)		
410°C	24 hours	3 days	6 days		
	mod P	good C	good C		
	mod C	fair H	good H		
	some H	(7.0)	(7.0)		
	(7.0)				
380°C	25 hours	3 days	7 days		
	X	poor P	mod C		
	(7.0)	poor C	fair H		
		poor H	(7.0)		
		(7.0)			
340°C	20 hours	3 days	7 days		
	X	trace P	good Q		
	(7.0)	(7.0)	(7.0)		
300°C	3 days	8 days	16 days		
	X	mod C	good K		
	(7.0)	(7.0)	(7.0)		
250°C	3 days	8 days	15 days	20 days	27 days
	X	X	X	good Q	X
	(7.0)	(7.5)	(8.0)	(7.0)	(7.5)
200°C	6 days	16 days	20 days		
	X	X	X		
	(7.0)	(6.5)	(7.0)		
150°C	6 days	16 days			
	X	X			
	(7.0)	(6.5)			
110°C	62 days	105 days			
	trace G	X			
	(>10.5)	(>10.5)			

TABLE 11 Products from gels of composition $SrO.Al_2O_3.7SiO_2$

435°C	21 hours	3 days	7 days	
	mod P	good C	good C	
	trace H	fair P	v.good H	
	(7.0)	fair H	(7.0)	
		(7.0)		
380°C	24 hours	2 days	3 days	3 days
	X	good D	good D	mod P
	(7.0)	some P	mod P	some D
		(7.0)	(7.0)	(7.0)
	4 days	7 days	10 days	
	mod P	poor P	fair C	
	trace C	(7.0)	v.good H	
	some H		(8.0)	
	some D			
	(7.5)			
340°C	16 hours	2 days	4 days	
	X	X	good D	
	(6.0)	(7.0)	some Q	
			(7.0)	
	7 days	8 days	11 days	
	X	good D	good D	
	(6.0)	good Q	good Q	
		(7.0)	(7.0)	

continued.

TABLE 11 (continued)

300°C	36 hours	3 days	5 days	6 days	9 days
	X	X	mod C	poor C	poor C
	(6.5)	(7.0)	good M	(7.5)	(7.0)
			(8.0)		
	12 days	13 days	15 days	23 days	
	mod C	poor C	mod C	fair C	
	mod Q	(7.0)	(7.0)	(8.0)	
	(7.0)				
250°C	36 hours	6 days	19 days		
	X	X	mod C		
	(7.0)	(6.5)	(7.0)		
200°C	36 hours	6 days	20 days		
	X	X	X		
	(7.0)	(7.5)	(7.0)		
150°C	6 days	20 days			
	X	X			
	(8.5)	(8.0)			

TABLE 12 Products from gels of composition $SrO.Al_2O_3.8SiO_2$

435°C	3 days good P v.good H (7.0)	5 days good P poor C good H (7.0)	6 days good P poor C good H (7.0)	8 days good P poor C good H (7.0)
410°C	24 hours poor P some H (7.0)	3 days mod P good H (7.0)	6 days mod P mod C good H (6.5)	
400°C	27 hours mod P good H (7.0)	4 days good K (7.0)	8 days mod P mod C good H (7.0)	
380°C	22 hours X (7.0)	2 days good D (7.5)	3 days poor P (7.0)	4 days mod D mod P some H (7.0)
	7 days good D good H trace P (7.0)	8 days good P strong H (7.5)	15 days v.good H good C (7.0)	
340°C	2 days X (7.0)	4 days good Q (7.0)	7 days good Q (7.0)	

continued.

TABLE 12 (continued)

300°C	5 days X (8.0)	9 days X (7.5)	12 days mod C (7.0)	15 days mod C some Q (7.0)	
280°C	4 days poor C (7.0)	8 days mod Q (7.0)	14 days poor C good H (7.0)		
250°C	4 days v.good I (brown) (10.5)	4 days X (7.0)	12 days X (7.0)	19 days X (7.0)	21 days mod Q (7.0)
200°C	8 days X (7.0)	14 days X (8.5)	19 days X some J (black) (8.5)	22 days X (8.5)	
150°C	8 days X (8.5)	19 days X some J (black) (>10.5)			
110°C	62 days X (>10.5)				

TABLE 13 Products from gels of composition $SrO.0.9Al_2O_3.8SiO_2$

340°C	2 days	4 days	6 days	12 days
	X	X	poor D	good D
	(8.0)	(8.0)	(8.0)	(9.0)

TABLE 14 Products from gels of composition $3SrO.Al_2O_3.9SiO_2$

300°C	4 days	8 days	21 days
	X	X	good Q
	(7.0)	(7.0)	(7.0)
250°C	4 days	12 days	21 days
	X	X	X
	(7.0)	(7.0)	(7.0)
200°C	7 days	29 days	
	X	X	
	(7.0)	(7.0)	
150°C	8 days		
	X		
	(10.0)		

TABLE 15 Products from gels of composition $1.5SrO.Al_2O_3.9SiO_2$

250°C	20 days	23 days	27 days
	good D	good D	good Q
	(8.5)	good M	(10.0)
		(9.0)	

TABLE 16 Products from gels of composition $SrO.Al_2O_3.9SiO_2$

435°C	25 hours mod P trace H (7.0)	4 days mod P mod H (7.0)	8 days v.good H (7.0)		
380°C	24 hours X (7.0)	3 days X (7.0)	3 days good D (4.0)	5 days good D mod H (7.0)	6 days trace D (7.0)
	10 days good H poor C (7.0)	10 days good D (7.0)	10 days mod D mod H (5.0)	10 days mod D good H (6.0)	12 days(2) good H mod P some D (6.5)
340°C	17 hours X (7.0)	2 days X (8.0)	3 days(2) X (7.0)	4 days trace Q (8.0)	
	6 days poor D (7.0)	7 days X (7.0)	10 days good D (8.5)	12 days poor D (8.0)	
300°C	11 days mod C good Q (7.0)	21 days(2) mod Q (8.0)	23 days good Q (8.0)		

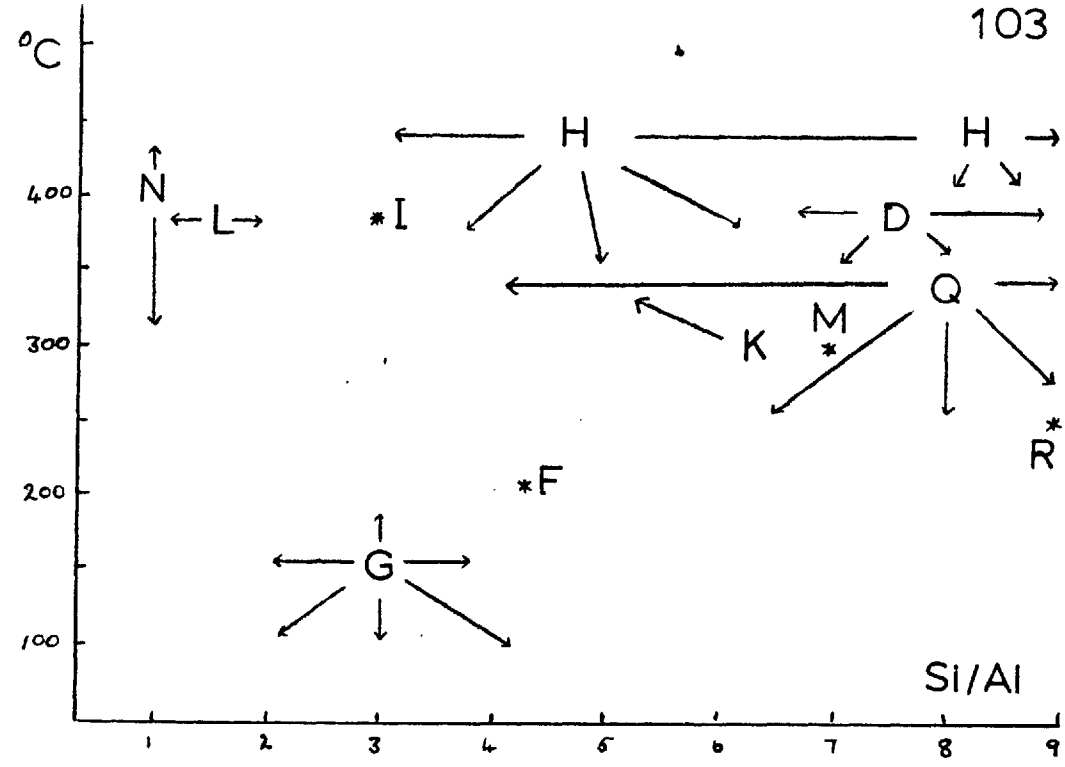
continued.

TABLE 16 (continued)

250°C	20 days	21 days	23 days	23 days(2)	27 days
	X	X	mod R	X	X
	(8.5)	(7.0)	(8.5)	(8.0)	(9.0)
200°C	11 days	21 days			
	X	X			
	(8.0)	(7.5)			
150°C	21 days				
	X				
	(8.0)				
110°C	62 days				
	X				
	(> 10.5)				

TABLE 17

Reference letter	Species	Yield
B	Montmorillonite	minor
C	Polymorph of strontium-felspar	100%
D	A Sr-zeolite	100%
E	Boehmite	minor
F	Gmelinite	major
G	near-Chabazite	100%
H	α-Cristobalite	major
I	Analcite	major
J	Cancrinite	minor
K	Unidentified	major
L	Strontium mica	major
M	Mordenite	minor
N	Unidentified	major
P	Hexagonal polymorph of Sr-felspar	100%
Q	Possibly a Sr-zeolite	100%
R	Heulandite	major
S	Unidentified	minor
T	Unidentified	minor
W	Strontium felspar	100%
X	Uncrystallised gel	



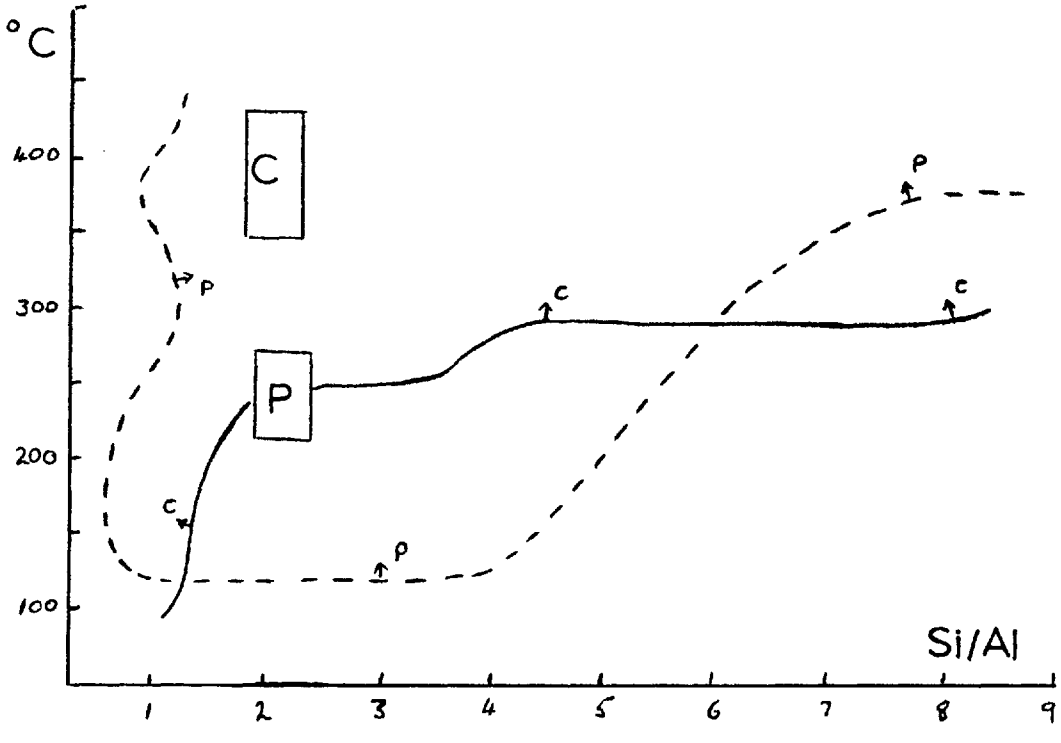


Fig.13. Sr Crystallisation Field.

8.1.1. General.

A few general remarks may be made before proceeding to consideration of the individual species. The parameters which were varied in this work were the alumina:silica ratio of the parent gel, the temperature of crystallisation, and the duration of the treatment at that temperature. It was found that crystallisation became increasingly difficult as the silica:alumina ratio increased and as the temperature was lowered. For example, even after three weeks the gels remained amorphous at temperatures below 200°C when n was greater than 5, and at 250°C a gel of $SrO.Al_2O_3.8SiO_2$ only crystallised after three weeks. However, the region in which gels failed to crystallise was noticeably smaller than that found in the analagous calcium system. When the silica:alumina ratio was low good crystallisation was obtained after periods of less than twenty-four hours but as the amount of silica increased three or four days were required to obtain well crystallised products even at high temperatures.

Some of the species, notably Sr-C and Sr-P and to a lesser extent Sr-Q, occurred over a very wide range of conditions whereas other species such as Sr-N, Sr-G and Sr-D occurred in very much more limited and relatively sharply defined regions of the field. It is difficult to trace any systematic effects resulting from increasing the

duration of the heat treatment, although there is some evidence that gels which produce mainly Sr-P after short heat treatments will tend to produce Sr-C after longer times at the same temperature. However a feature of the crystallisation of the strontium aluminosilicates has been the unpredictable and irreproducible appearance of many of the zeolite species. Thus gmelinite, analcite, mordenite and heulandite have been synthesised in one, or at most two runs, from gels of approximately the expected stoichiometric composition, but numerous attempts to repeat these syntheses, using identical or similar gels under the same conditions for both longer and shorter times resulted either in other products or in uncrystallised gel. Attempts to seed these gels with the desired product were also unsuccessful.

When the silica:alumina ratio of the parent gel was 3 or less it was not uncommon to find evidence of strontium carbonate among the products. This was formed by the reaction of the strontium hydroxide with carbon dioxide from the air, and although efforts were made to minimise this whilst mixing the parent gel, the formation of strontium carbonate could have occurred either at this stage, or during the processes of washing and drying the products after reaction. It was readily removed by washing with approximately 0.5N hydrochloric acid, which

had no harmful effects on the other products.

In addition to the minor species listed in table 17, on a number of occasions the X-ray powder pattern of the product revealed a few weak lines which could not be attributed to the major species present. Where these very minor species could not be identified and did not occur more than once, they have not been recorded.

8.1.2. Particular species.

The individual species listed in table 17 will now be considered in detail.

Sr-E Boehmite. This species was only observed once in the work with strontium gels and was formed in small yield at 150°C from a gel with a low silica:alumina ratio (table 4). Consideration of the other products formed at the same time makes the presence of free alumina expected and the conditions used fall in the stability field of boehmite[161]. The X-ray powder pattern of this species was faint with very diffuse lines, indicating poor crystallinity. This may be the reason why boehmite was not observed more often in other runs with gels whose composition would seem to make its formation likely. Boehmite was observed to form from similar gels in the calcium and barium fields, but over a rather wider range

of temperatures in the case of barium, and a much wider range of temperatures in the case of calcium.

Sr-H α-Cristobalite. When the parent gel contained a higher ratio of silica than the crystalline products which were formed then the excess silica crystallised out as α-cristobalite, often in the form of small spherules (Plate 1).



PLATE 1. Sr-H. α-cristobalite.
560 x

At these temperatures of formation α-cristobalite is metastable with respect to α-quartz, but in this work the excess silica either remained amorphous or crystallised as α-cristobalite. However when a pure aqueous solution of the silica sol used in these experiments was treated hydrothermally at 380°C and the product examined under the microscope it was seen to consist of well grown crystals showing the common habit of quartz, although X-ray examination did reveal traces of α-cristobalite in the product

of the shortest run. These results indicate that the pH of the liquor with strontium and alumina present is relatively low[162] and this is supported by the observation that the pH of the cold mother-liquor when the autoclave is opened is normally between 7 and 8. In addition to the pH effect, the alkaline earth cations appear to catalyse the formation of α-cristobalite[132,133]. The X-ray powder pattern for one of the best specimens is compared with that given by the A.S.T.M. Index for α-cristobalite in Table A.1.

Sr-B. Montmorillonite. This species was only observed once, from a gel of composition $SrO.Al_2O_3.3SiO_2$ after a day at 405°C (Table 6). The X-ray powder pattern showed only the lines due to Sr-P, but examination with the electron microscope showed the appearance characteristic of montmorillonite and an electron diffraction ring pattern was obtained (Plates 2 and 3) which confirmed the presence of this mineral. It is very difficult to detect in minor yield by X-ray methods, and so may have been an initial product in other runs of short duration in this region.

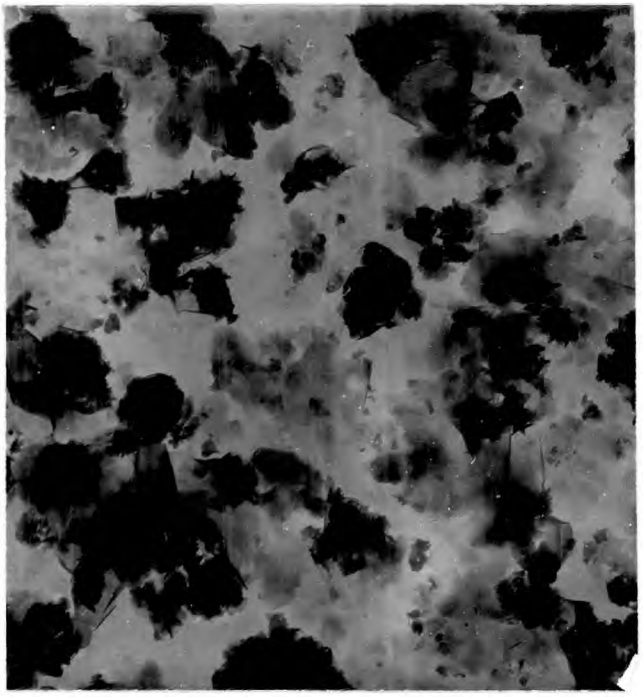


PLATE 2. Sr-B. Montmorillonite 11,000 x

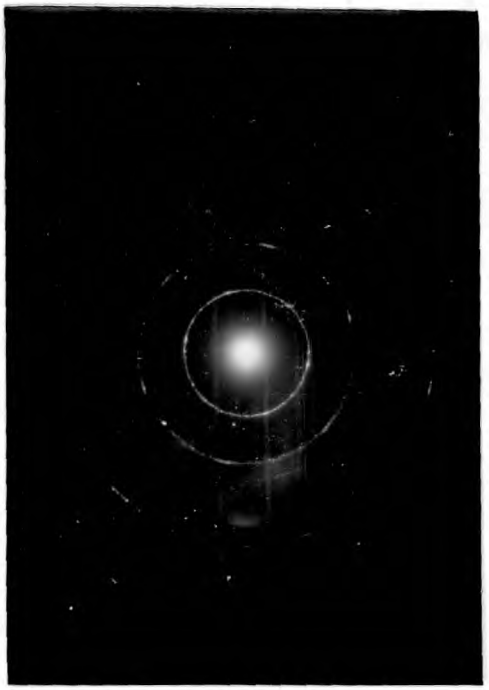


PLATE 3. Electron diffraction pattern from Sr-B. ~~10,200~~ x.

Sr-J. Cancrinite. This product appeared only on two isolated occasions in very minor yield, in each case from a gel of composition $SrO.Al_2O_3.8SiO_2$ at 200°C and 150°C respectively. In one instance the whole product was grey and faintly magnetic and the X-ray powder pattern showed the strongest lines of cancrinite. In the second specimen the product was white and amorphous but contained a number of black flakes and particles which could be readily separated out with a magnet and when X-rayed gave a strong clear pattern identical to that of cancrinite but with a heavy background as would be expected from a

sample containing iron. These samples were presumably formed as a result of attack on the walls of the autoclave but their formation was not reproducible. Attempts were made to promote the growth of this product by adding small amounts of ferrous chloride, ferric chloride or pure iron filings to identical gels, but without success. The X-ray powder pattern of the better sample of cancrinite is given in Table A3.

Sr-I. Analcite. This product has only been observed twice in this survey of the crystallisation field of the strontium aluminosilicates in contrast to its ready occurrence in the other systems investigated in these laboratories, for instance in the cases of sodium[127], potassium[128], and calcium[42]. In one case it was formed in about 50% yield, mixed with Sr-C, from a gel of composition $SrO.Al_2O_3.3SiO_2$ at 380°C (Table 6). The crystal habit was spherulitic (Plate 4) with a few spherules showing faint indications of faces, and the X-ray powder pattern ~~compared~~ agreed well with that of the natural mineral (Table A4). The unit cell was found to be cubic within experimental error, with a=13.74Å, and since the cationic radius of Sr is 1.175Å, this fits in well with the sequence drawn up by Barrer et al[163] for the variation of the unit cell parameter of cubic analcites

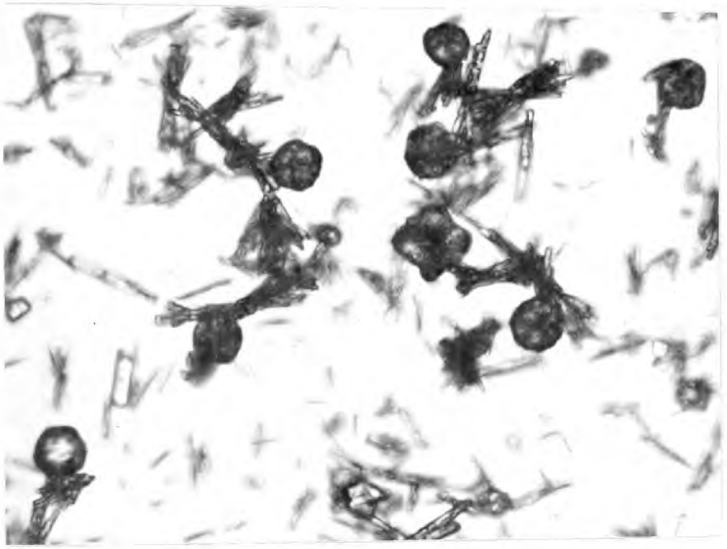


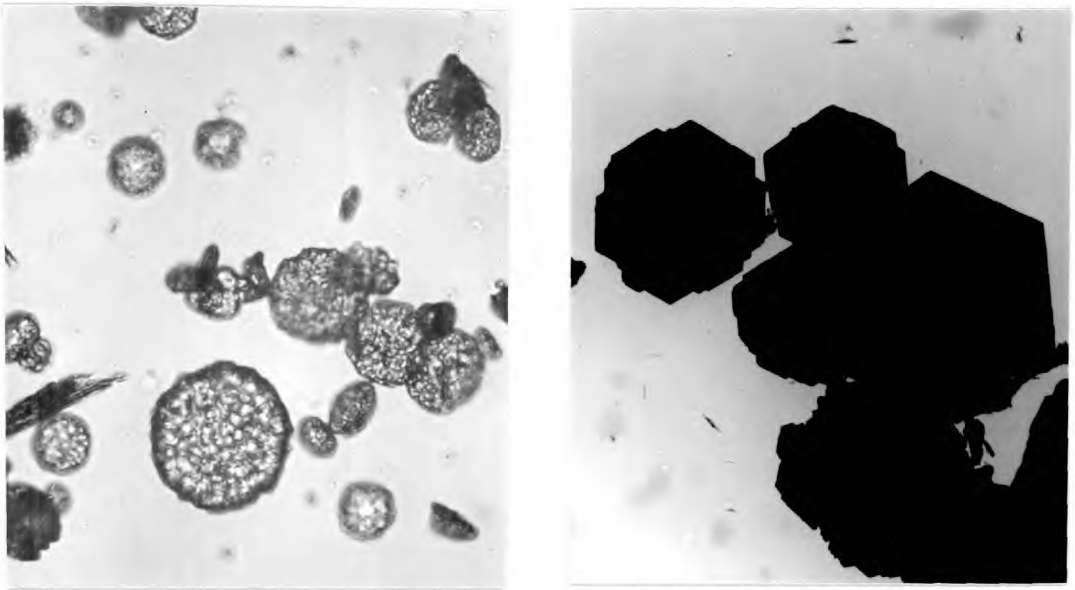
PLATE 4. Sr-I. Spherulites of analcite (together with laths of Sr-C). 630 x

with cationic radius.

The only other occurrence of this species was from a gel of composition $SrO.Al_2O_3.8SiO_2$ at 250°C, but the product was deep brown in colour and quite strongly magnetic, suggesting that considerable attack on the walls of the autoclave had occurred. The X-ray powder pattern is given in Table A3, and the unit cell was found to be cubic, with a=13.69Å. It was not found possible to repeat this result.

Sr-F. Gmelinite. Only one occurrence of this species was observed, from a gel of composition $SrO.Al_2O_3.4.4SiO_2$ at 205°C, and attempts to reproduce

this result, using gels of identical and slightly varied compositions were unsuccessful. The gmelinite produced was well crystallised in the form of spherulitic aggregates of small hexagonal crystals (Plate 5). The X-ray powder pattern shows good agreement with that of natural



(a) 510 x (b) 2,800 x

PLATE 5. Sr-F. Gmelinite.

gmelinite (Table A5) and the unit cell has been calculated, using hexagonal indices, to be a=13.80Å, c=10.01Å. The values quoted for the natural mineral are a=13.72 to 13.76Å, c=10.02 to 10.06Å (164). A few weak lines could not be accounted for on the basis of this unit cell, and they were ascribed to the presence of a small amount of a fibrous impurity, visible under the microscope.

The sorptive capacity of the sample was investigated, using oxygen at 90°K, and the gmelinite was found at saturation to sorb 55 N.T.P. cc/gram of equilibrated hydrated material (Fig. 14). There was an insufficient amount of the sample to carry out complete dehydration studies and differential thermal analysis, but ignition to red heat produced a loss in weight of 18.4%. This should be compared with a loss of 21.2% for the natural mineral with the formula $(Na_2,Ca)Al_2Si_4O_{12}.6H_2O$, and 19.5% for the ideal formula of strontium gmelinite.

Sr-M. Mordenite. This species was observed on two occasions and in both cases was mixed with another product. Once it formed in good yield, mixed with Sr-C, from a gel of composition $SrO.Al_2O_3.7SiO_2$ at 300°C. The other specimen was mixed with Sr-D and crystallised from a gel of composition $SrO.Al_2O_3.9SiO_2$ to which a little extra strontium hydroxide had been added (Table 15). In both cases the typical 'wheatsheaf' habit of mordenite was observed and the X-ray powder pattern showed good agreement with that of the natural mineral (Table A2). Also individual crystals were identified by electron diffraction and shown to have the unit cell dimensions a=18.13Å, b=20.5Å, c=7.52Å for a c-centred orthorhombic cell. The unit cell reported for the natural sodium mineral is a=18.13, b=20.49, c=7.52Å(166).

Sorption of O_2 at 90°K.

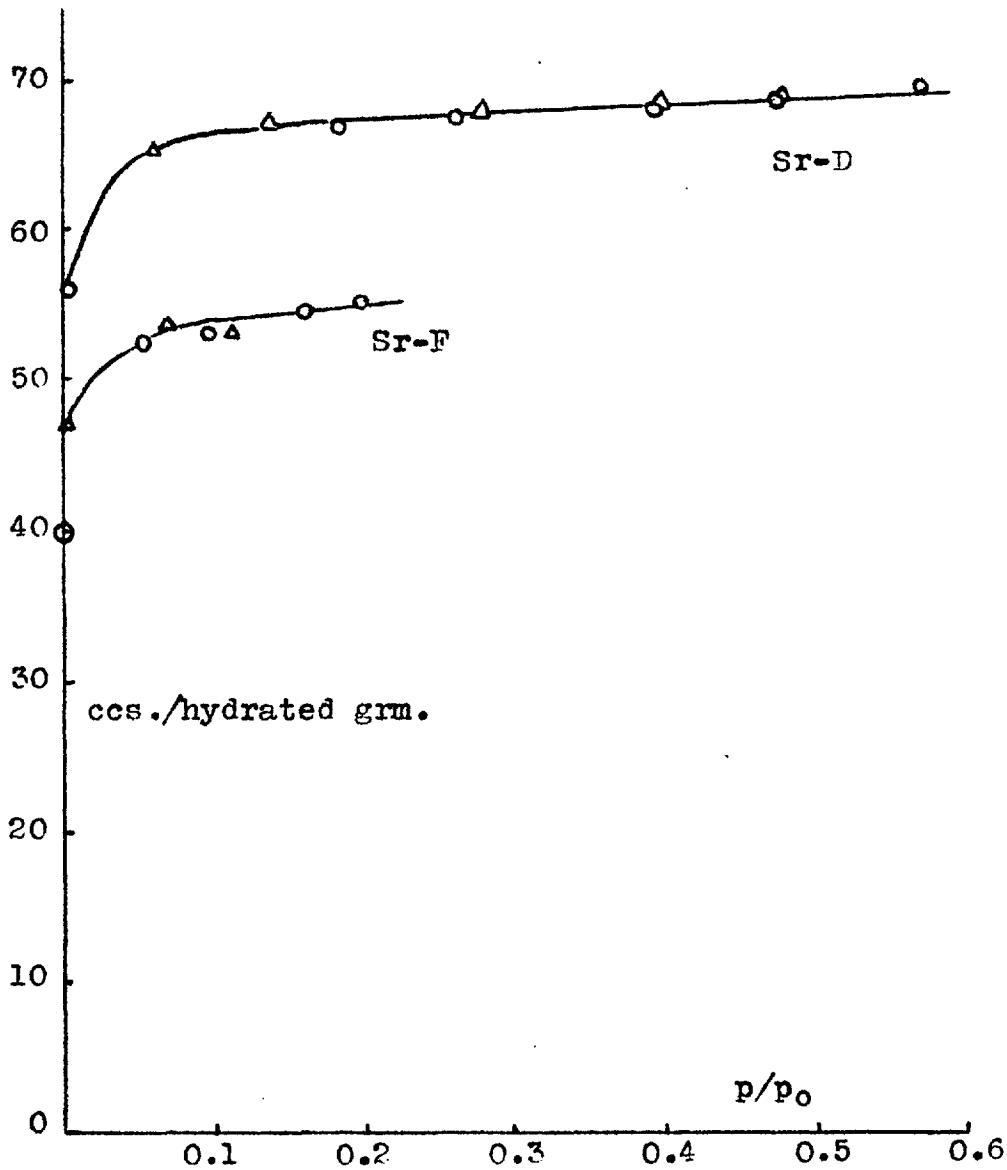


FIG. 14.



PLATE 6. Sr-M. Mordenite (plus some laths of Sr-C). 3,800 x

Sr-R. Heulandite. Only one specimen of this zeolite was obtained; it crystallised moderately well, but without any clearly defined crystal habit, from a gel of composition $SrO.Al_2O_3.9SiO_2$. Attempts to repeat this synthesis using gels of the same composition, and with added strontium hydroxide, were unsuccessful. The loss on ignition was 8.81%, but there was insufficient material to carry out any other tests. The natural mineral, if in the pure strontium form, would have a water content of about 14.6%. There is some uncertainty in the literature about the distinction between heulandite and clinoptilolite since their properties and X-ray patterns are very similar. Mason and Sand[157] suggest that heulandite

is the calcium-rich form and that clinoptilolite contains potassium and sodium as the cations. Mumpton[158] prefers to say that heulandite has a silica:alumina ratio around 6:1 whereas this ratio in clinoptilolite is between 8:1 and 10:1, and that there is a miscibility gap between the two forms. Sr-R clearly has the heulandite-clinoptilolite type of structure and as the silica:alumina ratio is undetermined it will be called a Strontium heulandite. The X-ray powder patterns of Sr-R and natural samples of heulandite and clinoptilolite are compared in Table A6. The differences are slight, but a visual comparison suggests that the pattern of Sr-R is nearest to that of the heulanidte.

Sr-G. Near-chabazite. This zeolitic species formed reproducibly in high yield below 200°C from gels of composition $SrO.Al_2O_3.nSiO_2$, where n is between 2 and 4. It was often obtained either alone, or mixed with a little strontium carbonate which could readily be removed by washing with very dilute hydrochloric acid. The characteristic crystal habit was spherulitic (Plate 7) and the X-ray powder pattern shows close, though not perfect, agreement with that of a natural chabazite (Table A7). The unit cell has been calculated, using hexagonal indices, to be a=13.67Å, c=15.49Å. The values obtained

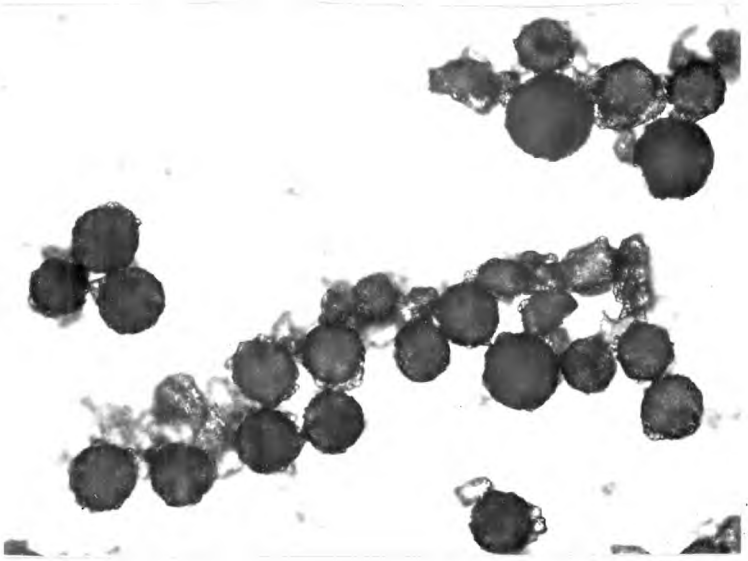


PLATE 7. Sr-G. Near-chabazite.
330 x

for natural chabazite[164] range from a=13.74Å, c=14.83Å to a=13.78Å, c=15.06Å. A good sample of this product shows a weight loss of 21.8% on thermogravimetric analysis and gave a d.t.a. curve typical of a zeolite (Fig. 15), similar to those obtained for natural and synthetic chabazite by Langley[167], except that for Sr-G there was no recrystallisation exotherm at high temperatures and the product on ignition was amorphous. However the sample used in the thermo-gravimetric analysis showed good recrystallisation to Sr-P. On the basis of these results this species is identified as belonging to the chabazite family and will be called strontium near-chabazite. A

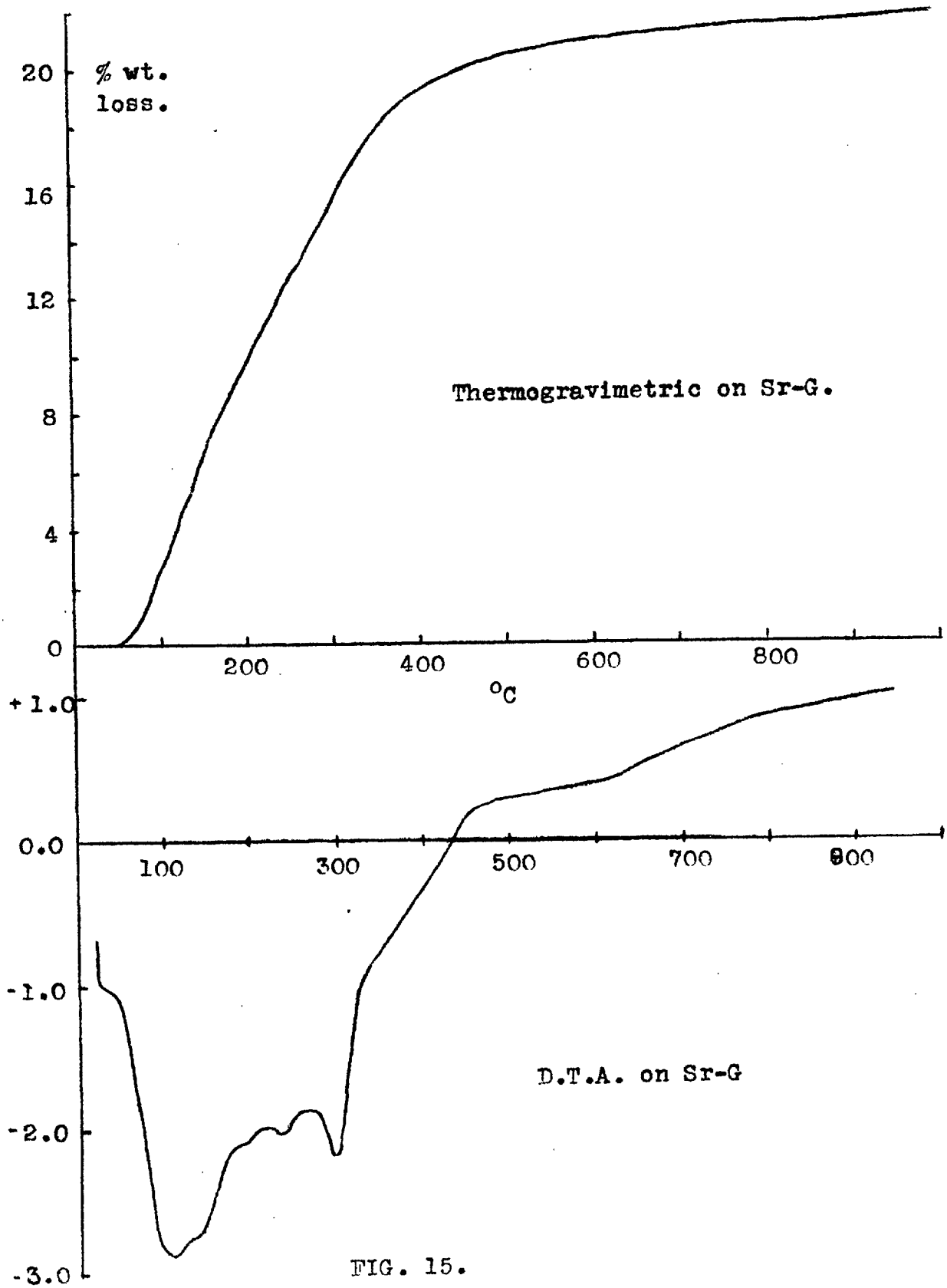

20
% wt.
loss.
16
12
8
4
0
200
400
600
800
°C
Thermogravimetric on Sr-G.
+1.0
0.0
-1.0
-2.0
-3.0
100
300
500
700
900
D.T.A. on Sr-G

FIG. 15.

similar species has been obtained in the corresponding region of the crystallisation field of the potassium aluminosilicates[128], but not from other alkalis or pure calcium aluminosilicate gels.

Sr-D. This species has not been identified with any known natural mineral but there is good reason to suppose that it is a strontium zeolite. It crystallised well between 340°C and 400°C from gels of composition $SrO.Al_2O_3.nSiO_2$ where n ranges from 7 to 9. The species could be formed reproducibly in 100% yield and crystallised in a number of different crystal habits, the two most characteristic of which are shown in Plates 8 and 9.

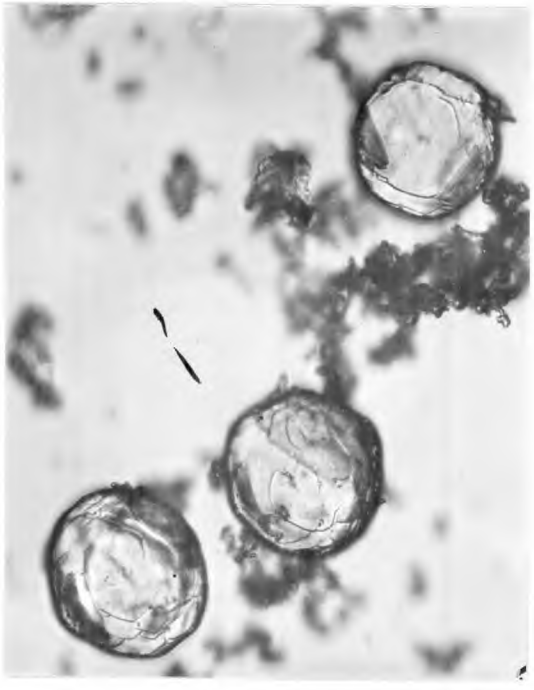


PLATE 8. Sr-D
385 x.

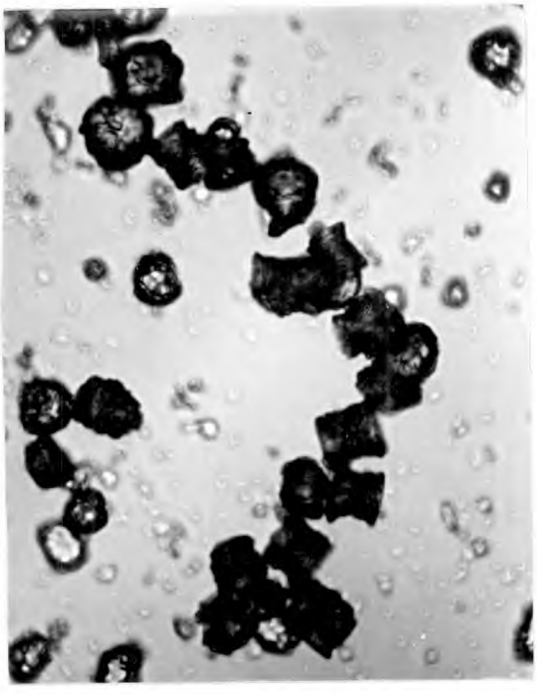


PLATE 9. Sr-D
650 x.

The results of thermogravimetric and differential thermal analysis are plotted in Fig. 16, showing a weight loss on ignition of 11.2%, and a d.t.a. curve compatible with zeolitic behaviour. On ignition to 1000°C, Sr-D recrystallised to an unidentified product, whose X-ray powder pattern is given in Table A8. The isotherm obtained for the sorption of oxygen at 90°K on an outgassed sample of Sr-D is shown in Fig. 14. The sample took up 70 cc at N.T.P. per gram of hydrated sample, comparable with such natural zeolites as mordenite[165]. Electron diffraction patterns taken from a lath in a specimen which X-rays indicated contained only Sr-D enabled the calculation of a unit cell for this sample. It was found to be orthorhombic, body-centred with a=18.5Å, b=21.0Å, c=7.12Å. These dimensions are close to those of mordenite but mordenite is c-centred and its laths lie on their bc plane whereas the laths of this species lie on their ac plane. However, because of the wide varieties of crystal habit observed there was no certainty that the crystal examined by electron diffraction was representative of the major species, and the unit cell obtained could not be fitted to the X-ray powder pattern observed for Sr-D (Table A9).

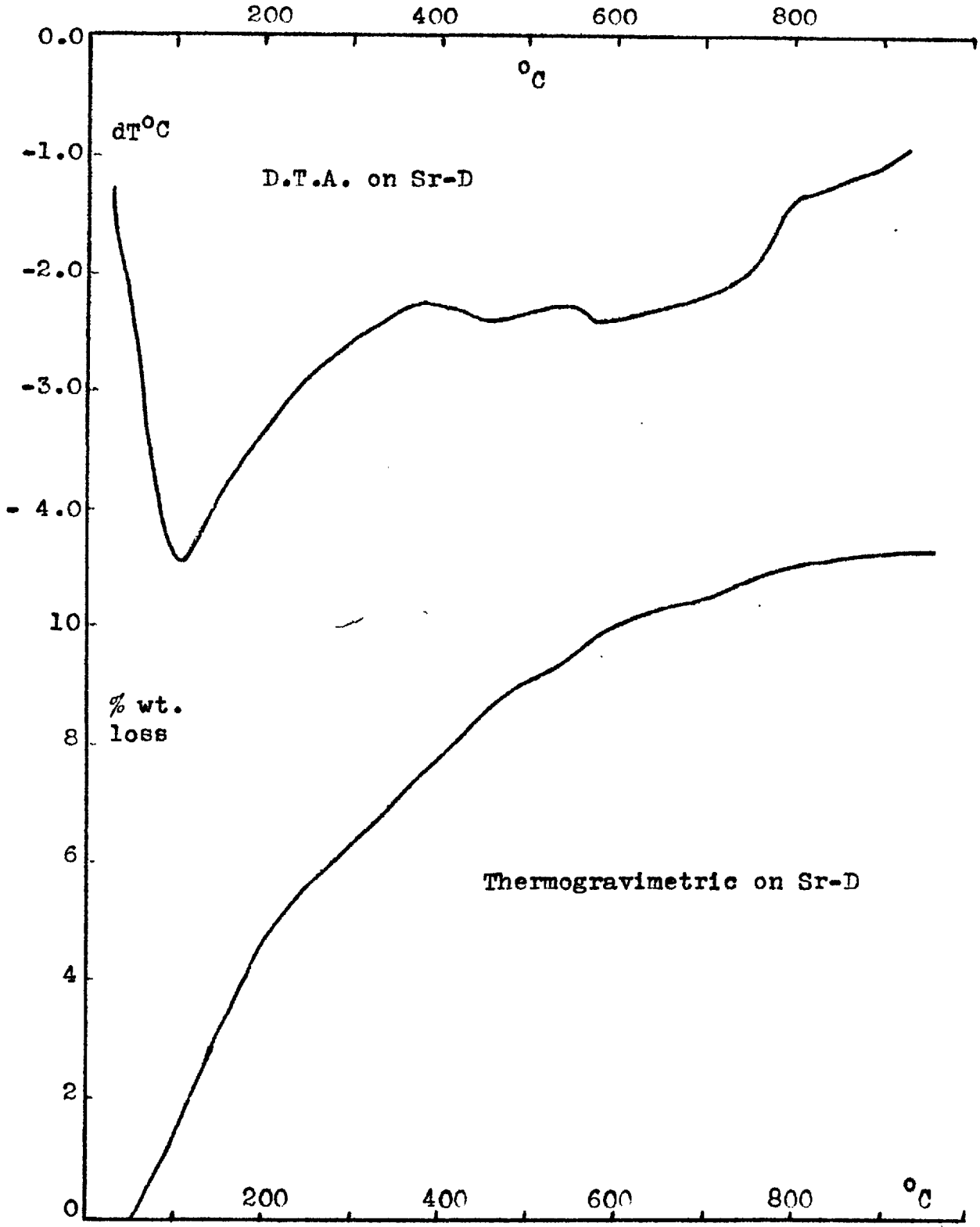

200
400
600
800
0.0
°C
dT°C
-1.0
D.T.A. on Sr-D
-2.0
-3.0
- 4.0
10
% wt.
loss
8
6
Thermogravimetric on Sr-D
4
2
0
200
400
600
800
°C

FIG. 16.

Sr-Q. This species occurred quite widely between 250°C and 350°C from gels with a high silica: alumina ratio, with 8 as the optimum value for this ratio. It could be crystallised fairly reproducibly in 100% yield, and although the crystals were often very small it normally displayed a fibrous or spherulitic habit (Plate 10). The results of thermogravimetric and differential



PLATE 10. Sr-Q 4,050 x.

thermal analysis are shown in Fig. 17. These show that the sample loses 10.5% by weight and is completely destroyed on heating to 1000°C. However 90% of this loss occurs below 450°C which suggests that the species may be a zeolite. The d.t.a. curve shows some interesting features which were completely reproducible for all the samples of Sr-Q investigated. The small but very

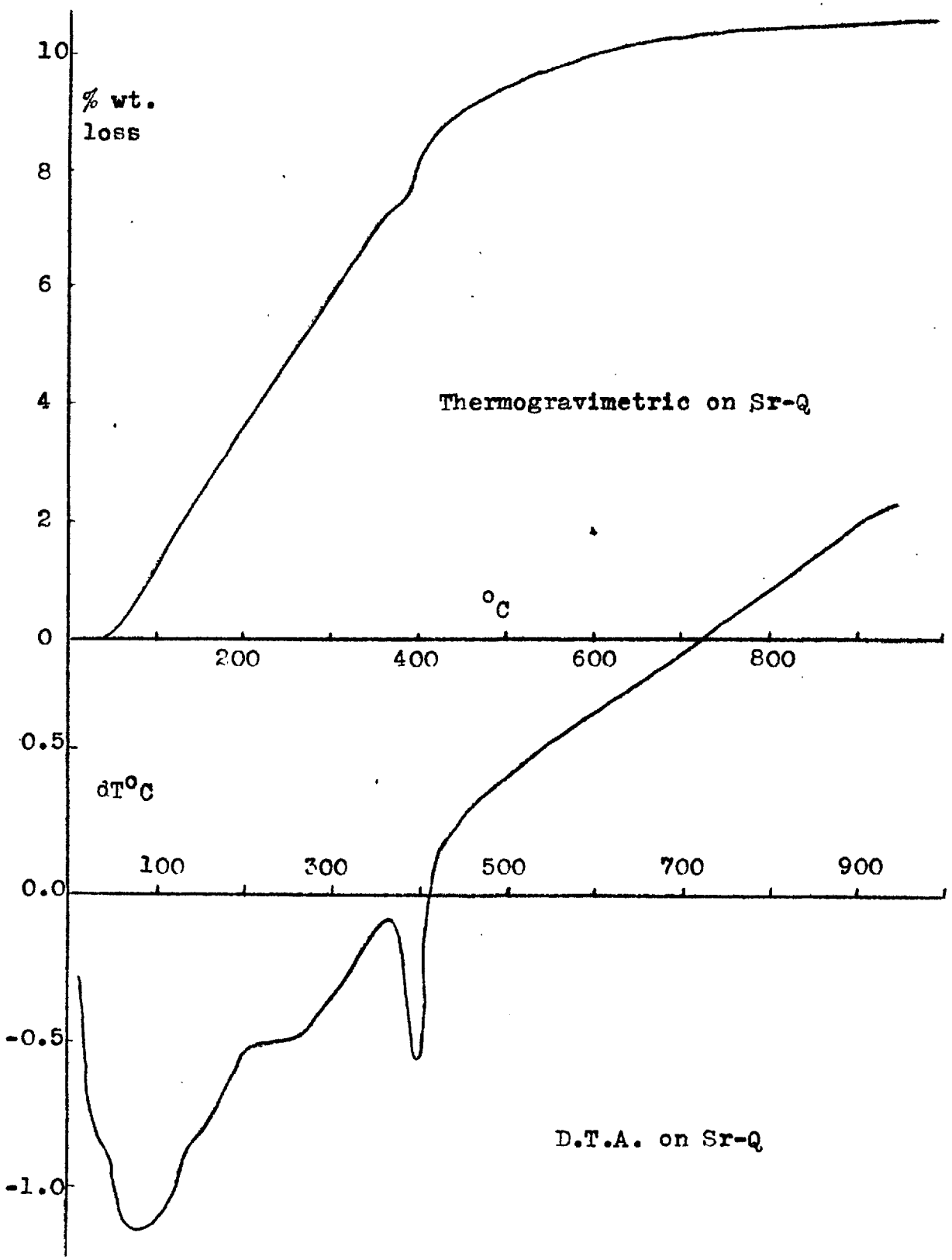

10
% wt.
loss
8
6
4
2
0
Thermogravimetric on Sr-Q
°C
200
400
600
800
0.5
dT°C
100
300
500
700
900
0.0
-0.5
-1.0
D.T.A. on Sr-Q

FIG. 17.

sharp peak which occurs at 400°C is probably associated with the slight but definite change in the slope of the thermogravimetric curve just below this temperature. If the d.t.a. run is stopped at 450°C and the sample cooled and X-rayed the pattern is found to be identical with that of the sample before treatment, thus indicating that no permanent structural alteration has taken place. Although it was found that Sr-Q did not sorb oxygen at 90°K the shape of the d.t.a. curve would suggest that it may be zeolitic with three different sites for the water molecules, the last molecule being held particularly firmly. The X-ray powder pattern (Table A10) could not be identified with that of any natural mineral.

Sr-L. Strontium mica. This species was detected by means of its X-ray powder pattern in samples produced from gels of composition $SrO.Al_2O_3.SiO_2$ at 380°C. After short treatments it was produced in good yield mixed with uncrystallised gel, but after longer times it formed in decreasing yield, and was mixed with Sr-C. A gel of composition $SrO.2Al_2O_3.2SiO_2$ which is the theoretical oxide composition of a strontium margarite, was treated at 455°C and runs of less than three days gave good yields of the mica, although still mixed with either Sr-P or Sr-C. In addition to these major occurrences, when some

specimens of Sr-C produced at 380°C from gels of composition $SrO.Al_2O_3.2SiO_2$ were examined under the electron microscope they were shown to contain a little Sr-L, in amounts which, except in one instance, were too small to be detected by X-ray methods. The mica crystallised in small very thin plates, showing a clear hexagonal outline under the microscope (Plates 11 and 12)

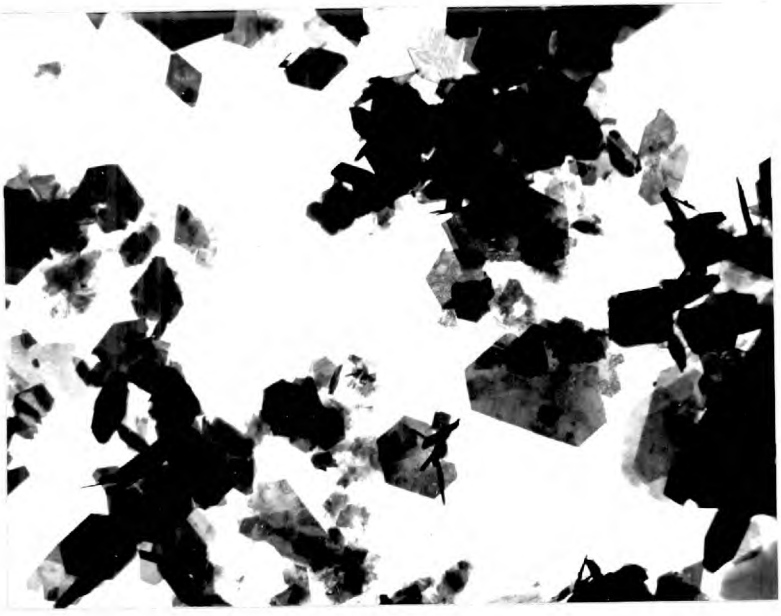


PLATE 11. Sr-L. Strontium mica.
3,150 x

The thermogravimetric and differential thermal analyses of two samples of the mica are shown in Fig. 18. The weights lost above 400°C, which can be assumed to be due to the elimination of the hydroxyl groups, are 3.1%

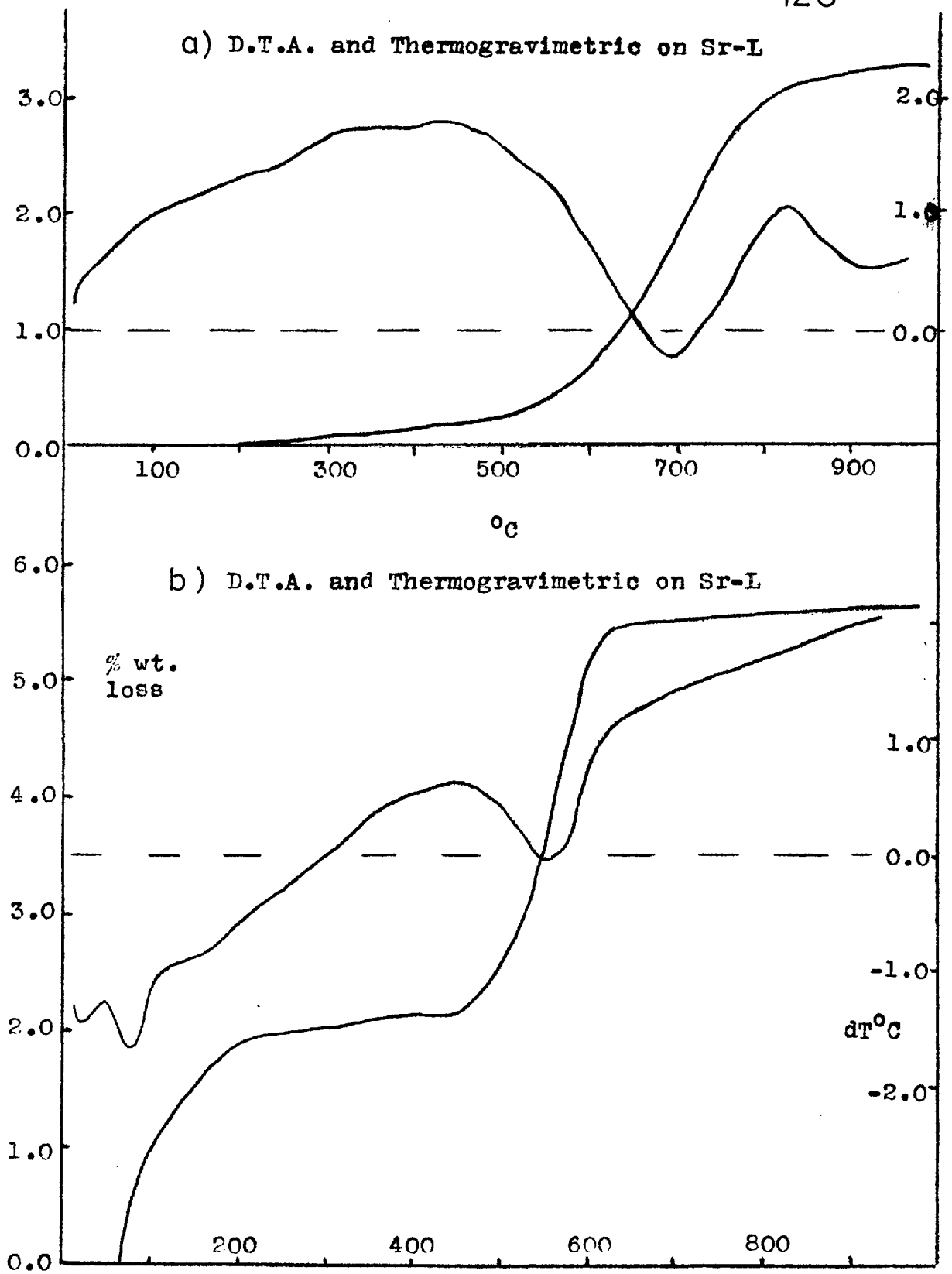

a) D.T.A. and Thermogravimetric on Sr-L
3.0
2.0
1.0
0.0
2.0
1.0
0.0
100
300
500
700
900
°C
b) D.T.A. and Thermogravimetric on Sr-L
% wt. loss
6.0
5.0
4.0
3.0
2.0
1.0
0.0
1.0
0.0
-1.0
-2.0
dT°C
200
400
600
800

FIG. 18.

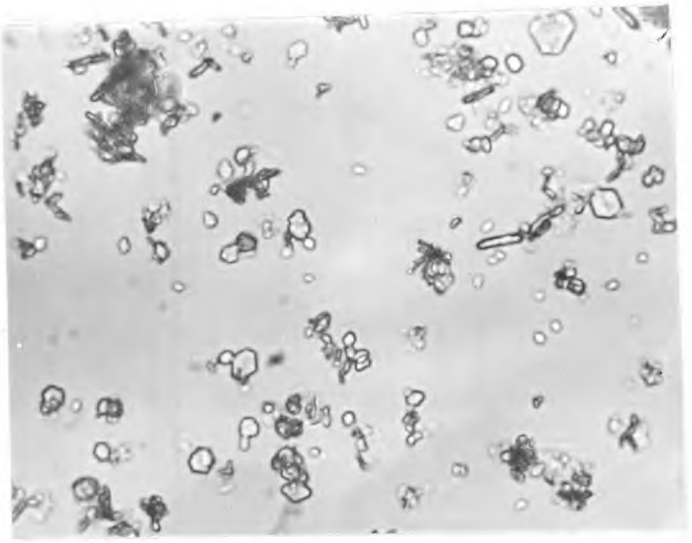


PLATE 12. Sr-L. Strontium mica (with some Sr-C) 565x.

and 3.5%. The calculated loss for a mica with the formula $SrAl_2(Al_2Si_2O_{10})(OH)_2$ is 4.04%, which indicates that the yield of mica was about 80% in the best samples. In each case the peak of the endothermic reaction on the d.t.a. curve corresponds to the temperature of maximum rate of loss of weight, and is due to the loss of the hydroxyl groups. However there is a difference of 150°C in the peak temperatures although the shape of the two graphs is the same. A survey of other published results shows that the dehydroxylation peak temperature for illites and micas undergoing d.t.a. varies considerably between 600°C and 950°C[14,15,16]. Yoder[10] suggests that one of the factors affecting the peak temperature is

grain size, and this may be the explanation in this case, as the crystals were much smaller in the sample which had the lower peak temperature. The seoondary product was also different in each case, being Sr-C in Fig. 18a and Sr-P in Fig. 18b.

X-ray diffraction patterns of samples which had been heated to 1,000°C showed that the structure had undergone a slight permanent expansion but was otherwise intact. This effect was also noted by Roy [16], although the natural micas which he studied decomposed when the temperature was raised a little above 800°C. Vacher[168] has suggested that the expansion observed may be accounted for by the buckling of the structural layers to accommodate the unsatisfied valencies of the oxygen atoms, which result from the expulsion of water. A partial return to the original dimensions was observed when an ignited sample was treated hydrothermally with distilled water at 110°C for three days.

Further evidence that the hydroxyl groups were lost on ignition is provided by the infra-red spectra of the fresh and ignited samples. The fresh samples of Sr-L and also a sample of natural margarite show a sharp peak at 2.74μ. This peak is characteristic of an inorganic hydroxyl group[169], and it was absent or very greatly reduced in the spectra of the ignited samples.

An attempt was made to index the powder pattern of the mica (Table A12) and so determine which polymorphic form had been synthesised and thus calculate the unit cell. However it was not possible to index the pattern with certainty because of the intrinsic differences between the patterns of muscovite and the strontium-mica, and also because a number of important reflections were masked by lines due to the other species present. By analogy with muscovite it would seem from the X-ray powder pattern that the mica obtained was most probably the 2M polymorph, but electron diffraction on some samples indicated very little ordering along the c-axis. Many of the crystals gave good electron diffraction patterns showing clear two-dimensional hexagonal symmetry, but it was not possible to obtain an interplanar spacing giving a value for the c-axis. The best value obtained for the repeat distance along the hexagonal a-axis was $a=5.12\text{Å}$.

It was also found that a product with an identical X-ray diffraction pattern can be obtained by simmering Sr-C with moderately concentrated (1:4) hydrochloric acid for two or three minutes in an open beaker. An electron micrograph of the product is shown in Plate 13. Milder treatment results in incomplete conversion, whereas more vigorous or prolonged treatment results in the complete decomposition and solution of the Sr-C. It may

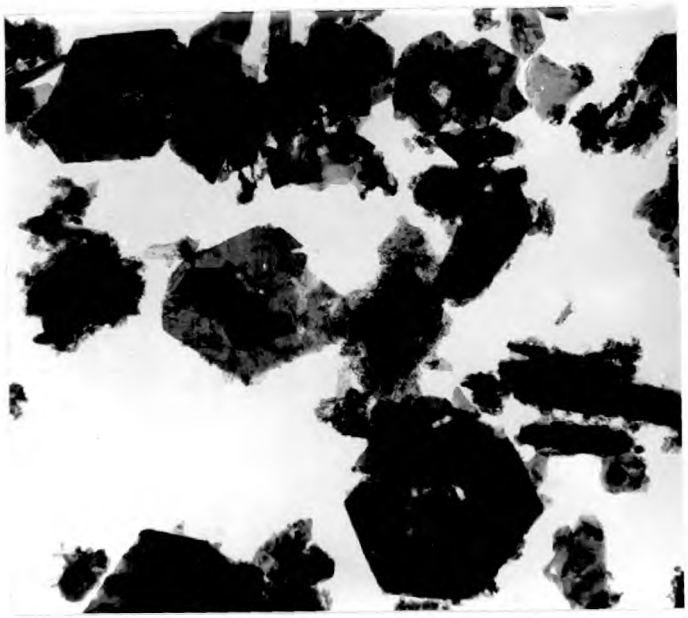


PLATE 13. Sr-L produced from Sr-C by acid attack. 8,000x

be that the samples used originally contained both Sr-L and Sr-C, but that the latter is preferentially dissolved in the acid at a faster rate than is the mica. If this were so then the fact that no mica could be detected in the X-ray pattern of the original samples is rather surprising when semi-quantitative estimates of the yields of mica produced by acid treatment are considered. However, the alternative possibility that the mica had recrystallised from the strongly acid aqueous solution at 100°C would be rather remarkable, although similar reactions are known to occur under hydrothermal conditions at elevated temperatures[170,171].

Sr-N. This species was formed from gels whose silica:alumina ratio was around 1:1, It formed best at temperatures above 400°C although lesser yields were recorded down to 300°C. It was always mixed with Sr-C in varying amounts, and no pure samples were obtained. The species crystallised as well-formed cuboid crystals up to 10μ long (Plate 14). Since Sr-C is completely

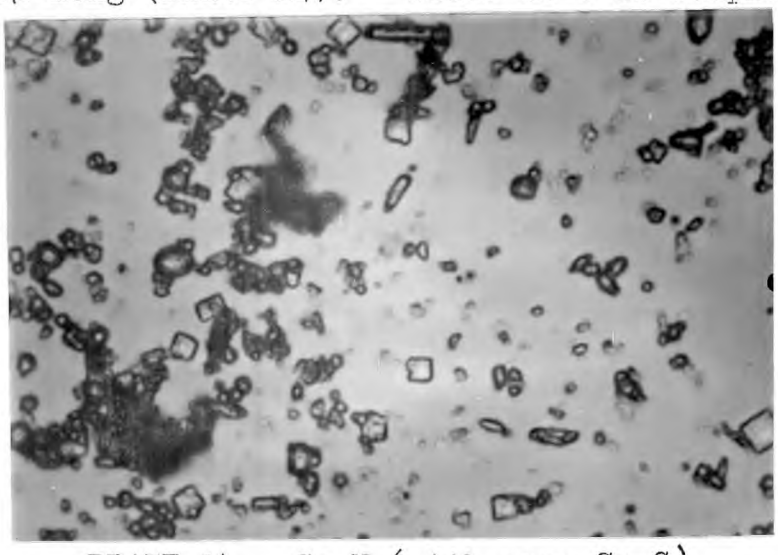


PLATE 14. Sr-N (with some Sr-C)
380 x.

unaffected by heating up to at least 1000°C it was possible to carry out differential and thermogravimetric analyses on the samples, although they were mixed with Sr-C (Fig. 19). Sr-N shows a weight loss between 400°C and 700°C, and an endothermic peak on the d.t.a. with its maximum at 640°C. This suggests that the compound contains hydroxyl groups which are lost on ignition. This

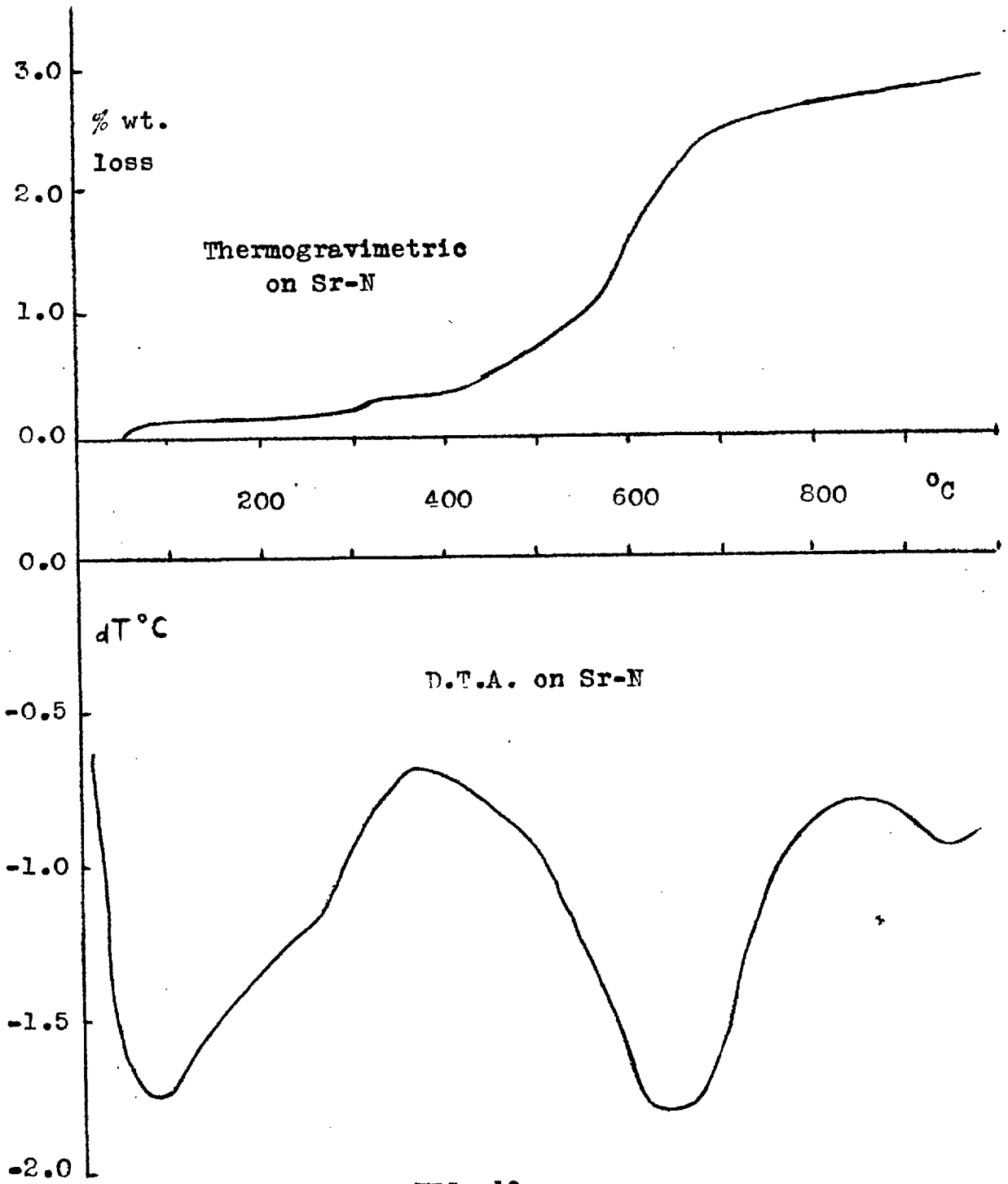

3.0
% wt.
loss
2.0
Thermogravimetric
on Sr-N
1.0
0.0
200
400
600
800
°C
0.0
dT °C
D.T.A. on Sr-N
-0.5
-1.0
-1.5
-2.0

FIG. 19.

is supported by the infra-red spectra which have a sharp peak at 2.75μ, characteristic of a hydroxyl group, in the spectrum of the fresh sample, and no trace of this peak in the spectrum of the sample after ignition.

The X-ray powder pattern (Table A11) was indexed to a tetragonal unit cell with the parameters a=12.48Å, c=16.00Å. The species was not a hydrogrossularite as might have been expected by analogy with the work of Denny[42] and it was not identified with any other mineral by means of its X-ray powder pattern.

Sr-C. This species occurred very widely and was formed from gels with silica:alumina ratios from 1 to 9 above 370°C and at 300°C, and at temperatures down to 150°C when the silica:alumina ratio was 1:1. The optimum yields were obtained from gels of composition $SrO.Al_2O_3.2SiO_2$ at 380°C or above for about 24 hours. In the case of shorter treatments the product sometimes contained a little strontium mica, and also some strontium carbonate which could be removed by washing with dilute acid. When formed under these optimum conditions Sr-C crystallised as well-formed acicular laths about 15μ in length (Plate 15). When formed from gels with a higher silica:alumina ratio the yield and crystallinity were much poorer, and the Sr-C was often mixed with other species.



PLATE 15. Sr-C. 300x.

Sr-C appeared to be quite unaffected by heating up to at least 1,050°C, as it suffered no appreciable weight loss or other reaction under the conditions of differential thermal analysis or prolonged ignition. An examination of the tables of products seems to suggest that in many cases the first product formed is Sr-P and that after longer treatments this is converted to Sr-C. Attempts to test this directly by the hydrothermal treatment of Sr-P were inconclusive, and the result of a pyrolytic study is discussed in the section on Sr-P.

The X-ray powder pattern of this species was sharp but complex, and was not similar to that of strontium anorthite[136] although there were some similarities with that of paracelsian (Table A13).

Paracelsian is a near orthorhombic polymorph of the barium felspar celsian, and there is a similar polymorph of calcium felspar. From its properties and its place in the crystallisation field it seems probable that Sr-C is an analogous polymorph of strontium felspar.

Sr-P. This is the hexagonal polymorph of strontium felspar, similar to that obtained by Denny(42) in the work on the hydrothermal synthesis of calcium aluminosilicates. It was formed from gels with a very wide range of compositions at temperatures from 150°C upwards when the silica:alumina ratio was between one and four, and at progressively higher temperatures as the proportion of silica increased. Above 400°C the excess silica crystallised as cristobalite, and at lower temperatures the Sr-P was mixed with uncrystallised gel or other species. The optimum conditions for the formation of this species were from gels of composition $SrO.Al_2O_3.2SiO_2$ and $SrO.Al_2O_3.3SiO_2$ either at 200°C for several days, or for short periods at 340°C, although under the latter conditions the product was sometimes mixed with Sr-C. The same gels which produced Sr-P after short treatments, often gave Sr-P and Sr-C or Sr-C alone after longer treatments, but the direct hydrothermal conversion of a sample of Sr-P into Sr-C was not conclusively proved. In an

attempt to determine the relative stability of the two forms, a sample containing principally Sr-P with a little Sr-C present, was heated for 14 days at 1250°C in a platinum bucket in a platinum tape wound furnace. Examination of the product (Sr-W) revealed that the whole sample had been completely converted to strontium anorthite. The X-ray powder pattern of this sintered product was extremely close to that found for the compound $SrO.Al_2O_3.2SiO_2$ analogous to anorthite, prepared pyrolytically by Dear[136] and Sorrell[137] (Table A14).

The samples of Sr-P showed no definite or reproducible features on differential thermal analysis up to 1,000°C, and there was no weight loss on ignition. There was no evidence for a phase transformation of the type observed with the analogous barium species.

The X-ray powder pattern was similar to those obtained for the calcium and barium hexagonal felspars, the corresponding lines showing a progressive displacement from calcium, through strontium, to barium. The pattern was indexed on the hexagonal system and the unit cell calculated to be a=5.19Å, c=7.59Å. This is in good agreement with the powder pattern and unit cell obtained by Sorrell (Table A15). The crystals of Sr-P were always extremely small and ill-defined. An electron micrograph of one of the best samples is shown in Plate 16.



PLATE 16. Sr-P. Hexagonal Sr-felspar. 3000x

Sr-K. This species occurred on one occasion with uncrystallised gel from a gel of composition $Sr.O.Al_2O_3.6SiO_2$ after 16 days at 300°C and on two occasions mixed with Sr-P from gels of composition $SrO.Al_2O_3.5SiO_2$ at 380°C. Examination under the microscope showed that the species was quite well crystalline but there was no characteristic crystal habit. A sample of Sr-K was ignited over a meker burner for 24 hours with no effect other than a slight sharpening of the X-ray pattern. The X-ray pattern had considerable similarities to that of strontium-anorthite, but careful comparison indicated that the resemblances were not close enough in detail to identify it as such. The pattern was not identified

with that of any other previously known mineral (Table A16).

Sr-S. Small amounts of this species were produced on three occasions from gels of composition $SrO.Al_2O_3.SiO_2$ at 380°C (Table 4). Since both Sr-P and Sr-C were present each time the minor species was only indicated by the presence of a number of weak extra lines in the X-ray powder photograph (Table A17). The minor species was not picked out under the microscope and the X-ray powder pattern was not identified with that of any known mineral.

Sr-T. This species was produced in very minor amounts on three occasions from gels of composition $SrO.Al_2O_3.SiO_2$ at 295°, 250° and 205°C. Its formation was not reproducible. The X-ray powder pattern, determined by subtracting the lines due to Sr-C from the total pattern obtained, is given in Table A17. The two strongest of these lines are the same as the two strongest lines of boehmite, whose other lines would be obscured by the pattern of Sr-C. The weakness of the diffraction lines observed makes a definite decision difficult but it is possible that Sr-T may be a mixture of boehmite and another very minor unidentified constituent.

8.2. The Barium Aluminosilicates

The hydrothermal crystallisation field of the barium aluminosilicates was investigated using gels of the composition $BaO.Al_2O_3.nSiO_2$, where n was varied from 1 to 9, at temperatures between 100°C and 435°C for varying times. The products obtained are recorded in Tables 18-28, and the code letters used are listed in Table 29, where the terms 100%, major, and minor have the same meanings as were explained in the section on the strontium aluminosilicates (p. 82).

8.2.1. General.

The region in which no crystallisation at all took place decreased steadily along the series calcium, strontium, and barium. Crystallisation was difficult below 250°C when n=5 and below 300°C when n=6, but harmotome crystallised down to 150°C from gels with n=7 and those with n=8 produced crystalline products at 250°C and above, whilst those with n=9 did so from 300°C upwards. No experiments were carried out with gels to which excess alkali had been added. In contrast to the crystallisation of the strontium aluminosilicates, the barium gels did not produce isolated and irreproducible occurrences of numerous, mainly zeolitic, species. Instead, all the products except Ba-Z were obtained in major or 100% and reproducible

TABLE 18 Products from gels of composition $BaO.Al_2O_3.SiO_2$

435°C	19 hours	5 days	9 days	
	good C	good C	mod C	
	good P	$BaCO_3$	good P	
	(7.5)	(10.5)	(7.0)	
380°C	19 hours	3 days	10 days	
	mod good P	mod good P	poor P	
	mod good A	mod good A	$BaCO_3$	
	$BaCO_3$	$BaCO_3$	(7.0)	
	(10.5)	(10.5)		
340°C	20 hours	2 days	4 days	8 days
	good A	good A	good A	mod good A
	$BaCO_3$	$BaCO_3$	$BaCO_3$	$BaCO_3$
	(>10.5)	(>10.5)	(>10.5)	(>10.5)
300°C	4 days	12 days	19 days	
	good A	v.good A	good A	
	$BaCO_3$	$BaCO_3$	$BaCO_3$	
	(≥10.5)	(10.5)	(7.5)	
250°C	4 days	12 days	19 days	
	good E	v.good A	good A	
	good P	$BaCO_3$	$BaCO_3$	
	good C	(10.0)	(10.5)	
	$BaCO_3$			
	(>10.5)			
200°C	4 days	12 days	19 days	
	good E	good E	good E	
	$BaCO_3$	good C	good C	
	(>10.5)	good P	good P	
		$BaCO_3$	$BaCO_3$	
		(>10.5)	(>10.5)	

continued

TABLE 18 (continued)

150°C	12 days	19 days
	good E	good E
	$BaCO_3$	$BaCO_3$
	(>10.5)	(>10.5)
110°C	123 days	
	mod good G	
	(>10.5)	

TABLE 19 Products from gels of composition $BaO.2Al_2O_3.2SiO_2$

435°C	20 hours	6 days	13 days
	good P	good P	good C
	trace C	trace C	(7.10)
	(7.0)	(7.0)	

TABLE 20 Products from gels of composition $BaO.Al_2O_3.2SiO_2$

435°C	23 hours good C (7.0)	4 days good C $BaCO_3$ (7.5)	8 days good C (7.0)
380°C	23 hours mod good C (7.0)	3 days mod good C (7.0)	7 days mod good C (7.5)
340°C	22 hours good C $BaCO_3$ (7.5)	3 days good C trace $BaCO_3$ (9.0)	7 days good C trace P (7.5)
300°C	3 days some C some P (10.5)	8 days good C mod good P (8.5)	16 days mod good P some C (7.0)
250°C	5 days good P some C (7.5)	16 days good P some C (7.0)	
200°C	5 days mod P trace C $BaCO_3$ (7.0)	16 days good P trace C (10)	
150°C	5 days poor P trace C (9.0)	16 days mod P trace C (>10.5)	
110°C	119 days mod good G	(>10·5)	

TABLE 21 Products from gels of composition $BaO.Al_2O_3.3SiO_2$

435°C	19 hours	4 days	8 days		
	mod C	mod good C	good C		
	(7.0)	(7.0)	(7.0)		
380°C	24 hours	3 days	7 days		
	mod C	mod C	good C		
	(7.0)	(7.0)	(7.0)		
340°C	24 hours	3 days	7 days		
	mod good C	mod C	mod good C		
	(9.0)	poor P	(8.0)		
		(8.0)			
300°C	3 days	7 days	12 days	18 days	25 days
	good P	good P	good P	good P	good P
	mod C	mod C	mod C	mod C	poor C
	(8.0)	(7.5)	(8.5)	(dry)	(8.5)
250°C	3 days	7 days	12 days	18 days	25 days
	good P	good P	good P	good P	good P
	mod C	poor C	good C	good C	mod C
	(8.5)	(9.0)	(9.0)	(7.0)	(9.0)
200°C	7 days	12 days	15 days	18 days	
	mod G	mod good G	mod G	mod good G	
	(7.5)	mod P	(9.0)	(9.0)	
		(8.5)			
	21 days	25 days	29 days		
	mod G	good P	mod good P		
	(8.5)	mod G	(8.5)		
		(9.5)			

continued

TABLE 21 (continued)

150°C	10 days	15 days	18 days
	mod good G	poor G	mod G
	(9.0)	(8.5)	(9.0)
	21 days	25 days	29 days
	mod G	good G	good G
	(9.0)	(9.0)	(8.5)
110°C	118 days		
	mod good G		
	(9.0)		

TABLE 22 Products from gels of composition $BaO.Al_2O_3.4SiO_2$

435°C	23 hours good P (7.0)	2 days good P trace H (7.0)	7 days good P some H (7.0)
380°C	23 hours good P (7.0)	3 days good P (7.0)	7 days v.good P (7.0)
340°C	21 hours good P (7.5)	3 days good P trace H (8.5)	7 days good P trace C (7.5)
300°C	2 days mod good P (7.0)	7 days good P (7.0)	14 days good P good C (7.5)
250°C	7 days mod P (7.0)	17 days mod P (9.0)	
200°C	2 days trace P (7.5)	7 days trace P (7.0)	14 days good P (7.0)
150°C	7 days trace P (7.0)	17 days trace P (9.0)	
110°C	116 days mod good G (9.0)		

TABLE 23 Products from gels of composition $BaO.Al_2O_3.5SiO_2$

435°C	18 hours	4 days	8 days
	good P	good P	good P
	trace H	some H	mod H
	(7.0)	(7.5)	(7.5)
380°C	24 hours	3 days	7 days
	good P	good P	v.good P
	(8.0)	trace H	some H
		(7.5)	(7.0)
340°C	17 hours	3 days	7 days
	good P	good P	good P
	(7.0)	(9.0)	(7.0)
300°C	5 days	14 days	21 days
	mod P	good P	good P
	(8.5)	(7.0)	(9.0)
250°C	5 days	14 days	21 days
	poor P	poor P	some P
	(9.0)	trace J	some M
		(8.0)	(9.0)
200°C	5 days	14 days	21 days
	X	trace P	trace P
	(9.0)	$BaCO_3$	$BaCO_3$
		(8.5)	(9.5)
150°C	5 days	14 days	21 days
	X	trace P	trace P
	(8.5)	$BaCO_3$	$BaCO_3$
		(9.5)	(9.0)

TABLE 24 Products from gels of composition $BaO.Al_2O_3.6SiO_2$

435°C	19 hours	5 days	9 days
	good P	good P	good P
	some H	good H	good H
	(7.0)	(7.0)	(7.0)
380°C	24 hours	3 days	7 days
	good P	good P	good P
	(7.0)	some H	good H
		(7.0)	(7.5)
340°C	2 days	6 days	9 days
	good P	good P	good P
	(7.5)	some H	some H
		(7.0)	(7.0)
300°C	5 days	13 days	22 days
	mod P	mod good P	poor P
	(7.5)	(8.0)	(7.0)
250°C	5 days	13 days	22 days
	trace P	trace M	X
	(8.0)	(8.5)	(7.0)
200°C	5 days	13 days	22 days
	X	X	X
	(9.0)	(9.5)	(7.0)
150°C	5 days	13 days	22 days
	X	X	X
	(9.0)	(9.5)	(7.0)

TABLE 25 Products from gels of composition $BaO.Al_2O_3.7SiO_2$

435°C	21 hours good P good H (7.0)	3 days good P good H (7.0)	7 days good P good H (7.0)	
380°C	17 hours good P (7.0)	3 days good P (7.0)	5 days good P some H (7.0)	7 days good P (7.0)
340°C	17 hours good P (7.0)	3 days good P poor H (7.0)	6 days good P mod H (7.0)	
300°C	5 days mod P trace K (7.0)	8 days mod P good K (7.0)	18 days mod P some K (7.0)	
250°C	5 days poor M (7.0)	12 days good M good J (7.0)	15 days mod M mod J (8.0)	
200°C	5 days poor M (>10.5)	12 days mod M (>10.5)	18 days good M (>10.5)	
	20 days(2) X (7.5)	33 days(2), X (8)	54 days good M (7.5)	

continued.

TABLE 25 (continued)

150°C	8 days	15 days	18 days
	mod M	X	mod good M
	(10.5)	(7.0)	(10.0)
110°C	102 days		
	X		
	trace $BaCO_3$		
	(9.5)		

TABLE 26 Products from gels of composition $BaO.Al_2O_3.7.5SiO_2$

250°C	12 days	13 days(2)	19 days	19 days	19 days
	good M	good M	trace J	poor J	good M
	(9.0)	(9.0)	(9.0)	(9.0)	(9.0)
220°C	13 days	19 days	30 days	33 days	
	X	poor M	good M	v.good M	
	(9.0)	(9.0)	(9.0)	(8.5)	

+	19 days at 220°C 3 days at 250°C	+ 19 days at 220°C 11 days at 250°C
	some M	good M
	(9.0)	(8.5)

TABLE 27 Products from gels of composition $BaO.Al_2O_3.8SiO_2$

430°C	21 hours good P trace H (7.0)	3 days v.good P good H (7.0)	7 days v.good P good H (7.0)		
380°C	3 days good P good H (8.5)	7 days good P good H (8.0)			
340°C	2 days X (8.0)	4 days mod P mod Z (9.0)	7 days(2) good P good H mod Z (8.5)	9 days(2) mod P mod H trace Z (8.5)	13 days good P good H trace Z (8.0)
300°C	2 days X (8.0)	3 days some K (9.0)	4 days trace J (8.5)	6 days good K (8.5)	
	6 days good J (8.0)	6 days some J (8.0)	6 days(2) fair K (8.0)	6 days fair J (8.0)	
	9 days good K (8.5)	9 days good J (8.0)	13 days good J (9.0)	15 days good K (8.0)	
	15 days some J trace P (8.5)	16 days good K (8.5)	20 days good K trace P (9.0)	20 days fair K some J some P (8.5)	

continued.

TABLE 27 (continued)

300°C	26 days mod P poor K (8.5)	30 days mod P trace J (8.5)	30 days some P some K some J (8.5)		
250°C	6 days X (9.0)	10 days mod M (9.5)	13 days good M (9.5)	15 days(2) X (8.5)	15 days(2) trace M (8.5)
	15 days mod M (8.5)	16 days good M (8.5)	17 days poor J (9.0)	17 days good M (8.5)	18 days(2) mod K (9.0)
	19 days poor J (8.5)	19 days mod K (8.5)	20 days X (9.5)	23 days(3) mod M mod J (9.0)	30 days good M (9.0)
200°C	6 days X trace $BaCO_3$ (9.5)	13 days X trace $BaCO_3$ (9.5)	19 days X trace $BaCO_3$ (10.0)	20 days X trace $BaCO_3$ (8.5)	25 days X $BaCO_3$ (9.0)
150°C	6 days X trace $BaCO_3$ (9.5)	13 days X trace $BaCO_3$ (9.5)	20 days X trace $BaCO_3$ (8.5)		
110°C	125 days X trace $BaCO_3$ (10.0)				

TABLE 28 Products from gels of composition $BaO.Al_2O_3.9SiO_2$

430°C	19 hours	3 days	7 days
	good P	good P	good P
	(7.0)	good H	good H
		(7.0)	(7.0)
380°C	3 days	7 days	
	good P	good P	
	good H	good H	
	(7.0)	(8.5)	
340°C	15 hours	3 days	6 days
	X	v.good K	good K
	(7.0)	(7.0)	(7.0)
300°C	3 days	9 days	14 days
	good P	v.good P	v.good P
	some Z	some H	(7.5)
	(7.5)	(7.0)	
250°C	3 days	9 days	14 days
	X	X	some J
	(8.0)	(8.5)	(8.5)
200°C	3 days	9 days	14 days
	X	X	X
	(9.5)	(9.0)	(8.5)
150°C	3 days	9 days	14 days
	X	X	X
	(10.0)	(9.5)	(10.5)
110°C	110 days	125 days	
	X	X	
	(10.0)	(10.0)	

TABLE 29 Species obtained from barium gels

A	Unidentified	major
C	Celsian (barium felspar)	100%
E	Boehmite	major
G	Barium zeolite	major
H	α-cristobalite	major
J	Barium zeolite	100%
K	Barium zeolite	100%
M	Harmotome	100%
P	Hexagonal polymorph of felspar	100%
Z	Unidentified	minor
X	Uncrystallised gel	

A diagrammatic representation of the crystallisation fields is given in Fig. 20.

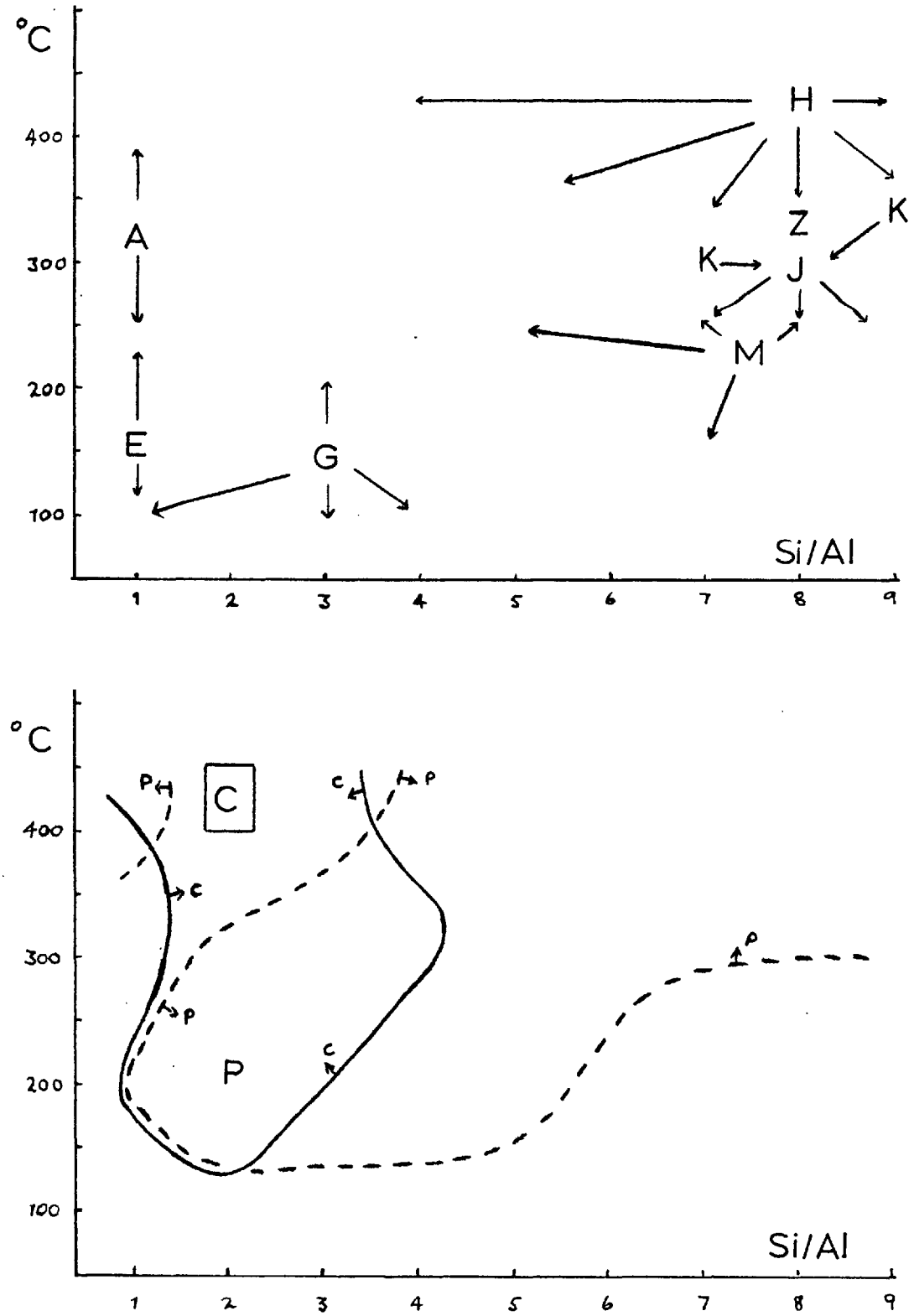


Fig. 20. Ba Crystallisation Field.

yield and occurred in a readily defined region of the crystallisation field, although a number of species did overlap considerably.

Above 400°C good crystallinity was nearly always obtained, even after only 24 hours treatment, but as the temperature was lowered and the silica:alumina ratio increased, the time required for a good yield of a crystalline product increased to about four weeks. Other systematic variations depending on the time of treatment will be discussed under the heading of the species involved.

8.2.2. Particular species.

Ba-E. This species was identified from its X-ray powder pattern as boehmite (Table A18) and it was found among the products from gels with the composition $BaO.Al_2O_3.SiO_2$ which had been treated at 250°C and below. It would appear that it is an initial product of the crystallisation of the alumina, which, at the higher temperatures at least, is wholly or partially converted by more prolonged treatment into other species containing barium and silicon.

Ba-H. α-cristobalite. As in the case of the strontium field, this species was often mixed with an aluminosilicate species in experiments carried out above

340°C, if the parent gel contained excess silica. Often it took several days to develop, although at 430°C it was in one case well crystallised in 24 hours. The X-ray powder pattern is compared with that of a standard sample in Table A1. When well crystallised the cristobalite formed small spheres as in the case of Sr-H.

Ba-C. Celsian. The X-ray powder pattern of this species was closely similar to the published data for the barium felspar celsian, and was identical to that of a sample of natural celsian kindly supplied by Dr. P. Gay of Cambridge (Table A20). Ba-C formed at all temperatures from gels of composition $BaO.Al_2O_3.2SiO_2$ although the yields were poor below 300°C and mixed with Ba-P. It also formed well from gels of composition $BaO.Al_2O_3.3SiO_2$ although again mixed with Ba-P below 300°C. The optimum conditions of formation were one or two days between 400°C and 450°C from gels of composition $BaO.Al_2O_3.2SiO_2$. The samples of celsian could be ignited to at least 1,100°C without change. The crystals were always extremely small and did not display a characteristic habit. An electron micrograph of a sample is shown in Plate 17.

Ba-P. This is the hexagonal polymorph of barium felspar and is identical with the product described by Ito[34]. It occurred very widely over the whole range



PLATE 17. Ba-C. Celsian
7,100 x

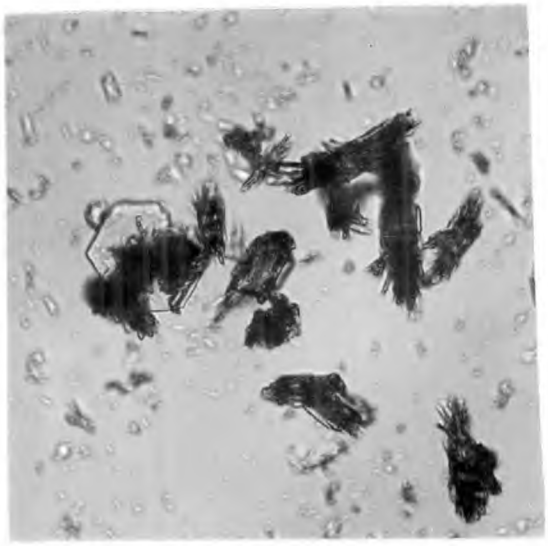


PLATE 18. Ba-J.
550 x

of compositions investigated but was in most cases accompanied by other species. The best samples were obtained from gels of composition $BaO.Al_2O_3.4SiO_2$ for short periods above 300°C, but even in these cases the product was not pure Ba-P but would have contained amorphous silica. The crystals were in all cases extremely small and of indefinite habit.

The differential thermal analysis curves for three samples of Ba-P are shown in Fig. 21. These show two endothermic peaks and thermogravimetric analysis shows that the first of these is due to the loss of the normal surface held moisture, but the second, the peak of which falls at 340°C, 354°C and 348°C respectively in the three samples, was not associated with any loss of weight. This suggests that the peak is caused by a phase transformation probably of the $\alpha \rightarrow \beta$ type, and is in agreement with the work of Yoshiki and Matusmoto[32]. These workers carried out dilatometric analysis on specimens cut from an aggregated mass of the compound produced pyrolytically. They found that as the sample was heated the plot of expansion vs. temperature had a marked step at about 300°C, and that this also occurred on cooling, although the graph did not retrace exactly the same path. They also found that there was a sharp discontinuity in the specific heat at about 300°C and therefore concluded that the compound has

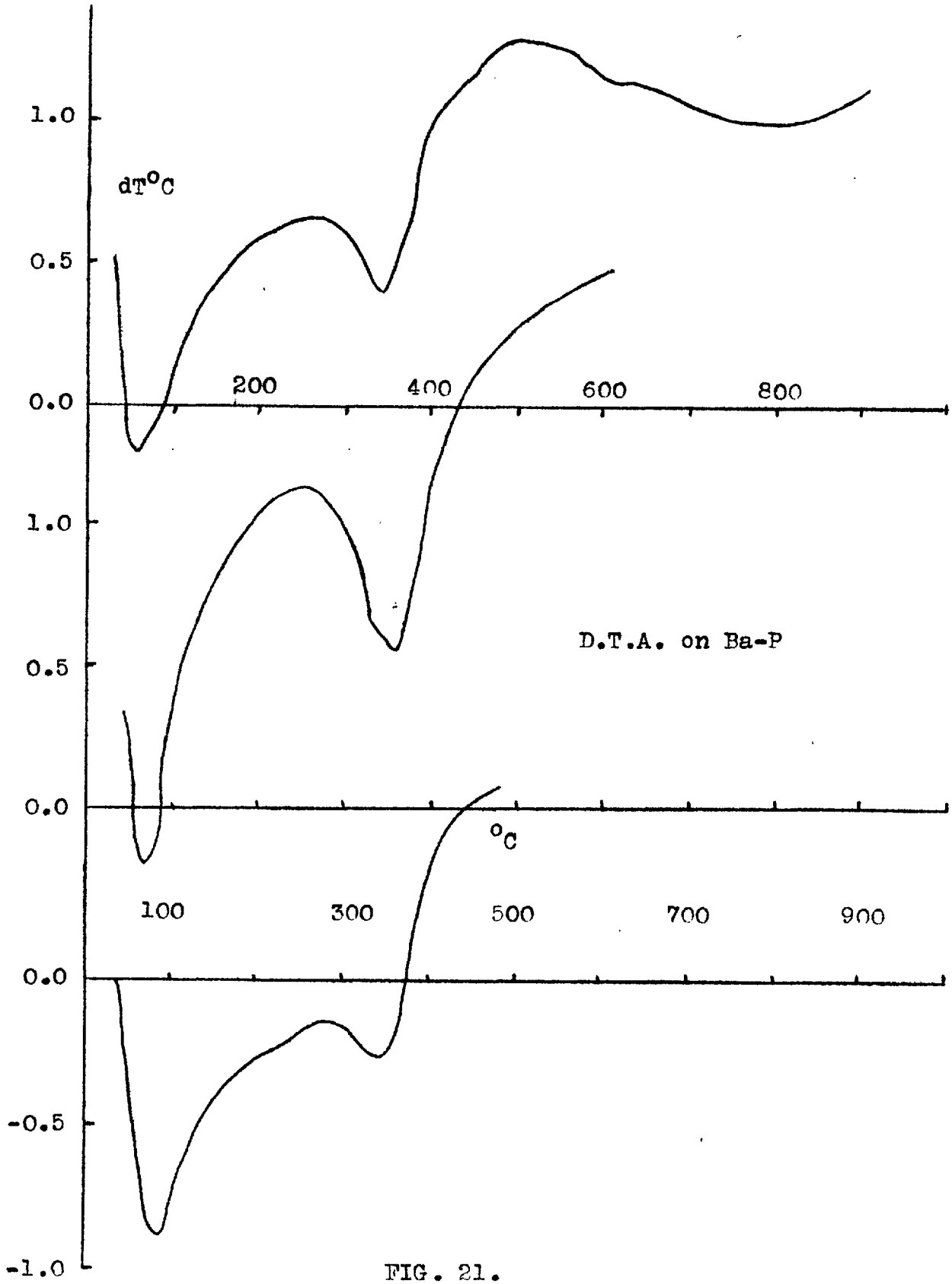

1.0
dT°C
0.5
0.0
200
400
600
800
1.0
0.5
D.T.A. on Ba-P
0.0
°C
100
300
500
700
900
0.0
-0.5
-1.0

FIG. 21.

an enantiotropic transformation similar to the $\alpha \rightleftharpoons \beta$ transformation in quartz. The transformation temperature observed in this work is 50°C higher than that quoted by Takeuchi[35]. Although this difference might be attributed to the dynamic heating used in the d.t.a. method compared with the steady state method using the dilatometer it should be noted that the d.t.a. apparatus used recorded the $\alpha \rightarrow \beta$ inversion of quartz at 570°C compared with the established value of 575°C[172]. Furthermore the apparatus could readily pick out the exothermic $\beta \rightarrow \alpha$ transition of quartz on cooling (at 567°C) and yet careful examination of many cooling curves for Ba-P showed no evidence for an exothermic reaction. The X-ray patterns of samples which had been heated above 450°C and then cooled showed slight but definite differences from those patterns of freshly prepared samples. It is therefore concluded that the $\alpha \rightleftharpoons \beta$ transition is more sluggish in these samples, possibly on account of their poorer crystallinity, and that the high temperature form may be frozen in during relatively rapid cooling.

Takeuchi has shown that the low temperature form is only pseudohexagonal and is in fact probably orthorhombic but invariably occurs in a trilling form. The X-ray powder pattern was in good agreement with the published data, but there is some divergence between the

unit cells quoted in the literature.

	a	c
Takeuchi[35]	5.293 Å	7.790 Å
Ito[34]	5.25	7.84

The pattern was indexed as shown in Table A15, and the unit cell calculated to be a=5.33Å, c=7.72Å, whilst that of the ignited sample was a=5.29Å, c=7.76Å.

Ba-G. This zeolitic species formed reproducibly in quite good yield from gels of composition $BaO.Al_2O_3.3SiO_2$ between 200°C and 150°C. About three or four weeks were required to obtain good yields as estimated from the X-ray powder photographs. Some Ba-G was also formed from gels with silica:alumina ratios between 1:1 and 4:1 treated at 110°C for about four months. The species was always obtained together with unreacted gel and often contained barium carbonate. It was difficult to purify the samples by treatment with dilute acid. The Ba-G formed as large irregular aggregates of very small crystals but a number of samples also contained a few well formed cuboid crystals.

The d.t.a. and thermogravimetric curves obtained from one of the better samples of Ba-G are shown in Fig. 22. The amount of gel in this sample

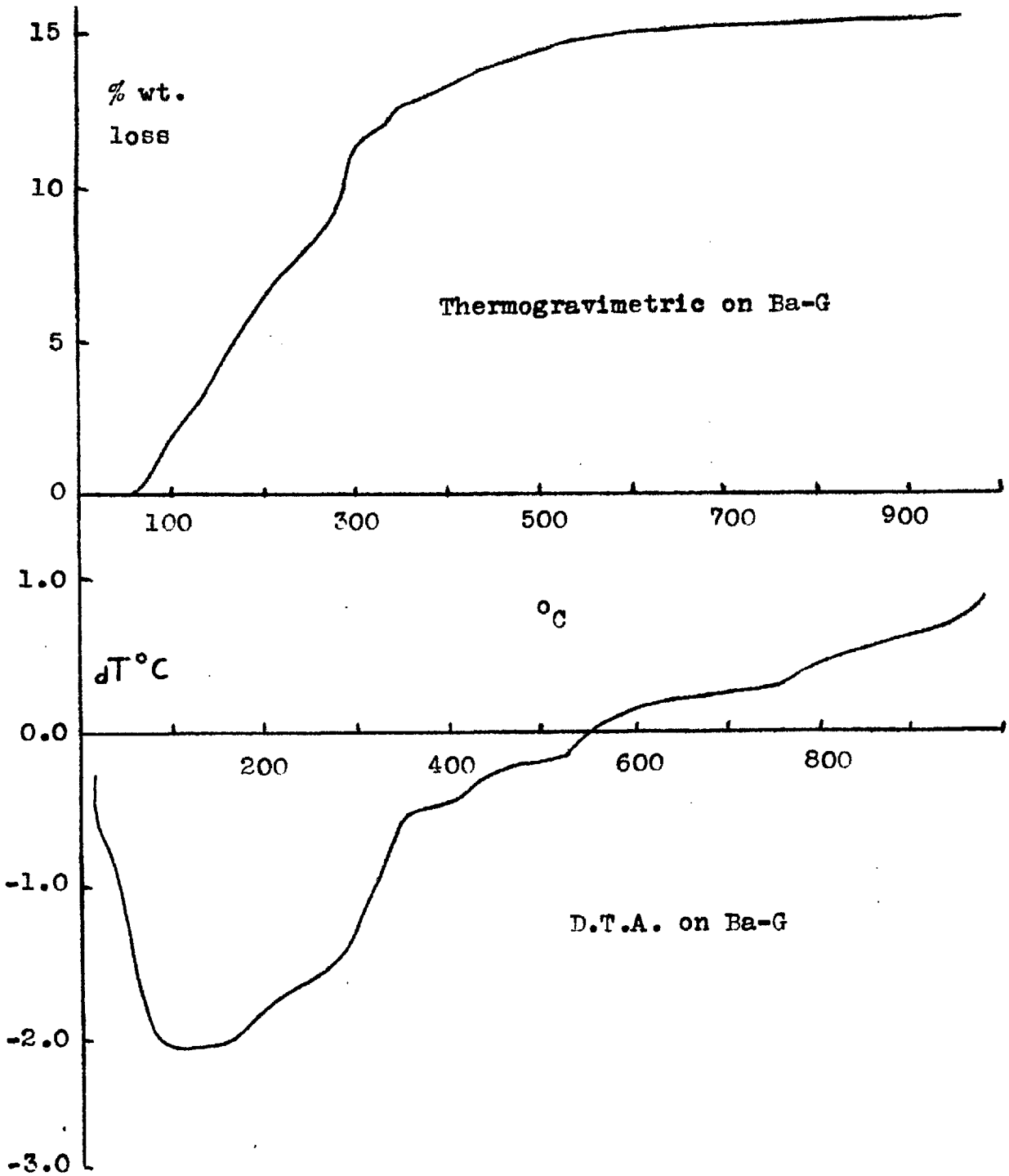

15
% wt.
loss
10
5
0
100
300
500
700
900
Thermogravimetric on Ba-G
1.0
°C
dT°C
0.0
200
400
600
800
-1.0
D.T.A. on Ba-G
-2.0
-3.0

FIG. 22.

is believed to be low. There is a total weight loss of 15% which follows the pattern of water loss from a zeolite. A qualitative ion-exchange experiment carried out on a small sample showed that the barium present could readily be replaced by sodium, without any noticeable effect on the X-ray powder pattern.

The X-ray powder pattern of this species is given in Table A24. It was not found possible to identify it with the pattern of any known zeolite, but the first 21 lines were indexed on the tetragonal system to give a unit cell with the parameters a=18.89Å, c=15.16Å.

Ba-J. This species occurred in a limited region of the crystallisation field, being formed from gels with a silica:alumina ratio between 7:1 and 9:1, at 250°C and 300°C. It was very often mixed with other species, particularly Ba-M and Ba-K. The best yields were obtained from gels of composition $BaO.Al_2O_3.8SiO_2$ after a number of days at 300°C (Table 27), but it was not possible to predict with certainty whether a particular gel under these conditions would give Ba-J or Ba-K or a mixture of the two. The crystals showed an irregular fibrous habit with some tendency towards spherulitic forms (Plate 18).

The results of differential thermal and thermogravimetric analysis are shown in Fig. 23. The sample

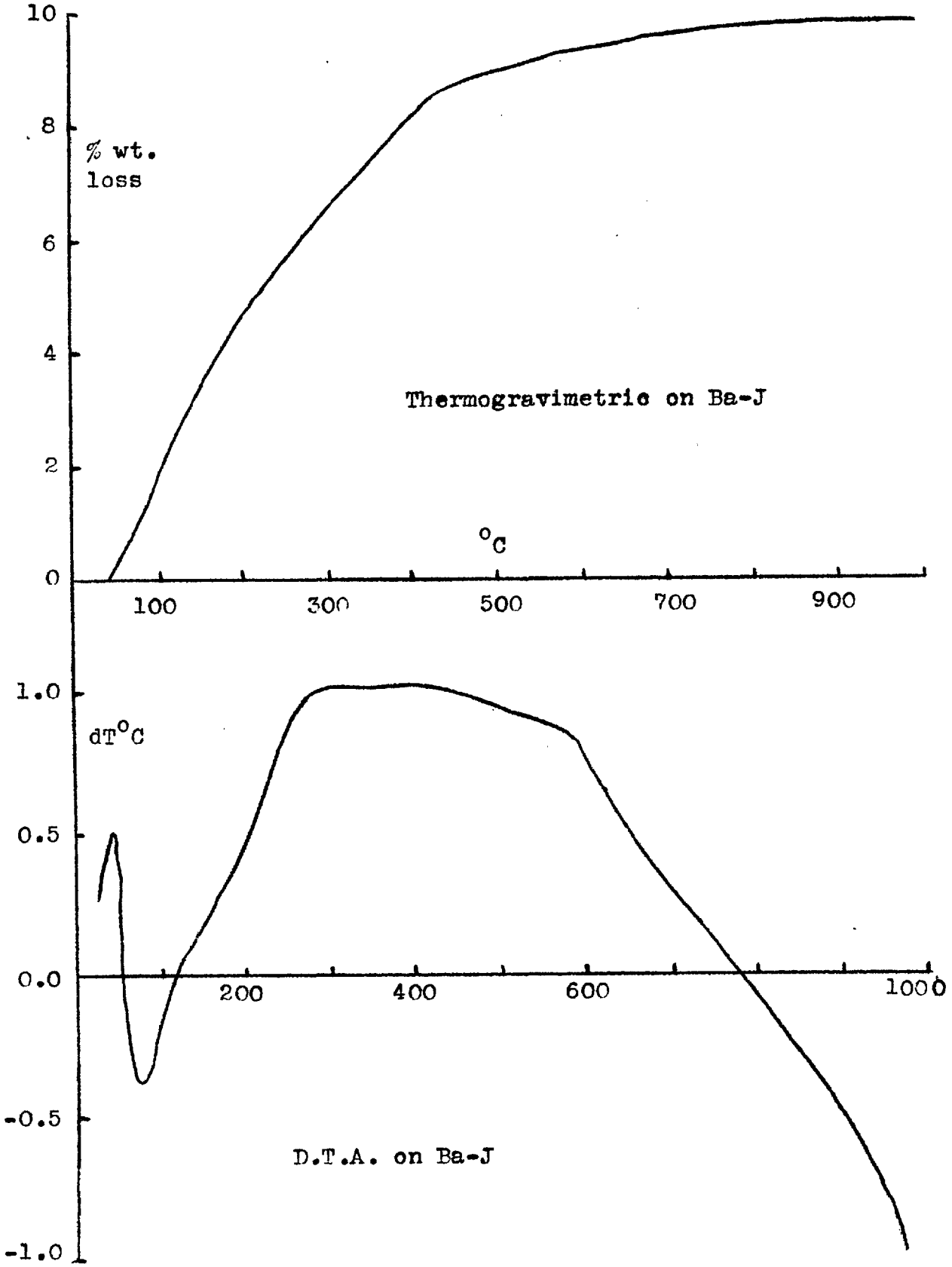

10
8
% wt.
loss
6
4
2
0
Thermogravimetric on Ba-J
°C
100
300
500
700
900
1.0
dT°C
0.5
0.0
200
400
600
1000
-0.5
D.T.A. on Ba-J
-1.0

FIG. 23.

lost 8.9% below 450°C and a further 1% between 450°C and 1,000°C, which is typical of a zeolite, although the percentage lost is somewhat low, indicating that even the best sample may have contained some amorphous material. The d.t.a. trace is also compatible with zeolitic behaviour, and the steep downward slope of the base line can probably be explained by the observation that X-ray examination showed that the sample had been completely destroyed by ignition. It was found that at saturation Ba-J took up 59 cc at N.T.P. of oxygen per gram of hydrated sample at 90°K (Fig. 24).

The X-ray pattern of the species is given in Table A21, but it was not found possible to match it with that of any known natural zeolite.

Ba-K. This was another zeolitic species which occurred in much the same region of the crystallisation field as Ba-J. It was formed from gels in which the silica:alumina ratio was 7:1 and 8:1 at 300°C and 9:1 at 340°C. At the lower temperature it was often mixed with Ba-J or Ba-P. The species crystallised well in a distinctive variation of the spherulitic habit (Plate 19) although even the best samples may have contained some amorphous silica.

The results of differential thermal and thermogravimetric analysis are shown in Fig. 25. The sample

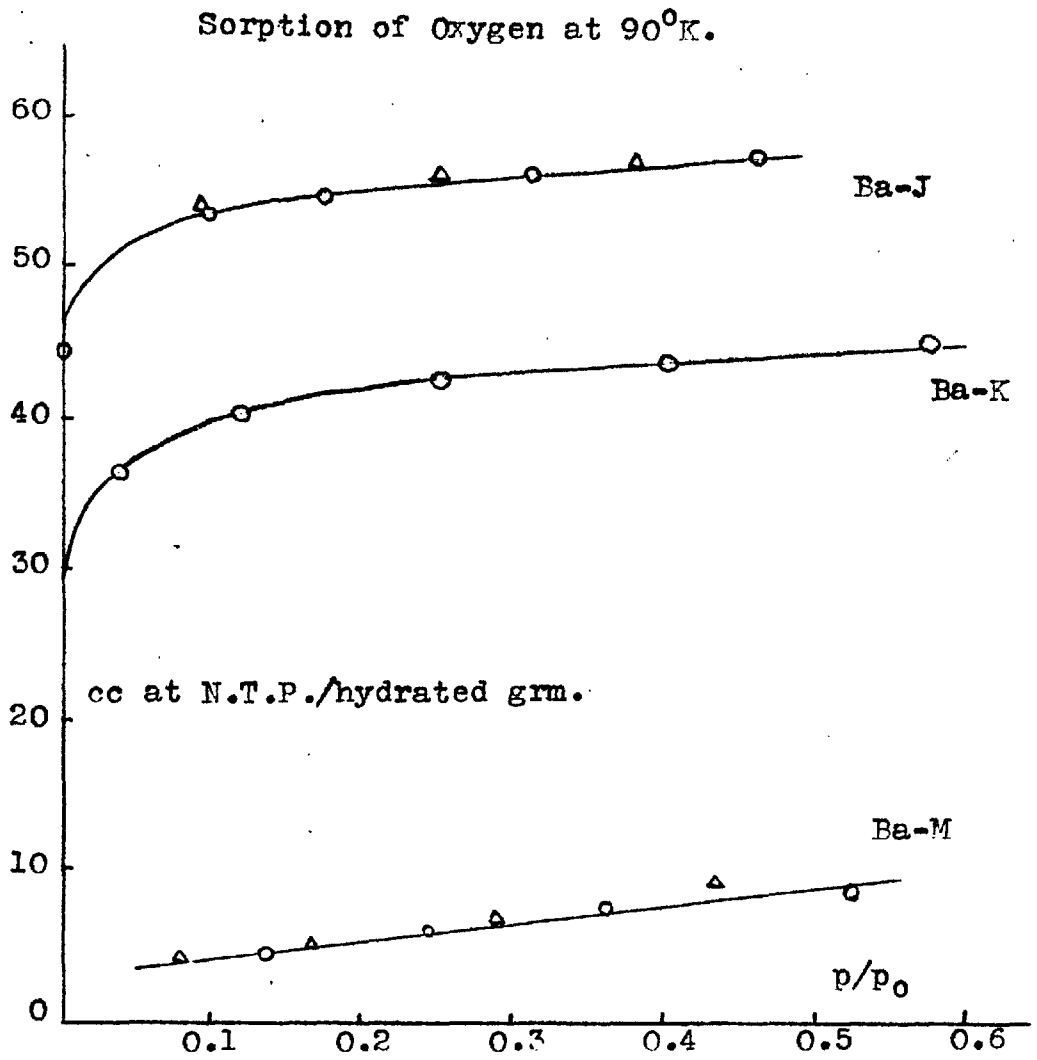

Sorption of Oxygen at 90°K.
60
50
40
30
20
10
0
Ba-J
Ba-K
Ba-M
cc at N.T.P./hydrated grm.
p/p0
0.1
0.2
0.3
0.4
0.5
0.6

FIG. 24.

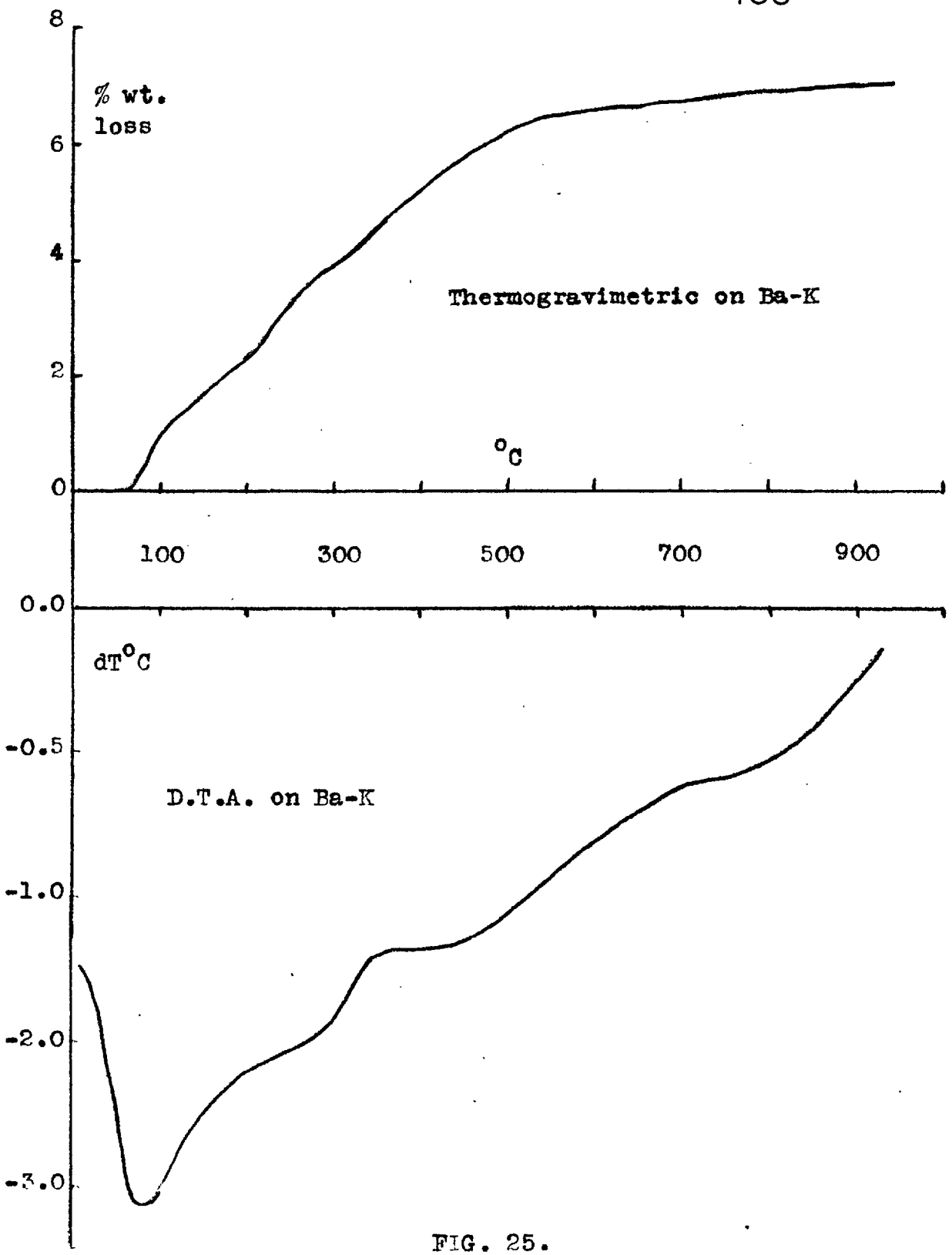

8
% wt.
loss
6
4
2
0
Thermogravimetric on Ba-K
°C
100
300
500
700
900
0.0
dT°C
-0.5
D.T.A. on Ba-K
-1.0
-2.0
-3.0

FIG. 25.

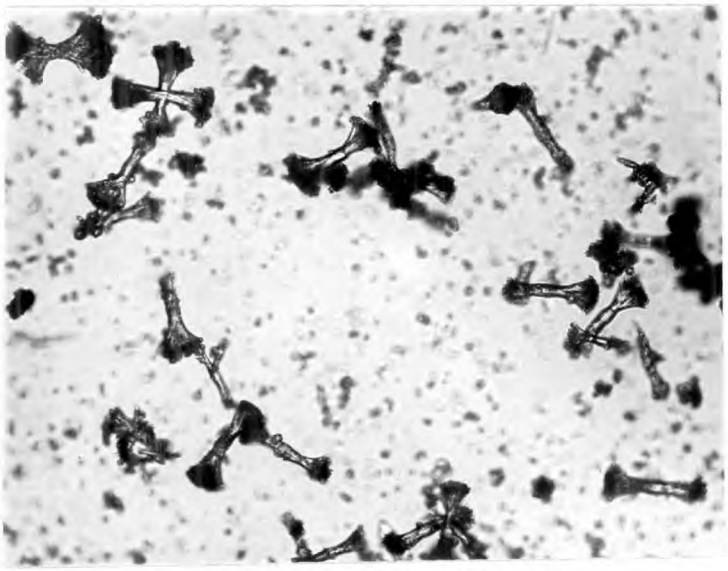


PLATE 19. Ba-K. 250 x

lost a total of 7% by weight on ignition to 950°C and had already lost 6% at 460°C, and this together with the shape of the d.t.a. curve indicated that the species might be a zeolite. This was confirmed by the observation that the outgassed sample had a sorption capacity at saturation of 46 cc of oxygen at N.T.P. per gram of hydrated sample at 90°K (Fig. 24).

Itwas found that one sample of Ba-K withstood a brief heating to about 1000°C without decomposition, but other samples were destroyed. The X-ray powder pattern is given in Table A21,but it was not possible to identify this species with any known zeolite.

Ba-M. Harmotome. This zeolite was produced in good yield between 200°C and 250°C from gels whose silica: alumina ratio was between 7:1 and 8:1, and small amounts were also formed at 250°C down to a silica:alumina ratio of 5:1. The optimum conditions of formation were found with gels of composition $BaO.Al_2O_3.7.5SiO_2$ at 220°C or 250°C for about three weeks. The crystals often display the cruciform twinning characteristic of the naturally occurring mineral which has the ideal formula $BaO.Al_2O_3.6SiO_2.6H_2O$ (Plate 20).

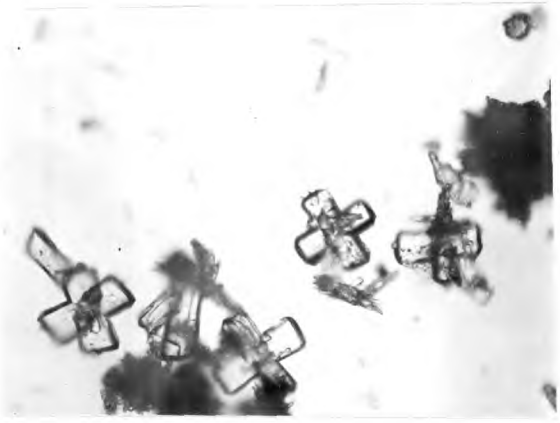


PLATE 20. Ba-M.
Harmotome. 320 x

The results of differential thermal and thermogravimetric analysis are presented in Fig. 26. The sample showed a weight loss of 11.5%, of which 10.6% was lost below 450°C, and the d.t.a. trace showed three endothermic peaks below 450°C, as did that of the Ca-harmotome obtained by Denny(42). The natural mineral

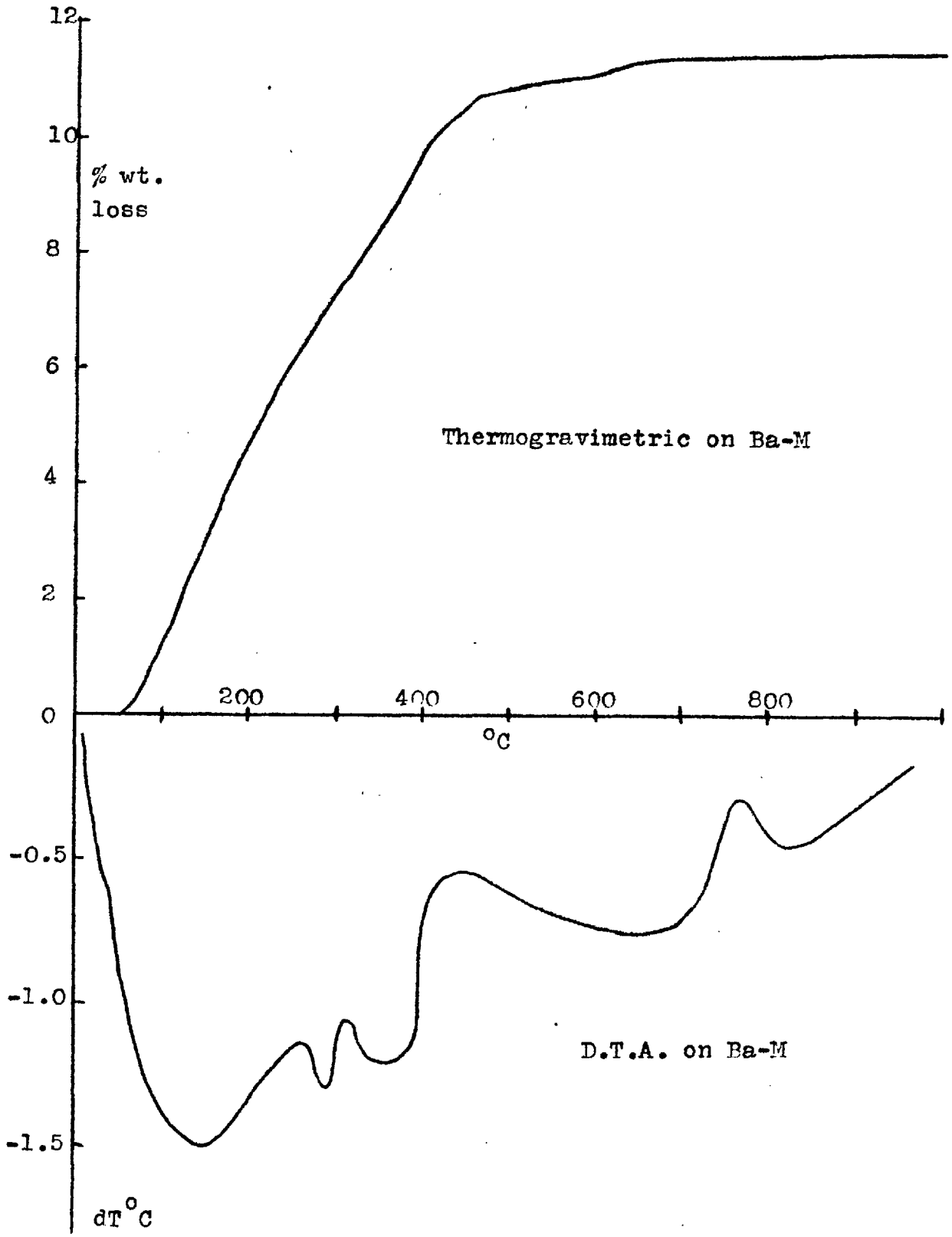

12
10
% wt.
loss
8
6
4
2
0
200
400
600
800
°C
Thermogravimetric on Ba-M
-0.5
-1.0
-1.5
dT °C
D.T.A. on Ba-M

FIG. 26.

has a water content between 13.9% and 15.0% and from analyses in the literature it would seem that the silica: alumina ratio can vary between about 4.5:1 and 7:1. This indicates that the yield of harmotome in these syntheses was of the order of 80%, the rest being amorphous silica. The harmotome did not sorb oxygen at 90°K to any appreciable extent, (Fig. 24), which also accords with the properties of the natural material.

The X-ray powder pattern of this species is given in Table A22. It is very close to that of the natural mineral, which is monoclinic, although it can be considered as pseudorhombic[44].

Ba-A. This species was formed from gels with the composition $BaO.Al_2O_3.SiO_2$ between 250°C and 380°C, the optimum yields being obtained at 300°C and 340°C, mixed with some barium carbonate which could readily be removed by washing with dilute hydrochloric acid (Table 18). The crystals were very small and did not display any distinctive habit.

The results of differential thermal and thermogravimetric analysis are shown in Fig. 27. Ba-A shows a total weight loss of 3.2% at 1,000°C with a steady loss of 2.3% between 400°C and 800°C associated with an endothermic peak on the d.t.a. curve having its maximum at 600°C.

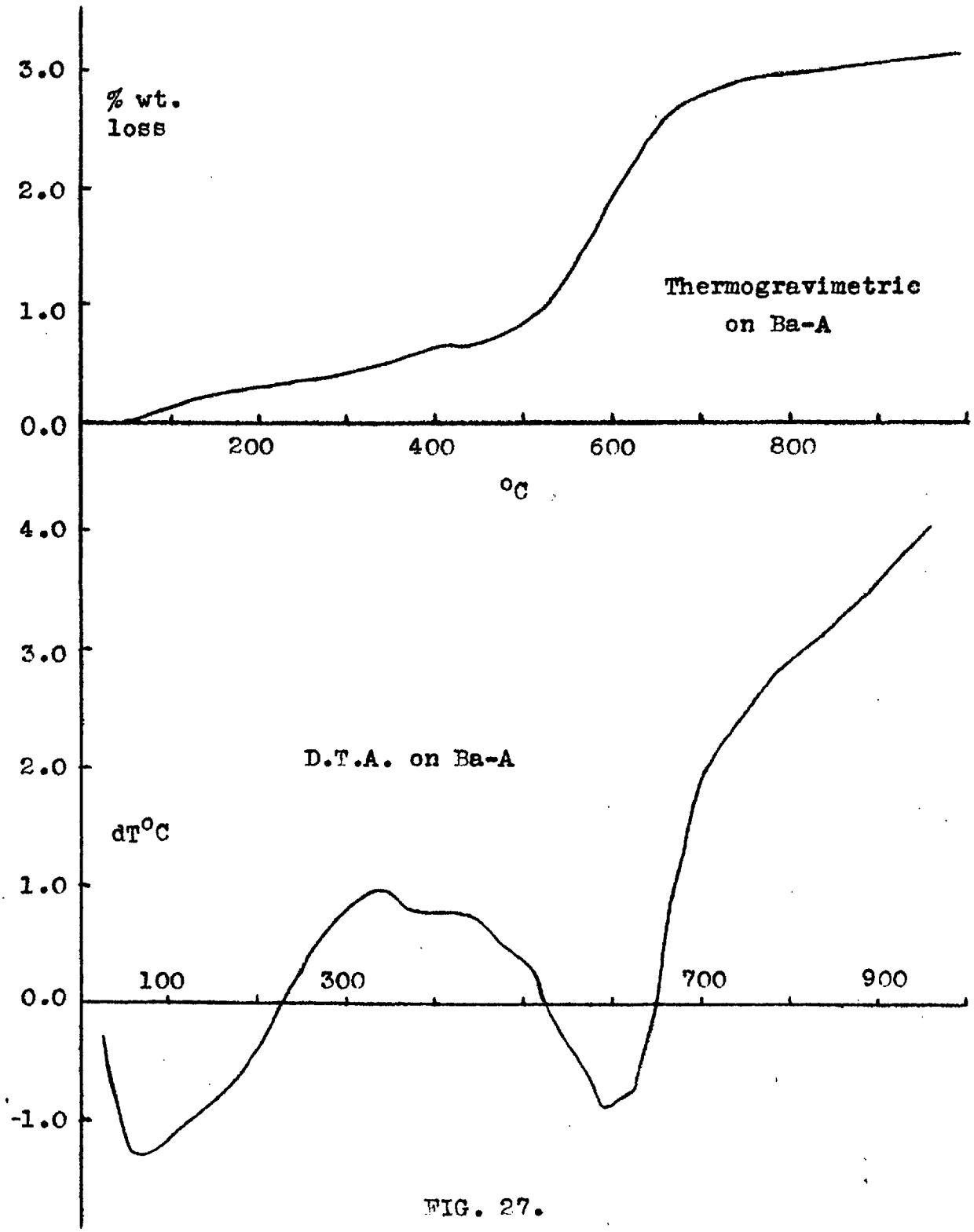

3.0
% wt.
loss
2.0
1.0
0.0
Thermogravimetric
on Ba-A
200
400
600
800
°C
4.0
3.0
2.0
D.T.A. on Ba-A
dT°C
1.0
100
300
700
900
0.0
-1.0

FIG. 27.

This behaviour could be explained by the presence of hydroxyl groups in the structure, which are driven off on ignition, although the infra red spectra of the species did not show the characteristic hydroxyl peak.

The X-ray powder pattern of Ba-A was very similar to that of the synthetic celsian, Ba-C. There were a few additional lines and a number of small shifts and intensity changes. The pattern of an ignited sample showed a few differences from that of the fresh sample, a number of the lines having shifted slightly, but the pattern did not become identical to that of Ba-C.(Table A23). The infra-red spectrum of Ba-A was also very similar to that of celsian, with the addition of a peak at 11.4μ, which was altered to 11.1μ in the ignited sample. The X-ray data indicates that the structure of Ba-A is closely related to that of celsian, the structure apparently being slightly altered to accommodate an hydroxyl or other volatile group. The possibility of the product being a mixture of species is ruled out by the sharp and reproducible nature of the powder pattern. Ba-A would therefore seem to be a new species.

Ba-Z. This species was formed from gels of composition $BaO.Al_2O_3.8SiO_2$ at 340°C and once from a gel of composition $BaO.Al_2O_3.9SiO_2$ at 300°C. It was never

produced pure and was usually only present in small amounts. In the best sample Ba-Z crystallised as large spherules (Plate 21) but it was not possible to identify the species by means of its X-ray powder pattern (Table A19) and there was insufficient material available to carry out other tests.

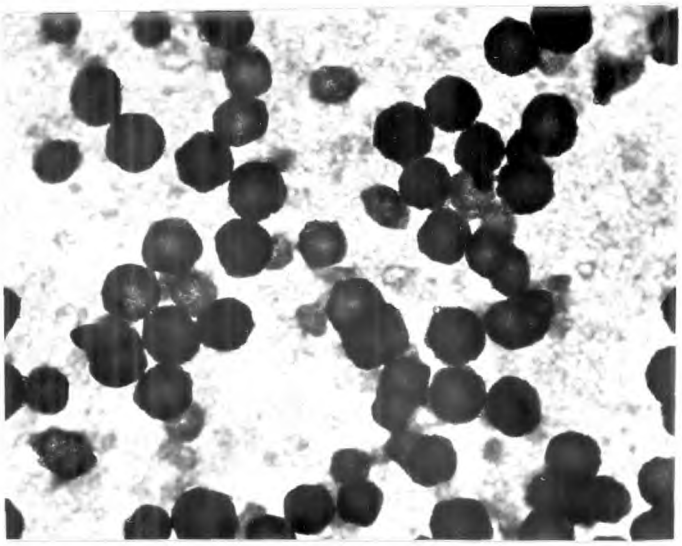


PLATE 21. Ba-Z. 245 x.

9. GENERAL DISCUSSION

The syntheses reported in this work and in previous work in these laboratories have been presented so as to define the crystallisation fields of the major species on a plot of temperature against silica:alumina ratio. The crystallisation fields for different species often overlap and usually the boundaries cannot be sharply drawn. These fields cannot be related to a simple thermodynamic concept, as, for instance, can stability fields, whose boundaries are definite, although it may be difficult to determine them accurately in a given experimental case. A crystallisation field indicates a complex thermodynamic and kinetic relationship between the given starting materials and the product species under the specified conditions. The crystallisation field of a species may be altered or eliminated by an alteration in the nature of one of the starting materials, e.g. by replacing silica sol by powdered silica glass[42]. Despite these limitations it is of some interest to compare the crystallisation fields of the major species obtained in the hydrothermal synthesis of the calcium, strontium and barium aluminosilicates. In the case of the calcium aluminosilicates[42] only those products obtained from gels using silica sol, as in the present work with strontium and barium, will be directly

compared.

It was found that there is a steady decrease along the series from calcium to barium in the region of the field which showed little or no crystallisation after comparable times. Greenberg has shown that in the case of $Ca(OH)_2$ the Ca^{++} cations are strongly adsorbed by silica gel[173]. The surface of the silica gel is believed to be covered with acidic -SiOH groups. These dissociate weakly and the system calcium hydroxide-silica gel acts as a strong base with a weak acid. Therefore on adding silica gel to a solution of calcium hydroxide there is a sharp fall in the pH of the solution and the cations are tightly bound to the surface of the gel. Evidence that this occurs also in the case of strontium and barium is found in the observation that the products from low temperature runs with gels of high silica content were completely amorphous gels, which, even after thorough washing, produced on ignition the hexagonal polymorph of the strontium or barium felspar. Since, in general, hydrothermal crystallisation of aluminosilicates is favoured by a high pH of the mother liquor, this effect would tend to suppress the crystallisation at low temperatures of gels with a high silica content. However, these considerations would apply approximately equally to each of the systems, leading to

poor crystallisation in that region of the field in each case. The increase in the reactivity down the series can probably be attributed to the very considerably enhanced solubility and increased basicity of the hydroxide of strontium compared with calcium, and of barium compared with strontium.

The synthesis of the hexagonal polymorphs of the felspars also shows a variation along the series. In each case the species was produced from gels having a wide range of silica:alumina ratios, particularly from runs of short duration. It was observed that in longer runs there was a tendency for the hexagonal phase to be replaced by the other forms of felspar, Ca-F, Sr-C, and Ba-C respectively. This, together with the results obtained by Sorrel[137] make it very probable that this is a metastable species. It is possible that the formation of the hexagonal phase is catalysed by the alkali earth cations, or possibly by hydroxide ions, since the crystallisation field moves progressively further into the silica rich region in going from calcium to barium. The unit cell dimensions show a regular progression and the X-ray powder patterns are very similar, so that the compounds form a clear sequence of structural analogues. A similar compound of lead, $PbO.Al_2O_3.2SiO_2$, has been

reported[137]. The unit cells of the hydrothermally prepared calcium, strontium and barium hexagonal felspar are tabulated, together with that of the pyrolytically prepared lead compound in table 30.

TABLE 30 Hexagonal felspars, $MO.Al_2O_3.2SiO_2$.

M	Cation radius (Å)	a (Å)	c (Å)	unit cell volume (Å^3)
Ca	1.05	5.10	7.44	502.7
Sr	1.18	5.19	7.59	531.2
Ba	1.40	5.33	7.72	569.8
Pb	1.28	5.25	7.60	544.2

There is a linear relationship between the unit cell volume and the cation radius, but not between the c-axis dimension and the cation radius. This indicates that the introduction of a larger cation does not merely push the parallel sheets further apart but that the channels in the framework of the layers expand slightly to accommodate it (see figure 3, p. 16).

It is not easy to discern any clear trend in the case of the other felspar polymorphs, however, particularly as Sr-C, the felspar obtained in the strontium

field, is not of the same monoclinic type as the synthetic anorthite and celsian obtained in the other two cases. In general, the monoclinic felspars do not crystallise from such a wide range of compositions as the hexagonal polymorphs. The crystallisation field of synthetic celsian is particularly limited since it only forms from gels with a silica:alumina ratio between 1:1 and 4:1. Although Ca-F and Sr-C are produced from gels with silica:alumina ratios up to 9:1 the crystallinity of the products is very poor in the case of the higher ratios. An anorthite type strontium felspar has been produced in sintering reactions by Dear[136] and also in this work, but it does not appear to be formed hydrothermally. This could be a kinetic effect following Ostwald's rule, but the reproducible and persistent formation of Sr-C, and the fact that it is unaffected by at least 24 hours treatment at 1000°C suggests that it may be a stable phase. The crystals produced were well formed laths, but they were too small to be suitable for X-ray examination by single crystal methods. Attempts to grow larger crystals were made by seeding the parent gel at high temperatures. This was not successful and no systematic attempt to grow large crystals was made.

A notable feature of previous work in these laboratories has been the very ready growth of minerals

with the analcite structure, both cubic and tetragonal, hydrated and anhydrous. In the case of calcium aluminosilicate gels a tetragonal analcite similar to the natural mineral wairakite was produced from a very wide range of compositions and temperatures, although never in 100% yield. A cubic form was also produced in rather better yield at higher temperatures. Both forms were hydrated. However, strontium analcite was obtained only once in the present investigations and barium analcite was not synthesised at all. If the cubic hydrated analcites only are considered then it is found that the minimum temperature at which they are observed to form hydrothermally under roughly comparable conditions increases with increase in cation radius, as shown in table 31.

TABLE 31 Minimum temperatures of formation of hydrated cubic analcites.

Cation	Ionic radius (Å)	Temperature	Reproducibility
Na^+	0.98	150°C	good
Ca^{++}	1.05	300°C	good
Sr^{++}	1.18	380°C	v. poor
K^+	1.33	400°C	good
Ba^{++}	1.40	-	-
NH_4^+	1.43	450°C	moderate

Since these temperatures do not refer to a true lower limit of stability no very definite conclusions may be drawn from them. It does seem that it becomes more difficult to synthesise hydrated cubic analcites as the cation radius increases although anhydrous tetragonal phases are formed readily at lower temperatures with larger cations such as rubidium and thallium and an anhydrous cubic caesium analcite is produced at about 120°C. Although the cavities in the structure of analcite are large enough to contain the ions of strontium and barium the maximum diameters of the channels through the framework are 2.3Å for the six-membered ring, and 2.4Å for the eight-membered ring. Also only small amounts of bivalent ions can be introduced into the analcite structure by ion-exchange[163]. One would not therefore expect the barium ion to be able to diffuse through the analcite structure, although Barrer and Rees did find that even caesium could migrate through the structure, but the process was very slow[174]. The size of the cation, or cation plus water, considerably influences the synthesis of the analcite framework, and it appears that at the temperatures which would be necessary to form a strontium or barium analcite the more compact felspar structure is the more stable phase.

The crystallisation field of barium harmotome shows some differences when compared with that found in

the case of the harmotome-phillipsite family for other cations. In the case of sodium the species Na-P was grown at all silica:alumina ratios from n=1 to n=12, in the temperature range 60° to 250°C. It grew best when the parent gel contained a 200 or 300% excess of sodium hydroxide. The X-ray powder pattern was not identical with that of the natural mineral and the compound, whose composition varied from $Na_2O.Al_2O_3.3.3SiO_2.4.3H_2O$ to $Na_2O.Al_2O_3.5.3SiO_2.5.7H_2O$ occurred in cubic, tetragonal and orthorhombic modifications[67,178]. An orthorhombic potassium phillipsite having approximately the same framework structure was synthesised between 200° and 300°C from gels in which n varied from 1 to 7, and at slightly lower temperatures with excess alkali and a higher silica ratio[128]. In the case of calcium little harmotome was obtained using silica sol in the parent gels, but with silica glass a tetragonal species of the harmotome-phillipsite family was produced at temperatures between 150°C and 300°C from gels with a silica:alumina ratio between 2 and 9, but most successfully when n=3 or 4[42]. A cubic harmotome type mineral was also produced with dimethyl ammonium as the cation[119]. According to the X-ray powder patterns none of these products were identical to the natural mineral and in general they had a composition with a lower silica:alumina ratio than ideal harmotome which is $BaO.Al_2O_3.6SiO_2.6H_2O$

and thus more akin to phillipsite. Barrer[175] produced a small yield of a compound very similar to the natural mineral by heating a gel of composition $BaO.Al_2O_3.3SiO_2$ plus excess $Ba(OH)_2$ at 220°C for two days followed by three days at 200°C. This result is a little surprising in the light of the present work. Harmotome, with an X-ray powder pattern identical to that of the natural mineral, was formed from gels with n between 7 and 8 at temperatures between 150° and 250°C and also in poor yields at 250°C when n=6 or 5. However this difference can probably be attributed to the presence of excess hydroxide in Barrer's synthesis and to unknown differences in the starting materials and methods. It is interesting to note that the natural monoclinic mineral always occurs with barium as the predominant cation, usually together with some potassium, which has a similar ionic radius, as the secondary cation. In view of the non-appearance of a strontium harmotome in the present investigation it seems quite likely that it would not be formed in nature, even if there was a sufficient concentration of strontium in a suitable environment. Sadanaga et al[44] have concluded that the space occupied by a barium ion in harmotome is too large for it to be satisfactorily filled by a calcium ion and that it does not seem possible to contract the co-ordination polyhedron by simple shifts of the neighbouring oxygen atoms so as to

fit a calcium ion. Hence they conclude that although harmotome and phillipsite have the same basic structure, there are differences in the dispositions of the cations and water molecules, and even perhaps slight changes in the framework. This has since been confirmed[179] but the exact structures of the previously synthesised synthetic species, although clearly of the same general type, are still not conclusively determined[178].

Although many micas have been synthesised from the melt[176,182] and micas of the muscovite type have been quite readily synthesised by hydrothermal methods[12], micas have been of rare occurrence from the typical parent gels used in this work, and the only examples are paragonite [127] and an ammonium mica produced by Barrer and Denny[119]. The hydrothermal synthesis of brittle micas of the margarite type containing divalent cations has in general proved more difficult, although a synthesis of margarite has been reported by Thu-Huan Chi[177].

This being so it is interesting that a strontium mica should be formed in moderate or good, though not 100%, yield with quite good reproducibility. An examination of the mica-structure does not give any indication that the size of the alkali cation will be a limiting factor preventing the growth of a barium mica, and indeed barium rich muscovite has been reported to occur naturally[180,181].

In this work however barium mica did not form in sufficient amounts to be detected by X-ray methods. Nevertheless on one occasion a gel of composition $BaO.Al_2O_3.SiO_2$ which had been treated at 435°C for 5 days was shown by the electron microscope to contain a number of flaky hexagonal crystals (Plate 22) which had the appearance of a mica and gave a



PLATE 22. Possibly barium mica
2,850 x

clear hexagonal electron diffraction pattern with a repeat distance in the a direction of 5.45Å. There was no evidence for the presence of a mica from the X-ray powder pattern, nor was it produced in noticeable quantities from gels of the optimum composition, $BaO.2Al_2O_3.2SiO_2$ at 435°C. Since the growth of micas is generally favoured by rather more acidic conditions it might be that the greater basic strength of the barium hydroxide,

compared with strontium hydroxide, operates against the formation of barium mica under the conditions used in this work. Against this suggestion must be set the fact that the mother liquor in the example quoted above was particularly alkaline.

With regard to the crystallisation processes involved in hydrothermal synthesis the prevalence of spherulitic growth, particularly among the zeolites produced, has been very striking. Also both among these species and those which grew as well-formed euhedral crystals, such as Sr-C and Sr-N, it was noticeable that all the crystals from a given autoclave were small and very uniform in size. This seems to suggest the solution suddenly produces a dense shower of nuclei which grow rapidly until the parent solution is exhausted. The occurrence of spherulitic growth also suggests that many of the species grew under conditions of high super-saturation. These qualitative observations are supported by the more quantitative work of Kerr[156] on the kinetics of formation of the Linde A and X zeolites. He showed that there was a period of induction followed by a period of rapid growth which continued at a logarithmic rate until the reactants were exhausted. He also found that the reaction was auto-catalytic and promoted by the presence of hydroxyl ions. The hypothesis based on these

results is that the amorphous solid starting materials dissolve rapidly to form a soluble active species, whose concentration remains constant during the growth period. The rate determining step is the reaction of this species with nuclei to form the crystalline zeolite. The Linde synthetic zeolites grow as very small crystals of a uniform size, although spherulitic growth is not normally observed, and it seems likely that the kinetics of formation for many species in the present work follow a similar pattern.

The synthesis of a number of apparently new zeolites in this work shows that the possibilities of linking together $[SiO_4]$ and $[AlO_4]$ tetrahedra into open frameworks are by no means exhausted. New structures can be obtained by slight changes in the conditions of the experiment or the reactants used, although there seems to be no way of predicting the results of such changes. The isolated and non-reproducible synthesis of a number of zeolites from strontium gels indicates that the production of a particular species may be governed by very minor variations in the circumstances of the experiment, which are difficult to control. It does not seem likely that any significant contamination by chemical impurities would have taken place so that if this is a source of variation it must be effective at

very low levels of concentration. In a few cases the interior surface of the autoclave appears to have entered into the reaction, and in others it may have exercised a catalytic effect on the nature of the products without being appreciably attacked. If this is the case such variations would be difficult to control without the use of an inert liner, and even the noble metals are not perfect in this respect. The autoclaves were cleaned between each run by scrubbing with an ordinary laboratory test-tube brush and rinsing well with water and finally distilled water. It was believed that an inert tightly adherent layer of oxides formed on the inner surface of the bomb and whilst this was true in the great majority of cases the surface film might have been damaged in a few cases, and thus perhaps permitted some catalytic effect on the reaction. Other possible sources of variation could be the amount of carbon dioxide adsorbed from the air whilst preparing the gels and small variations in the temperature or concentration of the reactants. All these variables would be small and difficult to eliminate, and it would be hard to determine whether they did in fact cause the variation in the products observed.

Summary

The products obtained in the work have been reviewed and comparisons made between those obtained in the calcium, strontium and barium fields. Possible effects arising from the variation of ion size and alkalinity of the respective hydroxides have been discussed. Factors affecting the crystallisation and reproducible growth of a number of the products have been considered.

Workers in these laboratories have now studied a similar region of the crystallisation field for the aluminosilicates of the alkali and alkaline earth metals except radium. Except in the case of caesium, where only two species were observed[129], a wide range of products has normally been produced. Under the alkaline conditions employed the formation of framework structures has been favoured. Felspars, in the high temperature form, have been produced in the case of sodium, potassium, rubidium, calcium and barium, and a felspar polymorph in the case of strontium. It would seem that lithium and caesium are respectively too small and too large to fit into the felspar framework. Species having the analcite structure or its anhydrous analogue have been produced containing each of the metal cations except lithium and barium. Nine zeolites, identical or very similar to naturally

occurring minerals, have been synthesised, in four cases with two or more different metals. A further eight zeolites have been produced which have not been identified with any naturally occurring counterparts. Besides these, several felspathoids, two micas, and a number of unidentified products have been produced.

10. REFERENCES

1. V. M. Goldschmidt, "Geochemistry", Clarendon Press, Oxford.

2. L. Pauling, J.Amer.Chem.Soc., 51, 1010, 1929.

3. W. Loewenstein, Amer.Min., 39, 92, 1954.

4. W. L. Bragg, "Atomic Structure of Minerals", O.U.P., for Cornell U.P., 1937.

5. C. Mauguin, (a) Compt.Rend.Acad.Sci., 185, 288, 1927; (b) Compt.Rend.Acad.Sci., 186, 879, 1928; (c) Compt.Rend.Acad.Sci., 186, 1131, 1928.

6. L. C. Pauling, Proc.Nat.Acad.Sci.,Wash., 16, 123, 1930.

7. W. W. Jackson and J. West, Z.Krist., 76, 211, 1930.

8. W. W. Jackson and J. West, Z.Krist., 85, 160, 1933.

9. S. B. Hendricks and M. E. Jefferson, Amer.Min., 24, 729, 1939.

10. H. S. Yoder, 6th Nat.Conf.Clays and Clay Minerals, p.42, 1959 (Pergamon Press, London).

11. J. V. Smith and H. S. Yoder, Min.Mag., 31, 209, 1956.

12. H. S. Yoder and H. P. Eugster, Geochim. et Cosmochim. Acta, 8, 225, 1955.

13. A. A. Levinson, Amer.Min., 40, 41, 1955.

14. R. E. Grim and R. A. Rowland, Amer.Min., 27, 746, 1942.

15. R. E. Grim and R. A. Rowland, Amer.Min., 27, 801, 1942.

16. R. Roy, J.Amer.Ceram.Soc., 32, 202, 1949.

17. V. S. Fadeev and L. P. Ivanova, Trudy Issledovaniya Tekhol. Proizvodstra Gruboi Keram, 5, 103, 1951.

18. I. M. Threadgold, Amer.Min., 44, 488, 1959.

19. W. M. Taylor, Z.Krist., 85, 425, 1933.

20. W. M. Taylor, J. A. Darbyshire and M. Strunz, Z.Krist., 87, 464, 1934.

21. T. F. W. Barth, Amer.J.Sci., 27, 273, 1934.

22. W. F. Cole, H. Sörum and O. Kennard, Acta Cryst., 2, 280, 1949.

23. S. W. Bailey and W. M. Taylor, Acta Cryst., 8, 621, 1955.

24. H. Sörum, Acta Cryst., 6, 413, 1953.

25. R. E. Newnham and H. D. Megaw, Acta Cryst., 13, 303, 1960.

26. R. B. Ferguson, R. J. Traill and W. M. Taylor, Acta Cryst., 11, 331, 1958.

27. P. Gay, Acta Cryst., 9, 474, 1956.

28. C. J. E. Kempster, Ph.D. Thesis, Camb. Univ., 1957.

29. A. S. Ginzberg, Ceram. Absts., 3, 136, 1924.

30. E. Dittler and H. Lasch, Anzeiger Akad. Wiss. Wien, Math.naturwiss.Kl., 67, 201, 1930.

31. R. H. Thomas, J.Amer.Ceram.Soc., 33, 35, 1950.

32. B. Yoshiki and K. Matusmoto, J.Amer.Ceram.Soc., 34, 283, 1951.

33. B. Yoshiki, S. Koide and M. Waki, Reports Research Lab.Asahi Glass Co., 3, 135, 1953.

34. T. Ito, "X-ray studies on polymorphism", p. 19, Maruzen, Tokyo, 1950.

35. Y. Takeuchi, Min.J.Japan, 2, 311, 1958.

36. W. C. Smith, F. A. Bannister and M. H. Hey, Min.Mag., 28, 676, 1949.

37. J. V. Smith, Acta Cryst., 6, 613, 1953.

38. W. Eitel, "Physical Chemistry of the Silicates", p. 63, Univ. of Chicago Press, 1954.

39. G. C. Davies and O. F. Tuttle, Amer.J.Sci.Bowen Vol., 107, 1952.

40. G. Donnay, Acta Cryst., 5, 153, 1951.

41. J. R. Goldsmith and E. G. Ehlers, J.Geol., 60, 386, 1952.

42. R. M. Barrer and P. J. Denny, J.Chem.Soc., 983, 1961.

43. U. Ventriglia, Periodico Miner. Rome, 24, 49, 1955.

44. R. Sadanaga, F. Marumo and Y. Takeuchi, Acta Cryst., 14, 1153, 1961.

45. M. H. Hey, Min.Mag., 22, 422, 1930.

46. W. O. Milligan and H. B. Weiser, J.Phys.Chem., 41, 1029, 1937.

47. J. Wyart, Compt.Rend., 191, 1343, 1930.

48. O. Weigel, Z.Krist., 58, 183, 1923.

49. O. Glemser, Z.anorg.Chem., 252, 305, 1944.

50. J. V. Smith, Quoted by R. F. Bartholomew, Ph.D. Thesis, London Univ., 1961.

51. R. M. Barrer and W. M. Meier, Trans.Farad.Soc., 54, 1074, 1958.

52. R. M. Barrer, Proc.Chem.Soc., 99, 1958.

53. R. M. Barrer, Ann.Reports, 41, 31, 1944.

54. L. A. Garden, G. L. Kington and W. Laing, Trans.Farad.Soc., 51, 1558, 1955.

55. P. H. Egli and S. Zerfoss, Discuss.Farad.Soc., 5, 61, 1949.

56. M. Volmer and A. Weber, Z.Phys.Chem., 119, 227, 1925.

57. R. Becker and W. Doring, Ann.Phys., 24, 719, 1935.

58. R. M. Barrer, J.Phys.Chem.Solids, 16, 84, 1960.

59. N. Cabrera and W. K. Burton, Discuss.Farad.Soc., 5, 40, 1949.

60. M. Volmer and H. Flood, Z.Physik.Chem., 170, 273, 1934.

61. J. Stauff, Z.Physik.Chem., 187, 107, 1940.

62. J. R. Goldsmith, J.Geol., 61, 439, 1953.

63. E. L. Brady, J.Phys.Chem., 57, 706, 1953.

64. W. S. Fyfe and D. S. McKay, Amer.Min., 47, 83, 1962.

65. G. W. Money and W. T. Chen, Amer.Min., 40, 996, 1955.

66. G. W. Devore, Proc.6th Nat.Conf.Clays and Clay Minerals, 1957 (Publ. 1959).

67. R. M. Barrer, J. W. Baynham, F. W. Bultitude and W. M. Meier, J.Chem.Soc., 195, 1959.

68. W. J. Dunning Discuss.Farad.Soc., 5, 79, 1949.

69. H. E. Buckley, "Crystal Growth", 1951.

70. Faraday Discussions, Vol. 5, Symposium on Crystal Growth, 1949.

71. "Growth and Perfection of Crystals", Proc.Internat. Conf. on Crystal Growth, U.S.A., 1958.

72. W. Kossel, (a) Nach.Ges.Wiss.Gottingen Math.physik. Klasse, 135, 1927.
(b) Physik Z., 29, 553, 1928.

73. I. N. Stranski, Discuss.Farad.Soc., 5, 13, 1949.

74. W. K. Burton and N. Cabrera, Discuss.Farad.Soc., 5, 33, 1949.

75. C. W. Bunn and H. Emmett, Discuss.Farad.Soc., 5, 119, 1949.

76. A. F. Seager, Min.Mag., 30, 1, 1953.

77. M. Volmer and W. Schultze, Z.Physik.Chem.A, 156,1,1931.

78. F. C. Frank, Discuss.Farad.Soc., 5, 48, 1949.

79. F. C. Frank, Adv. in Phys., 1, 91. 1952.

80. W. K. Burton and N. Cabrera, Phil.Trans.Roy.Soc., A.243. 299, 1951.

81. C. M. Heck, Phys.Revs., 51, 686, 1937.

82. L. J. Griffin, Phil.Mag., 42, 1337, 1951.

83. I. M. Dawson and V. Vand, Proc.Roy.Soc., 206A, 555, 1951.

84. A. J. Forty, Phil.Mag., 43, 72, 1952.

85. A. J. Verma, Phil.Mag., 43, 441, 1952.

86. A. J. Verma, Min.Mag., 31, 136, 1956.

87. D. Turnbull and J. C. Fisher, J.Phys.Chem., 17, 71, 1949.

88. O. Knacke, Z.Physik., 130, 259, 1951.

89. (a) H. W. Morse, C. H. Warren and J. D. H. Donnay, Amer.J.Sci., 23, 421, 1932;
(b) H. W. Morse and J. D. H. Donnay, Amer.J.Sci., 23, 440, 1932;
(c) H. W. Morse, J. D. H. Donnay and E. Ott, Amer.J.Sci., 25, 494, 1933.

90. H. W. Morse and J. D. H. Donnay, Amer.Min., 21, 391, 1936.

91. A. V. Shubnikov, Kristallografia, 5, 584, 1957.

92. R. M. Barrer and I. S. Kerr, J.Chem.Soc., in press.

93. G. W. Sears, J.Phys.Chem., 65, 1738, 1961.

94. J. W. Cahn and J. E. Hilliard, J.Chem.Phys., 31, 688, 1959.

95. J. E. Coleman, B. J. Allan and B. L. Vallee, Science, 131, 350, 1960.

96. R. M. Barrer, Discuss.Farad.Soc., 5, 326, 1949.

97. J. J. Frankel, Min.Mag., 28, 111, 1947.

98. G. R. Rigby and H. M. Richardson, Min.Mag., 28, 75, 1947.

99. E. Baur, Z.Physik.Chem., 48, 483, 1904.

100. I. D. Sedletsky, Compt.Rend.Acad.Sci.U.R.S.S., 17, 375, 1937.

101. J. H. Schulman, E. W. Claffy and R. J. Ginther, Amer.Min., 34, 68, 1949.

102. D. C. Stockbarger, (a) Rev.Sci.Inst., 7, 133, 1936; (b) Discuss.Farad.Soc., 5, 294, 1949; (c) Discuss.Farad.Soc., 5, 299, 1949.

103. S. Kyropoulos, (a) Z.anorg.Chem., 154, 308, 1926; (b) Z.Physik., 63, 849, 1930.

104. E. A. D. White, Quart.Revs., 15, 1, 1961.

105. A. Michel-Lévy, Discuss.Farad.Soc., 5, 325, 1949.

106. F. P. Bundy, H. T. Hall, H. M. Strong and R. H. Wentorf, Nature, 176, 51, 1955.

107. H. T. Hall, Rev.Sci.Instr., 31, 125, 1960.

108. L. Coes, Science, 118, 131, 1953.

109. F. Dachille and R. Roy, Z.Krist., 111, 451, 1959.

110. R. A. Laudise, J.Amer.Chem.Soc., 81, 562, 1959.

111. W. S. Fyfe, J.Geol., 68, 553, 1960.

112. W. S. Fyfe, F. J. Turner and J. Verhoogen, Geol.Soc.Amer.Mem. 73, 1958.

113. I. N. Stranski and D. Totomanov, Z.Phys.Chem., A.163, 399, 1933.

114. G. C. Kennedy, (a) Econ.Geol., 39, 25, 1944; (b) Econ.Geol., 45, 629, 1950.

115. F. G. Keyes, J.Amer.Chem.Soc., 72, 433, 1950.

116. E. U. Frank, Z.Phys.Chem., 8, 107, 1956.

117. H. S. Yoder, Amer.J.Sci. Bowen Vol., 569, 1950.

118. J. A. Wood, Amer.J.Sci., 256, 40, 1958.

119. R. M. Barrer and P. J. Denny, J.Chem.Soc., 983, 1961.

120. R. Mosebach, Neues.Jahrb.Min.Abhandl., 87, 351, 1955.

121. S. Glasstone, E. J. Laidler and H. Eyring, "Theory of Rate Processes", p. 433, 1941.

122. J. K. Fogo, S. W. Benson and C. S. Copeland, J.Chem.Phys., 22, 209, 1954.

123. G. W. Morey and P. Niggli, J.Amer.Chem.Soc., 35, 1086, 1913.

124. G. W. Morey and E. Ingerson, Econ,Geol., 32, 607, 1937.

125. G. W. Morey and C. N. Fenner, J.Amer.Chem.Soc., 39, 1173, 1917.

126. R. M. Barrer and E. A. D. White, J.Chem.Soc., 1167, 1949.

127. R. M. Barrer and E. A. D. White, J.Chem.Soc., 1561, 1952.

128. R. M. Barrer and J. W. Baynham, J.Chem.Soc., 2882, 1956.

129. R. M. Barrer and N. McCallum, J.Chem.Soc., 4029,1953.

130. H. F. W. Taylor, J.Chem.Soc., 1253, 1949.

131. E. T. Carlson and L. S. Wells, J.Res.Nat.Bur.Stand., 51, 73, 1953.

132. J. F. Corwin, R. G. Yalman, J. W. Edwards and E. R. Shaw, J.Phys.Chem., 61, 1437,1957.

133. J. F. Corwin, R. G. Yalman, J. W. Edwards and G. E. Owen, J.Phys.Chem., 61, 939, 1957.

134. R. M. Barrer, J.Chem.Soc., 127, 1948.

135. R. M. Barrer and D. W. Riley, J.Chem.Soc., 133, 1948.

136. P. S. Dear, Bull.Virg.Polytech.Inst., Eng.Expt. Station, Series 117, Vol.50, No.6,1957.

137. C. A. Sorrel, Amer.Min., 47, 291, 1962.

138. P. Eskola, Amer.J.Sci., 4, 331, 1922.

139. N. A. Toropov, F. Ya. Galakhov and I. A. Bondar,
(a) Izvest.Akad.Nauk.SSSR, Otdel.Khim.Nauk, 753, 1954;
(b) Izvest.Akad.Nauk.SSSR, Otdel.Khim.Nauk, 3, 1955.

140. W. Wislicenus, Z.agnew chem., 17, 805, 1904.

141. A. Guinier, Compt.Rend., 204, 1115, 1937.

142. "Index of X-ray Diffraction Data", 1960, American Society for Testing Materials.

143. W. Parrish and B. W. Irwin, "Data for X-ray Analysis", Vol. 1, Philips Tech.Lib. 1953.

144. L. V. Azaroff and M. J. Buerger, "The Powder Method in X-ray Crystallography", 1958.

145. R. A. Harrington, Rev.Sci.Inst., 9, 429, 1938.

146. R. Hesse, Acta Cryst., 1, 290, 1948.

147. H. Lipson, Acta Cryst., 2, 43, 1949.

148. T. Ito, "X-ray Studies in Polymorphism", Appendix, Tokyo, 1950.

149. R. C. Mackenzie, "The differential thermal analysis of clays", Min. Soc., London, 1957.

150. E. C. Sewell, Research Notes, Building Research Station, D.S.I.R., 1955-1958.

151. R. C. Mackenzie, Anal. Edafol. Fisiol. Veg., 11, 159, 1952.

152. H. Strunz, Neues Jahrbuch. Miner. Monatsh., 11, 250, 1956.

153. H. E. Swanson, R. K. Fuyat and G. M. Ugrinic, Nat. Bur. Stand. Circ. 539, Vol. III, 38, 1954.

154. H. E. Swanson, and E. Tatge, Nat. Bur. Stand. Circ. 539, Vol.I, 39, 1953.

155. F. H. S. Vermas, Amer. Min., 38, 845, 1953.

156. G. T. Kerr, Zeolite Symposium A.A.A.S., New York, 1960. Submitted to J.Inorg.Chem.

157. B. Mason and L. B. Sand, Amer. Miner., 45, 341, 1960.

158. F. A. Mumpton, Amer. Miner., 45, 351, 1960.

159. M. Koizumi and R. Kiriyama, J. Geol. Soc. Japan, 59, 88, 1953.

160. D. A. Langley, Ph.D. Thesis, London University, 1957.

161. G. Erwin and E. F. Osborn, J. Geol., 59, 381, 1951.

162. J. F. Corwin, A. H. Herzog, G. E. Owen, R. G. Yalman and A. C. Swinnerton, J. Amer. Chem. Soc., 75, 3933, 1935.

163. R. M. Barrer, J. W. Baynham and N. McCallum, J. Chem. Soc., 4035, 1953.

164. R. M. Barrer and I. S. Kerr, Trans. Farad. Soc., 55, 1915, 1959.

165. R. M. Barrer, Trans. Farad. Soc., 40, 555, 1944.

166. W. M. Meier, Z. Krist., 115, 439, 1961.

167. R. M. Barrer and D. A. Langley, J. Chem. Soc., 3804, 1958.

168. H. C. Vacher, J. Res. Nat. Bur. Stands., 35, 339, 1945.

169. B. D. Saksena, Trans. Farad. Soc., 57, 242, 1961.

170. J. J. Hemley, J. Phys. Chem., 63, 320, 1959.

171. F. H. Norton, Amer. Min., 26, 1, 1941.

172. W. Eitel, "The Physical Chemistry of the Silicates", p. 616, 1954.

173. S. A. Greenberg, J. Phys. Chem., 60, 325, 1956.

174. R. M. Barrer and L. V. C. Rees, Trans. Farad. Soc., 56, 709, 1960.

175. R. M. Barrer, unpublished work.

176. R. Roy, P.B.Report 111,428, Office of Tech. Services, Wash., D.C., 1952.

177. Thu-Huan Chi, Bull. Geol. Soc. China, 36, 229, 1956.
see Chem. Abst., 53, 2951h, 1959.
Chem. Abst., 55, 6730a, 1961.

178. R. M. Barrer, F. W. Bultitude and I. S. Kerr, J. Chem. Soc., 1521, 1959.

179. H. Steinfink, Acta Cryst., 15, 644, 1962.

180. L. H. Bauer and H. Berman, Amer. Min., 18, 20,1933.

181. E. W. Heinrich and A. A. Levinson, Amer. J. Sci., 253, 39, 1955.

182. R. A. Hatch, R. A. Humphrey, W. Eitel and J. E. Comeforo, U.S. Bureau of Mines, Rept. of Invest. 5337, 1955.

A P P E N D I X

X-ray data:

Tables A1 to A25. pp. 201-221

D.T.A. data:

Tables A26 to A43. 222-239

Thermogravimetric data:

Tables A44 to A54. 240-250

X-ray data for minerals marked thus * have been obtained from natural samples in the collection of this Department.

Table A1.

α-cristobalite (154)		synthetic cristobalite*		Sr-H		Ba-H	
d(A)	int	d(A)	int	d(A)	int	d(A)	int
				6.50	w		
		4.27	w				
4.04	100	4.03	vvs	4.05	vs	4.04	vs
				3.93	vw		
		3.795	vw	3.75	m	3.74	w
						3.54	w
				3.45	m	3.48	w
		3.250	vw			3.245	s
3.138	12	3.130	m	3.23	s		
						3.171	mw
				3.09	w		
				2.975	vw		
		2.950	vw				
				2.90	vw		
						2.868	m
2.845	14	2.837	m	2.848	w		
				2.758	w		
				2.543	mw		
2.489	18	2.481	ms	2.489	ms	2.507	m
2.468	6	2.464	w				
						2.328	vw
				2.160	w		
2.121	4	2.110	m	2.12	vw		
2.024	3	2.012	mw	2.06	vw		
				1.96	vw		
1.932	4	1.925	m	1.93	vw		
1.874	4	1.864	m	1.87	vw		
				1.79	w		
		1.687	w				
1.613	5	1.605	m	1.61	w		
				1.59	vw		
		1.527	mw				
		1.489	mw	1.49	vw		
		1.427	mw				

Table A2.

Mordenite* d(A)	int	Sr. M d(A)	int
13.56	m	13.56	mw
9.04	ms	9.10	m
6.60	m	6.63	m
6.41	mw	6.43	w
6.08	w	6.07	vw
5.80	mw	5.86	m
5.11	vw		
4.66	vw	4.76	mw
4.53	m	4.55	m
4.26	vvw	4.32	vw
4.14	vw	4.18	m
4.00	s	4.00	ms
3.84	vw	3.84	vw
3.77	w	3.76	w
3.63	vw	3.64	w
3.49	vs	3.48	s
3.41	s	3.40	ms
3.22	s(b)	3.23	s(b)
2.98	vw	3.04	mw
2.90	ms	2.92	s(b)
2.75	w		
2.703	w	2.69	mw
2.642	w		
2.569	mw	2.563	ms
2.529	m	2.523	ms
2.464	w(b)		
2.442	w(b)		
2.174	vw	2.182	w
2.102	w	2.090	w
1.887	m	1.886	w
1.818	w	1.821	w
1.796	w	1.798	vw
1.710	vw	1.705	vw
1.626	vw	1.638	vw

Table A3.

Cancrinite* d(A)	int	Sr-J d(A)	int
6.36	ms	6.33	m
		4.85	w
4.69	s	4.69	ms
4.16	w	4.16	w
3.67	s	3.67	m
3.24	vs	3.24	s
2.99	w	2.97	m
2.90	vw		
2.753	m	2.75	m
2.632	w	2.63	w
2.596	m	2.594	w
2.526	w	2.526	vs
2.434	m	2.432	mw
2.273	w	2.271	vw
2.185	vw		
2.123	m	2.118	w
		2.094	mw
1.890	m		
1.812	m	1.812	w
1.764	m	1.764	w
1.711	w	1.709	w
1.595	m(b)	1.611	m
1.504	m(b)		
1.463	m(b)	1.480	ms
1.356	mw		
1.331	mw	1.327	vw(b)
1.300	w		

Table A4.

Analcite[xx]		Sr-I		Sr-I (Brown product)	
d(A)	int	d(A)	int	d(A)	int
6.87	50				
5.61	80	5.60	s	5.60	s
4.86	40	4.87	mw	4.85	m
3.67	20	3.68	vw	3.66	w
3.43	100	3.44	vs	3.43	vs
2.925	80	2.93	s	2.917	s
2.801	20	2.806	vw	2.796	w
2.693	50	2.691	m	2.686	ms
2.505	50	2.509	m	2.500	m
2.426	30	2.423	m	2.421	mw
2.226	40	2.227	m	2.219	m
2.168	5			2.165	vw
2.022	10				
1.903	50	1.906	ms	1.899	ms
1.867	40			1.863	m
1.743	60	1.757	ms	1.739	s
1.716	30	1.719	vw	1.712	mw
1.689	40	1.695	vw	1.695	m
1.664	10			1.660	vw
1.618	20			1.612	w
1.596	30	1.596	mw	1.592	m
1.498	20				
1.480	20			1.457	mw
1.415	40	1.415	ms	1.410	m
1.372	10			1.367	vw
1.359	40	1.360	ms	1.353	m
1.308	10			1.304	w
1.285	20			1.281	w
1.263	20			1.281	w
1.220	30			1.258	w

Table A5

Sr-F		natural gmelinite*		gmelinite (152)	
d(Å)	int	d(Å)	int	d(Å)	int
11.91	ms	11.94	s	12.0	90
9.40	w	9.42	w		
7.65	vw	7.70	ms	7.69	60
6.93	vw	6.91	ms	6.81	40
5.95	vvw	5.91	w(b)	5.99	10
5.54	vw	5.55	vw		
5.14	w	5.14	mw		
4.99	s	5.05	ms	5.07	60
		4.64	vw		
4.53	mw	4.50	m	4.53	20
		4.41	vvw		
4.32	m	4.32	m		
4.12	s	4.11	vs	4.10	100
3.98	m	3.97	vw		
3.89	vw	3.87	vw		
3.54	mw				
3.46	ms	3.45	ms	3.44	20
3.32	w	3.31	w		
3.19	w	3.24	s	3.22	60
				3.09	05
2.99	s	2.98	s	2.96	80
2.93	ms	2.93	s		
2.87	m	2.86	s	2.85	60
2.675	ms	2.700	s	2.67	60
2.608	s	2.605	m	2.57	10
		2.520	w		
2.302	m	2.323	w	2.292	20
2.091	ms	2.092	ms	2.076	40
2.050	vvw	2.060	vw	1.989	05
1.947	vvw	1.949	w	1.941	10
1.912	vvw	1.914	w		
		1.877	w		
		1.843	w		
1.801	m	1.815	m	1.807	40
		1.793	w		
1.727	s	1.724	m	1.722	40
1.694	w	1.700	w		
		1.683	mw	1.678	20
1.658	w	1.653	vvw		
1.640	w	1.634	vw	1.631	05
1.599	vw	1.600	w	1.598	05

Table A6.

Heulandite[159]		Sr-R		Clinoptilolite[157]	
d(Å)	int	d(Å)	int	d(Å)	int
9.0	s	9.04	m	8.96	vs
7.9	m	7.99	m	7.94	m
6.78	m			6.80	w
				5.98	vw
		5.28	mw		
5.09	m	5.12	ms	5.13	m
4.64	w	4.66	m	4.65	w
4.33	vw	4.37	w	4.35	w
3.96	vs	3.98	vs	3.97	vs
		3.92	w		
		3.84	vw		
3.70	vw	3.73	vw	3.72	w
3.54	vw	3.58	mw	3.55	w
		3.44	w		
3.40	m	3.41	w	3.43	m
3.29	vw	3.33	w	3.33	w
3.16	m	3.18	mw	3.18	w
		3.13	mw		
3.09	vw	3.08	vw		
2.96	s	2.97	ms	2.98	s
2.80	m	2.80	m	2.81	m
		2.74	m	2.74	w
		2.67	vw	2.68	vw
2.53	vw			2.54	w
2.42	vw			2.44	w
2.35	vw			2.36	vw
		2.28	vw		
1.96	vw	1.96	vw	1.96	w
		1.83	vw	1.83	vw

Table A7.

Sr-G		Natural Chabazite*	
d(Å)	int	d(Å)	int
9.43	m	9.47	s
6.80	m	6.93	mw
5.54	m	5.55	m
5.12	m	5.02	m
4.48	vvw		
4.37	vw		
4.30	ms	4.32	s
3.95	m	3.89	ms
3.68	w	3.57	ms
3.21	w	3.34	ms
3.12	m	3.16	mw
2.95	vw		
2.91	s	2.91	vs
2.82	vvw		
2.78	vw		
2.74	vvw		
2.54	m	2.59	m
2.28	mw	2.30	m
2.09	mw	2.08	m
		1.87	m
1.81	mw	1.80	s
1.71	mw	1.72	ms
		1.65	m
		1.56	m

Table A8.
Ignition product of Sr-D.

d(Å)	int	d(Å)	int
11.13	s	2.159	vw(b)
8.61	w	2.041	w(b)
6.91	s	1.943	ww
6.66	w	1.878	ms
5.57	m	1.726	m
5.49	s	1.665	vw
5.29	vw	1.623	vw
4.97	w	1.592	vw
4.65	m	1.434	w
4.31	m	1.413	vw
4.05	s	1.358	vw
3.88	w		
3.72	w		
3.68	m		
3.65	w		
3.56	vs		
3.34	m		
3.19	w		
3.13	w		
3.07	s		
2.92	s		
2.88	m		
2.83	m		
2.688	w		
2.656	w		
2.626	w		
2.494	w		
2.450	vw		
2.318	w		
2.302	mw		
2.267	w		

Table A9. Sr-D.

d(Å)	int	d(Å)	int
9.55	ms	2.479	vw
7.13	vw	2.411	m
6.96	vvw	2.352	w
6.63	ms	2.307	w
5.88	mw	1.923	w
4.97	vw	1.867	m
4.75	w	1.483	w
4.65	vw	1.422	w
4.31	vw	1.308	vvw
3.99	m	1.268	vw
3.94	mw	1.233	vw
3.86	w		
3.78	m		
3.73	vw		
3.68	w		
3.54	s		
3.48	s		
3.44	vvw		
3.39	vvw		
3.31	w		
3.26	vvw		
3.22	w		
3.14	ms		
3.06	ms		
3.03	vw		
2.96	w		
2.93	w		
2.89	m		
2.712	mw		
2.644	mw		
2.580	vw		

Table A10.

Sr-Q

d(A)	int	d(A)	int
9.66	w	2.374	vw
7.89	vvw	2.328	w
6.96	mw	2.196	w
6.61	vw	2.146	w
6.30	w	2.129	wv
5.88	vs	2.095	w
4.76	vs	2.076	wv
4.65	s	2.032	vw
4.31	s	2.000	m
4.16	ms	1.976	vw
4.06	w	1.954	vw
3.94	ms	1.924	vw
3.76	mw	1.894	ms
3,67	vw	1.828	vwd
3.54	w	1.730	m
3.48	w	1.701	mw
3.30	wd	1.651	mw
3.27	s	1.609	mw
3.14	w	1.586	mw
3.10	ms	1.568	vw
3.03	vs	1.527	w
2.95	w	1.497	vvw
2.9[illegible]	ms	1.475	vw
2.89	vvw	1.465	vw
2.768	mw	1.455	vw
2.738	mw	1.427	w
2.657	md	1.396	w
2.542	vvw	1.346	vw
2.454	w	1.333	vw
2.416	m	1.306	vw

Table A11.

Sr-N

d(A)	int	d(A)	int
6.68	m	2.125	vs
5.89	m	1.973	m
5.30	mw	1.861	m
4.56	vs	1.847	mw
3.84	m	1.818	ms
3.334	m	1.800	m
3.277	ms	1.772	m
3.166	ms	1.754	mw
2.940	vs	1.742	m
2.815	m	1.697	vw
2.793	mw	1.666	mw
2.751	s	1.636	ms
2.660	mw	1.612	ms
2.594	m	1.580	ms
2.576	m	1.549	vw
2.495	m	1.509	m
2.397	w	1.432	mw
2.336	vw	1.411	m
2.276	m	1.404	m
2.258	mw	1.393	m
2.222	m	1.372	m
2.142	ms		

Table Al2. Sr-L. Strontium mica.

(1) Fresh sample		(2) Ignited sample		(3) Sample (2) after hydrothermal treatment		(4) Prepared by acid attack on Sr-C	
d(Å)	int	d(Å)	int	d(Å)	int	d(Å)	int
9.85	vw	9.87	m	9.55	m	9.78	m
4.47	m	4.49	ms	4.49	mw	4.49	w
4.29	m	4.30	m	4.31	m	4.29	w
3.84	mw	3.86	m	3.86	m	3.85	m
3.46	m	3.47	mw	3.47	mw	3.46	w
3.31	w	3.34	mw	3.33	w	3.34	w
3.27	mw	3.28	m	3.28	m	3.27	m
3.17	m	3.19	m	3.19	mw	3.18	vw
2.95	m	2.97	w	2.97	w	2.97	vvw
2.93	m	2.93	mw	2.95	mw		
2.90	mw	2.92	m	2.93	m		
		2.89	mw	2.89	mw	2.85	vvw
2.754	mw	2.766	vw	2.760	vw		
2.582	s	2.604	ms	2.602	ms	2.586	ms
2.550	vs	2.568	vs	2.568	vs	2.555	vs
2.441	mw	2.460	w	2.455	vw	2.447	vw
2.240	ms	2.253	ms	2.250	ms	2.241	w
2.190	w	2.212	w	2.208	w	2.207	w
2.113	ms	2.130	ms	2.127	m	2.122	ms
						1.966	w
1.949	mw	1.964	m	1.961	ms	1.946	w
						1.712	mw
1.631	ms	1.638	ms	1.636	ms	1.633	m
1.492	vs	1.504	s	1.503	vs	1.495	vs
1.288	m	1.301	m	1.299	m	1.291	m

Table A13.

Sr-C		paracelsian[37]		Sr-C		paracelsian	
d(Å)	int	d(Å)	int	d(Å)	int	d(Å)	int
6.46	mw	6.582	20	2.101	mw	2.144	15
6.22	m	6.375	20	2.088	m		
5.12	vw	5.217	7	2.022	vw	2.054	7
4.17	m			2.007	w	2.034	7
3.93	vs	4.004	100	1.986	mw	2.030	7
3.71	s	3.797	70	1.903	w		
3.62	w	3.696	4	1.862	m	1.874	20
3.50	s	3.593	45	1.833	m	1.849	10
3.22	ms	3.290	35	1.812	mw	1.831	5
3.11	mw	3.194	15	1.794	w	1.807	5
3.045	w	3.115	7	1.771	vw	1.798	7
		3.074	7	1.752	m	1.782	7
		3.010	35	1.713	w	1.744	7
2.940	m	2.990	50	1.703	w	1.718	13
2.920	ms	2.961	30	1.694	vvw		
2.900	mw			1.630	mw	1.664	13
2.890	mw			1.615	vvw		
2.830	w	2.880	5	1.599	vvw		
2.681	m	2.731	50	1.557	m(b)	1.590	20
2.666	vw	2.621	20	1.533	vvw		
2.553	s	2.609	35	1.520	mw	1.551	15
2.506	m	2.555	50	1.516	mw		
2.349	vw	2.393	20	1.483	w		
2.338	m	2.370	45	1.470	m		
2.308	ms			1.438	vw		
2.291	vw			1.434	vw		
2.227	vw	2.281	3	1.417	w		
2.180	ms	2.229	20	1.395	w		
2.151	ms	2.194	45	1.388	mw		
2.109	mw	2.154	5	1.340	w(b)		

Table A14.

$SrO.Al_2O_3.2SiO_2$ (136)		Sr-W		$SrO.Al_2O_3.2SiO$		Sr-W	
d(A)	int	d(A)	int	d(A)	int	d(A)	int
6.44	35	6.48	ms	1.895	3	1.891	m
5.77	11	5.79	w	1.872	7	1.867	w
4.55	17	4.57	mw	1.846	7	1.847	w
4.11	9	4.11	mw	1.834	7	1.832	w
		3.77	w	1.794	11	1.793	w
3.75	40	3.74	s	1.784	20	1.780	s
3.58	20	3.59	w	1.744	7	1.739	w(b)
3.47	20	3.48	w			1.715	vw
3.43	70	3.44	vs	1.657	7	1.655	w
3.27	100	3.26	vvs	1.621	9	1.619	w
3.22	100	3.22	vvs	1.564	11	1.562	m
2.97	45	2.97	m	1.503	7	1.504	w(b)
2.89	25	2.885	mw	1.491	13	1.487	ms
2.74	35	2.747	s			1.445	w
2.55	65	2.69	s(b)			1.431	w
2.47	5	2.476	w			1.421	w
2.40	9	2.402	w			1.413	vw
2.34	9	2.341	w			1.391	m
2.31	9	2.307	w			1.373	w
2.22	11	2.222	mw			1.361	vw
		2.203	vw			1.343	vw
2.19	13	2.191	vw			1.333	mw
2.16	9	2.158	m			1.322	vw
		2.112	vw			1.294	mw
2.10	7	2.095	vw			1.270	m
		2.070	vw			1.261	w
2.06	11	2.057	vvw			1.233	w
2.04	11	2.041	w				
		2.025	vw				
1.965	3	1.961	ms				

Table A15.

Ca-P[42]		Sr-P		Ba-P		
d(Å)	int	d(Å)	int	d(Å)	int	hkl
7.49	vw	7.65	m	7.75	m	001
4.42	s	4.49	vvw			100
3.79	s	3.875	vvs	3.96	vs	101
3.68	vw	3.80	vw			002
2.83	s	2.905	vs	2.96	s	102
2.555	s	2.601	s	2.665	ms	110
		2.252	w	2.310	w	200
		2.210	m	2.249	m	103
2.120	w	2.159	ms	2.213	ms	201
		1.937	mw	1.980	vw	202
1.842	vvw	1.901	m	1.930	mw	004
1.778	vw	1.814	ms	1.850	ms	113
1.632	vw	1.659	m	1.701	m	211
1.552	vw	1.551	m	1.589	m	212
		1.531	m	1.561	mw	114
		1.498	m	1.538	w	300
		1.438	w	1.463	w	105
		1.409	vw	1.445	vw	213
				1.331	w	220
		1.296	w			303
				1.319	vw	205
		1.257	mw			310
		1.229	vw	1.282	w	222
		1.183	mw	1.262	vw	312

Table A16. Sr-K

d(Å)	int
6.46	vw
4.05	s
3.95	vw
3.88	mw
3.74	ms
3.54	vw
3.45	ms
3.22	vs(b)
3.14	vw
2.95	vw
2.91	mw(b)
2.845	w
2.761	w
2.602	w
2.53	mw(b)
2.487	m
2.310	w
2.160	m
2.116	mw
1.94	mw(b)
1.788	m
1.755	vw
1.715	w
1.61	vw(b)
1.56	vw(b)
1.48	mw(b)
1.37	w(b)

Table A17.

Sr-S		Sr-T	
d(Å)	int	d(Å)	int
5.81	m	6.10	s
4.57	m	6.69	mw
3.79	w	3.82	m
3.76	mw	3.31	mw
3.60	mw	3.15	ms
3.44	ms	2.706	m
3.27	ms	2.206	m
2.98	m		
2.751	ms		
2.407	m		
2.024	w		
1.784	mw		
1.612	mw		

Table A18.

Boehmite[153]		Ba-E	
d(A)	int	d(A)	int
6.11	100	6.16	ms(b)
3.164	65	3.16	s
2.346	53	2.346	ms
1.980	6	1.984	vw
1.860	32	1.863	w
1.850	27	1.848	s
1.770	6	1.769	m
1.662	13	1.662	m
1.527	6	1.53	vw(b)
1.453	16	1.450	ms
1.434	9	1.434	ms
1.396	2	1.396	vw
1.383	6	1.382	vw
1.369	2		
1.312	15	1.308	ms(b)
1.303	3		
1.224	1		
1.209	2	1.205	w

Table A19.

Ba-Z	
d(A)	int
10.56	w
8.90	m
6.90	mw
5.07	w
4.60	s
3.45	vs
3.29	w
3.17	m
2.91	m
2.84	w
2.421	ms
2.373	w
1.988	vw
1.785	vw
1.765	vw
1.592	mw

Table A20.

Celsian (155) S.W. Africa		Celsian* Jakobsberg		Ba-C	
d(A)	int	d(A)	int	d(A)	int
6.39	4	6.53	s	6.51	s
		5.88	m	5.85	w
		4.63	ms	4.62	mw
		3.90	mw	3.90	w
3.77	3	3.81	ms	3.80	m
		3.63	w	3.63	w
		3.56	ms	3.56	mw
3.44	6	3.50	s	3.47	s
3.33	7	3.35	s	3.35	s
		3.29	w	3.28	mw
		3.27	w		
3.24	7	3.25	w	3.25	mw
3.00	7	3.03	m	3.02	m
2.901	4	2.92	mw	2.91	mw
2.758	5	2.778	m	2.77	m
		2.613	w	2.608	w(b)
2.574	10	2.590	m	2.583	ms
2.406	3	2.430	vw	2.425	w
2.316	3	2.337	vw	2.326	mw
		2.275	vw		
2.263	2	2.258	vw	2.260	w(b)
		2.221	vw	2.218	w(b)
2.167	10	2.178	w	2.173	m
2.104	1			2.110	w
				2.093	w
2.056	1			2.061	w
				2.014	vw
1.994	2			1.995	vw
1.946	2			1.950	mw
				1.910	w
1.857	1				
1.801	5			1.797	mw
1.676	1			1.672	w
				1.649	w
1.625	2			1.627	w
1.576	2			1.577	w
				1.533	w
1.521	1			1.522	w
				1.502	mw
1.455	5			1.450	vw
1.428	6				
1.342	2				

Table A21.

Ba-K				Ba-J			
d(A)	int	d(A)	int	d(A)	int	d(A)	int
10.59	ms	2.648	w	11.39	s	2.88	m
7.39	mw	2.613	mw	10.53	vw	2.82	w
6.87	w	2.553	w	10.22	w	2.797	w
6.07	ms	2.493	m	7.39	m	2.709	m
5.58	ms	2.469	w	7.04	w	2.664	m
5.29	w	2.433	w	6.23	m	2.636	vw
5.08	w	2.336	w	6.08	vw	2.605	w
4.72	m	2.301	m	5.84	m	2.455	ms
4.59	ms	2.234	vw	5.73	mw	2.419	ms
4.30	ms	2.206	w	5.63	vw	2.370	ms
4.20_5	ms	2.117	w	4.79	m	2.334	w
3.88_5	w	1.965	w	4.58	s	2.307	vw
3.67	vw	1.919	w	4.52	s	2.287	vw
3.52_5	ms	1.846	m	4.29_5	vw	2.262	m
3.49	m	1.801	w	4.19	w	2.213	vw
3.44_5	w	1.760	w	4.08	w	2.189	vw
3.34	vw	1.730	w	4.02	ms	2.169	vw
3.29	mw	1.694	vw	3.97	m	2.125	vvw
3.16	s	1.650	vw	3.91	ms	2.107	vvw
3.06	w	1.559	vw	3.81	m	2.028	vw
3.025	ms	1.539	w	3.70	w	1.987	vw
2.94	m	1.525	vw	3.56	ms	1.953	vw
2.88	vw	1.509	vw	3.51	s	1.847	ms
2.791	vw	1.286	w	3.45	s	1.819	wd
2.719	m	1.271	vw	3.28	w	1.794	wd
				3.20	w	1.775	vw
				3.16	w	1.708	m
				3.12	vs	1.670	mw
				2.98	m	1.632	w
				2.82	w	1.596	w

Table A22.

Natural Harmotome*		Ba-M		Natural Harmotome*		Ba-M	
d(A)	int	d(A)	int	d(A)	int	d(A)	int
8.14	vs	8.09	s			2.608	w
7.56	vw	7.86	vw	2.557	w	2.560	vw
7.18	s	7.14	s	2.525	w	2.517	m
7.03	w	6.99	w	2.508	w		
6.39	vs	6.37	s	2.464	m	2.460	w
6.11	vw	6.26	w			2.406	vw
		5.60	m	2.368	m	2.368	w
5.02	ms	5.01	m	2.315	ms	2.320	mw
				2.295	m	2.294	mw
		4.72	vw	2.256	w	2.258	vw
4.29	ms	4.27	m	2.236	m	2.235	mw
4.10	s	4.08	s	2.213	w	2.205	w
4.06	s			2.147	m	2.145	m
4.03	s	4.03	ms	2.119	w		
3.89	m	3.93	mw	2.084	vw	2.088	vw
		3.88	mw	2.062	m	2.065	w
		3.76	vw	2.052	m	2.049	mw
3.66	w	3.67	vw	2.021	mw	2.020	w
3.57	vvw			2.008	vw		
3.52	w			1.996	vw	1.998	mw
3.46	mw	3.46	vw	1.964	w		
3.23	s	3.24	m	1.947	m	1.948	m
3.19	mw	3.19	m	1.921	w	1.919	vw
3.16	ms	3.16	m	1.894	mw	1.897	vw
3.12	vs	3.11	ms	1.840	vw	1.837	w
3.07	m	3.07	w	1.818	mw	1.822	w
		3.00	w	1.802	w	1.799	w
2.91	ms	2.91	mw	1.761	m(b)	1.770	vw
2.838	w	2.803	mw	1.709	ms(vb)	1.709	m
2.745	w			1.670	m	1.675	w
2.724	s	2.725	m	1.639	w	1.638	w
2.674	s	2.693	mw	1.530	m	1.530	w
2.668	s	2.669	m	1.473	w	1.478	w
2.624	w	2.628	w			1.459	vw

Table A23.

Ba-C		Ba-A		Ba-A (ignited)	
d(A)	int	d(A)	int	d(A)	int
6.51	s	6.54	m	6.52	ms
5.85	w	5.88	vw	5.18	w
4.62	mw	4.82	vw	4.64	w
		4.56	vs	4.54	vs
				3.95	w
3.90	w	3.92	w	3.91	w
3.80	m	3.81	mw	3.80	m
3.63	w	3.64	w	3.63	w
3.56	mw	3.56	mw	3.56	m
3.47	s	3.48	m	3.48	ms
3.35	s	3.36	ms	3.35	s
3.28	mw	3.30	ms	3.28	s
3.25	mw				
3.02	w	3.02	m	3.02	m
				2.97	w
2.91	mw	2.92	w	2.92	mw
2.77	m	2.797	s	2.796	s
2.608	w(b)	2.768	s	2.751	s
2.583	ms	2.587	s	2.580	s
2.425	w				
2.326	mw	2.334	vw	2.336	m
2.260	w(b)	2.278	w	2.277	mw
		2.248	w		
2.218	w(b)	2.218	vw	2.225	mw
2.173	m	2.172	w	2.176	w
		2.152			
2.110	w	2.132	s	2.126	s
2.093	w			2.023	w(b)
2.061	w				
2.014	vw				
1.995	vw				

Table A23 continued.

Ba-C		Ba-A		Ba-A (ignited)	
d(A)	int	d(A)	int	d(A)	int
1.950	mw	1,957	w	1.956	w
1.910	w	1.914	vw	1.914	w
		1.813	m	1.811	ms
1.797	mw	1.789	m	1.774	w
		1.752	m	1.740	m
1.672	w	1.694	m	1.690	m
1.649	w	1.645	m	1.637	m
1.627	w	1.614	vw		
		1.607	m	1.604	m
1.577	w	1.568	mw	1.567	m
1.533	w	1.538	w	1.540	vw
1.522	w	1.524	vw	1.526	vw
		1.514	w		
1.502	mw	1.504	w	1.508	mw
1.450	vw	1.441	mw	1.442	w
		1.398	ms	1.396	m
		1.319	w	1.319	w
		1.310	vw	1.304	w
		1.273	vw	1.287	w(b)
				1.262	w
		1.246	w	1.244	w
		1.211	w		

Table A24. Ba-G

d(Å)	int	hkl
16.15	s	100
9.35	vvw	111
8.10	vvw	102
7.53	m	200
6.83	mw	210
5.85	vw	103
5.38	w	220
4.85	w	203
4.72	w	004
3.95	vs	204
3.84	w	322
3.75	vw	005
3.49	m	323
3.32	m	421
3.23	m	403
3.19	m	422
3.08	s	225
2.92	s	206
2.874	vw	216
2.817	vw	325
2.753	vw	424
2.690	s	
2.635	mw	
2.502	w	
2.447	mw	
2.390	vw	
2.294	vvw	
2.224	m	
2.203	m	
2.187	w	
1.874	m	
1.800	w	
1.790	w	
1.745	vw	
1.714	w	
1.593	vw	
1.553	vw	
1.539	w	
1.441	vw	
1.430	vw	
1.345	vw	

Table A25.

Ba-P		Ignited Ba-P		α-hexagonal $BaAl_2Si_2O_8$		β-hexagonal $BaAl_2Si_2O_8$	
d(A)	int	d(A)	int	d(A)	int	d(A)	int
7.74	m	7.77	m	7.79	100	7.79	112
3.96	s	3.95	vs	3.949	43	3.963	47
				3.899	18	3.901	20
2.97	s	2.96	s	2.968	49	2.977	59
2.67	ms	2.65	ms	2.647	13	2.659	15
				2.597	20	2.603	22
2.31	mw	2.29	w	2.292	4	2.300	5
2.250	m	2.254	m	2.259	18	2.266	15
2.215	m	2.196	ms	2.195	11	2.206	11
1.982	vw	1.971	vw		65		60
1.933	w	1.942	w	1.947	7	1.951	6
1.854	m	1.850	m	1.853		1.860	(at 450°C)
1.702	m	1.690	m				
1.592	m	1.582	m				
1.561	mw	1.565	mw				
1.540	w	1.526	w				
1.464	w	1.469	w				
1.445	vw(b)	1.440	vw				
1.331	w	1.322	w(b)				
1.319	vw						
1.282	w	1.288	mw				
1.262	vw	1.253	vw(b)				

Table A26.

D.T.A. on Sr-C. Heating rate 9.71°C/min.

T°C	dT°C
16	+0.44
24	0.88
70	1.33
115	1.53
161	1.63
208	1.75
300	1.99
400	2.25
501	2.50
560	2.60
616	2.63
670	2.50
720	2.38
822	2.23
923	2.13
1020	2.00

Table A27.

D.T.A. on Sr-D. Heating rate 9.86°C/min.

T°C	dT°C	T°C	dT°C
30	-1.25	440	-2.36
40	-2.00	480	-2.34
50	-2.38	520	-2.29
60	-3.00	560	-2.34
70	-3.50	570	-2.38
80	-4.00	580	-2.44
90	-4.25	590	-2.38
100	-4.44	600	-2.38
110	-4.43	630	-2.33
120	-4.30	650	-2.28
130	-4.19	700	-2.19
150	-3.94	730	-2.09
160	-3.84	770	-1.75
190	-3.53	780	-1.46
200	-3.40	790	-1.40
210	-3.25	800	-1.38
230	-3.05	810	-1.13
240	-2.98	820	-1.03
260	-2.81	830	-1.23
280	-2.70	840	-1.38
300	-2.63	860	-1.48
320	-2.50	870	-1.25
340	-2.38	880	-1.06
360	-2.25	890	-1.08
370	-2.25	900	-1.19
380	-2.25	910	-0.90
400	-2.25	920	-0.75
420	-2.31	930	-0.90

Table A28. D.T.A. on Sr-G. Heating rate 9.56°C/min.

T°C	dT°C	T°C	dT°C
19	-0.66	250	-1.89
21	-0.76	260	-1.88
21	-0.84	270	-1.85
21	-0.91	274	-1.84
24	-0.99	279	-1.94
26	-1.00	282	-2.04
31	-1.00	288	-2.16
37	-1.03	291	-2.20
44	-1.11	298	-2.15
52	-1.25	303	-1.88
61	-1.50	308	-1.65
70	-1.88	314	-1.34
80	-2.25	324	-1.10
90	-2.56	334	-0.89
95	-2.81	344	-0.81
100	-2.83	354	-0.75
109	-2.85	366	-0.63
118	-2.79	376	-0.57
128	-2.76	386	-0.44
136	-2.75	395	-0.35
144	-2.56	405	-0.25
152	-2.41	430	-0.04
162	-2.31	445	0.14
171	-2.19	455	0.20
182	-2.14	485	0.24
190	-2.10	510	0.29
200	-2.07	570	0.35
210	-1.99	625	0.43
215	-1.98	680	0.61
219	-1.99	730	0.73
223	-2.09	781	0.84
228	-2.11	830	0.88
232	-2.11	880	0.93
236	-2.00	940	1.04
240	-1.96		

Table A29. D.T.A. on Sr-Ja. This sample also contained Sr-C. Heating rate 9.18°C/min.

T°C	dT°C	T°C	dT°C
15	0.23	457	1.78
17	0.38	470	1.75
30	0.53	495	1.65
41	0.68	548	1.26
43	0.70	567	1.03
45	0.60	572	1.03
47	0.50	577	1.03
48	0.40	581	0.99
49	0.55	599	0.78
51	0.66	626	0.43
55	0.76	652	0.13
63	0.81	680	-0.13
72	0.88	700	-0.20
99	1.00	710	-0.14
105	1.01	739	0.11
106	1.23	766	0.55
108	1.23	798	0.85
110	1.06	824	1.08
112	1.01	852	0.93
121	1.05	868	0.75
164	1.19	881	0.69
199	1.30	889	0.63
239	1.41	891	0.75
274	1.63	895	0.78
314	1.73	899	0.86
356	1.75	901	0.78
400	1.76	905	0.70
425	1.84	911	0.60
441	1.81	918	0.56
445	1.69	930	0.58
447	1.63	940	0.63
449	1.58	960	0.65
450	1.69	973	0.66
452	1.76		

Table A30. D.T.A. on Sr-Ib Heating rate 9.57°C/min. The sample used also contained Sr-P.

T°C	dT°C	T°C	dT°C
10	-1.35	318	0.15
12	-1.38	341	0.34
20	-1.39	364	0.44
27	-1.38	390	0.50
32	-1.33	413	0.58
35	-1.28	438	0.60
40	-1.25	454	0.63
45	-1.24	470	0.58
52	-1.25	490	0.50
62	-1.46	510	0.35
72	-1.60	521	0.25
78	-1.65	532	0.13
85	-1.60	543	0.01
90	-1.35	554	0.00
101	-1.13	565	0.01
110	-1.00	576	0.13
120	-0.95	585	0.38
140	-0.86	595	0.65
161	-0.81	605	0.88
170	-0.76	619	1.03
178	-0.68	626	1.13
188	-0.59	645	1.23
195	-0.54	654	1.25
203	-0.50	711	1.48
224	-0.38	774	1.64
249	-0.25	830	1.81
270	-0.13	883	1.95
294	0.00	940	2.09

Table A31. D.T.A. on Sr-N. This sample also contained Sr-C. Heating rate 9.46°C/min

T°C	dT°C	T°C	dT°C
17	-0.63	360	-0.68
19	-0.88	382	-0.70
21	-1.13	403	-0.76
28	-1.25	430	-0.79
31	-1.40	454	-0.83
38	-1.50	482	-0.90
47	-1.60	509	-1.04
57	-1.65	532	-1.19
64	-1.68	560	-1.35
73	-1.73	587	-1.59
86	-1.74	614	-1.78
95	-1.73	644	-1.88
101	-1.70	672	-1.75
110	-1.65	702	-1.50
130	-1.58	734	-1.23
150	-1.50	762	-1.00
170	-1.43	797	-0.88
190	-1.35	825	-0.83
210	-1.28	857	-0.80
230	-1.24	887	-0.88
250	-1.20	920	-0.94
273	-1.06	948	-0.98
293	-0.94	976	-0.88
317	-0.88	1002	-0.81
339	-0.75		

Table A32. D.T.A. on Sr-P. Heating rate 9.47°C/min.

T°C	dT°C	T°C	dT°C
18	0.0	128	1.03
18	0.04	137	1.14
18	0.31	147	1.20
18	0.63	167	1.25
20	0.88	212	1.38
29	1.10	261	1.50
31	1.15	310	1.69
32	1.16	361	2.00
33	1.15	418	2.26
39	1.03	467	2.50
49	0.88	576	2.63
59	0.50	676	2.56
69	0.40	776	2.55
78	0.24	826	2.56
88	0.16	875	2.49
99	0.23	927	2.25
107	0.38	979	1.96
118	0.66		

Table A33. D.T.A. on Sr-Q. Heating rate 9.24°C/min.

T°C	dT°C	T°C	dT°C
20	-0.50	362	-0.10
28	-0.75	372	-0.09
37	-0.78	381	-0.14
48	-0.93	385	-0.25
59	-1.05	389	-0.39
70	-1.13	392	-0.49
75	-1.15	396	-0.55
79	-1.14	399	-0.56
90	-1.13	401	-0.55
105	-1.09	403	-0.38
127	-0.94	408	-0.06
148	-0.83	413	0.06
165	-0.74	418	0.13
183	-0.63	436	0.23
199	-0.55	441	0.26
220	-0.54	456	0.34
239	-0.51	505	0.43
259	-0.50	605	0.64
278	-0.44	716	0.89
298	-0.38	835	1.14
320	-0.25	955	1.35
341	-0.13		

Table A34. D.T.A. on Ra-A. Heating rate 9.60°C/min.

T°C	dT°C	T°C	dT°C
24	0.0	460	0.63
26	0.0	481	0.44
28	-0.26	506	0.35
33	-0.58	520	0.0
41	-0.75	530	-0.13
50	-0.99	550	-0.38
57	-1.19	562	-0.50
62	-1.25	572	-0.63
67	-1.26	581	-0.75
70	-1.29	587	-0.85
76	-1.25	592	-0.85
85	-1.23	597	-0.84
111	-1.06	663	-0.81
135	-0.90	608	-0.79
161	-0.73	614	-0.78
184	-0.51	620	-0.75
207	-0.25	624	-0.69
221	0.0	629	-0.59
230	0.13	637	-0.44
248	0.33	645	0.0
257	0.50	658	0.50
271	0.63	670	1.00
290	0.75	680	1.45
316	0.81	691	1.75
328	0.90	720	2.19
339	0.98	749	2.50
350	0.90	775	2.71
359	0.85	800	2.89
370	0.81	840	3.13
390	0.79	870	3.35
412	0.81	900	3.63
424	0.81	930	3.81
436	0.75	960	4.03

Table A35. D.T.A. on Ba-C. Heating rate 9.57°C/min.

T°C	dT°C	T°C	dT°C
17	-0.65	206	0.28
18	-0.65	228	0.48
19	-0.83	250	0.63
20	-0.94	271	0.76
22	-1.00	301	0.94
26	-1.03	317	1.09
31	-1.01	340	1.25
37	-1.00	364	1.39
41	-0.98	388	1.48
46	-0.94	413	1.55
49	-1.00	438	1.63
53	-1.25	488	1.88
58	-1.38	540	2.10
62	-1.45	595	2.35
68	-1.38	650	2.70
71	-1.25	708	3.03
77	-1.15	765	3.39
100	-0.75	825	3.76
121	-0.48	883	4.14
142	-0.24	936	4.56
162	-0.04	990	4.75
184	0.11		

Table A36. D.T.A. on Ra-G. Heating rate 9.53°C/min.

T°C	dT°C	T°C	dT°C
15	-0.28	362	-0.53
16	-0.41	378	-0.50
19	-0.56	388	-0.48
22	-0.68	412	-0.38
28	-0.75	437	-0.30
45	-1.21	465	-0.25
65	-1.81	490	-0.23
75	-2.00	520	-0.23
85	-2.06	522	-0.16
93	-2.13	534	-0.03
102	-2.13	544	0.0
111	-2.13	555	-0.03
131	-2.13	570	0.08
145	-2.10	600	0.14
156	-2.05	678	0.19
175	-1.91	656	0.20
199	-1.81	683	0.23
211	-1.69	716	0.24
241	-1.63	745	0.25
265	-1.51	772	0.38
280	-1.49	825	0.46
290	-1.25	879	0.58
310	-1.00	930	0.63
320	-0.90	950	0.63
338	-0.63	958	0.73
345	-0.54	985	1.13

Table A37. D.T.A. on Ba-J. Heating rate 9.34°C/min.

T°C	dT°C	T°C	dT°C
19	0.0	173	0.30
21	0.13	200	0.50
25	0.28	224	0.75
30	0.43	250	0.91
37	0.49	272	1.00
41	0.51	323	1.00
46	0.38	376	1.03
49	0.25	428	1.00
54	0.0	480	0.96
58	-0.16	532	0.91
67	-0.34	583	0.75
72	-0.39	631	0.56
77	-0.38	720	0.21
87	-0.28	780	0.0
100	-0.13	856	-0.31
115	0.0	910	-0.53
124	0.06	963	-0.90
149	0.18	990	-1.25

Table A38. D.T.A. on Ba-K. Heating rate 9.47°C/min.

T°C	dT°C	T°C	dT°C
11	-0.98	353	-1.19
12	-1.23	376	-1.19
29	-1.39	425	-1.18
50	-1.73	475	-1.11
71	-2.03	530	-0.98
95	-2.03	581	-0.84
115	-1.91	640	-0.74
156	-1.73	699	-0.63
197	-1.63	655	-0.58
240	-1.55	819	-0.49
284	-1.38	878	-0.32
330	-1.25	931	-0.13

Table A39. D.T.A. on Ba-M. Heating rate 9.58°C/min.

T°C	dT°C	T°C	dT°C
10	-0.06	373	-1.18
12	-0.23	382	-1.15
21	-0.41	390	-1.00
42	-0.63	400	-0.79
62	-1.00	410	-0.65
88	-1.25	420	-0.60
110	-1.38	447	-0.53
131	-1.46	470	-0.55
150	-1.48	499	-0.60
171	-1.46	527	-0.64
190	-1.38	552	-0.66
213	-1.29	580	-0.71
232	-1.23	636	-0.74
255	-1.16	694	-0.73
270	-1.14	723	-0.63
278	-1.19	754	-0.38
285	-1.28	766	-0.29
290	-1.29	778	-0.28
295	-1.19	790	-0.38
303	-1.09	801	-0.41
313	-1.05	816	-0.44
324	-1.05	876	-0.38
332	-1.13	935	-0.25
349	-1.19	990	-0.13
362	-1.18		

Table A40. D.T.A. on Ba-M. This sample also contained Ba-P. Heating rate 9.53°C/min.

T°C	dT°C	T°C	dT°C
20	0.50	245	0.98
25	0.55	250	1.00
36	0.51	257	1.00
45	0.48	260	1.00
53	0.48	267	0.96
63	0.50	310	0.88
72	0.59	332	0.75
80	0.65	355	0.53
104	0.83	380	0.48
127	0.91	409	0.56
147	0.98	430	0.63
169	1.00	458	0.63
190	1.01	570	0.53
212	0.96	566	0.48
218	0.88	677	0.33
222	0.75	732	0.04
227	0.53	756	0.00
232	0.43	780	-0.09
236	0.50	882	-0.34
240	0.75	960	-0.50

Table A41. D.T.A. on Ra-P. Heating rate 9.21C°/min.

T°C	dT°C	T°C	dT°C
20	0.08	301	0.61
20	0.25	312	0.55
28	0.45	320	0.50
31	0.53	333	0.44
33	0.54	342	0.41
36	0.44	352	0.44
41	0.25	361	0.56
46	0.04	374	0.65
53	-0.13	383	0.84
62	-0.18	394	0.96
72	-0.13	403	1.01
82	-0.06	429	1.12
91	0.01	452	1.20
100	0.11	501	1.28
110	0.19	551	1.25
134	0.36	600	1.14
156	0.45	662	1.12
183	0.53	710	1.03
208	0.60	758	1.00
230	0.65	807	1.00
254	0.66	855	1.03
278	0.66	903	1.11
		951	1.25
		1000	1.63

Table A42. D.T.A. on Ba-P. Heating rate 9.20°C/min.

T°C	dT°C	T°C	dT°C
17	0.0	212	1.06
20	0.10	258	1.13
31	0.25	281	1.06
40	0.34	310	0.90
48	0.25	330	0.66
52	0.05	340	0.63
56	-0.10	350	0.56
60	-0.15	358	0.56
65	-0.20	368	0.63
74	-0.15	381	0.85
78	0.0	407	1.25
81	0.10	430	1.50
90	0.26	458	1.63
101	0.48	570	1.69
124	0.65	564	1.86
170	0.90	618	1.90

Table A43. D.T.A. on Ba-P. Heating rate 8.97°C/min.

T°C	dT°C	T°C	dT°C
20	0.0	334	-0.24
40	0.0	346	-0.25
56	-0.40	355	-0.24
66	-0.63	366	-0.19
75	-0.83	370	-0.08
85	-0.88	380	0.08
94	-0.81	395	0.28
107	-0.70	410	0.48
130	-0.50	438	0.58
151	-0.40	463	0.62
175	-0.35	487	0.69
220	-0.25	491	0.75
266	-0.14	500	0.94
290	-0.14	510	1.03
315	-0.20		

Table A44. Thermogravimetric on Sr-D.

0.2260 g. Heating rate 10.44°C/min.

T°C	% loss	T°C	% loss
20	0.0	387	7.63
35	0.0	405	7.92
45	0.0	425	8.18
55	0.04	435	8.43
63	0.25	455	8.69
69	0.55	485	8.94
84	0.89	505	9.13
120	2.25	535	9.49
131	2.63	573	9.87
143	3.05	603	10.04
155	3.39	625	10.17
166	3.73	658	10.34
177	4.07	689	10.47
189	4.36	728	10.68
201	4.66	770	10.93
212	4.87	846	11.10
223	5.13	930	11.23
244	5.55	950	11.23
268	5.89		
279	6.02		
291	6.19		
299	6.31		
307	6.48		
318	6.63		
328	6.78		
337	6.91		
347	7.05		
357	7.20		
367	7.33		
377	7.50		

Table A45. Thermogravimetric on Sr-G
0.2536g. Heating rate 9.30°C/min.

T°C	% loss	T°C	% loss
10	0.0	303	15.69
25	0.0	311	16.09
37	0.0	319	16.44
44	0.08	325	16.74
51	0.24	333	17.05
62	0.41	342	17.35
81	1.32	354	17.94
93	2.05	365	18.20
103	2.82	374	18.39
115	3.69	384	18.61
125	4.51	391	18.81
131	5.28	397	18.99
140	6.01	405	19.18
150	6.57	415	19.34
156	7.20	423	19.50
162	7.73	430	19.66
170	8.22	436	19.75
180	8.71	447	19.85
187	9.13	466	20.03
194	9.60	475	20.11
202	9.99	486	20.19
210	10.35	506	20.35
218	10.78	536	20.52
223	11.22	566	20.74
232	11.65	605	20.94
241	12.11	632	21.02
249	12.52	673	21.25
255	12.95	739	21.37
263	13.39	794	21.53
272	13.82	851	21.61
279	14.29	910	21.69
286	14.73	968	21.73
294	15.26	1030	21.73

Table A46. Thermogravimetric on Sr-La. This sample also contained Sr-C. 0.1550g. Heating rate 9.07°C/min.

T°C	% loss	T°C	% loss
20	0.0	622	0.839
50	0.0	648	1.161
80	0.0	670	1.483
100	0.0	693	1.742
120	0.0	715	2.000
150	0.0	735	2.387
186	0.013	746	2.548
202	0.045	758	2.710
237	0.058	768	2.774
271	0.058	781	2.903
314	0.097	805	3.013
358	0.129	827	3.116
402	0.180	860	3.161
449	0.213	899	3.213
496	0.258	919	3.226
546	0.387	955	3.226
571	0.452	970	3.226
595	0.645		

Table A47. Thermogravimetric on Sr-Ib .
The sample used also contained Sr-P.
0.1347g. Heating rate 10.25°C/min.

T°C	% loss	T°C	% loss
20	0.0	433	2.14
40	0.0	452	2.23
60	0.0	471	2.26
77	0.4	492	2.48
89	0.82	502	2.56
99	1.04	510	2.71
111	1.19	520	2.89
122	1.26	530	3.12
133	1.37	540	3.30
153	1.56	550	3.71
162	1.63	560	4.01
171	1.74	570	4.19
182	1.82	579	4.71
193	1.89	590	4.97
202	1.89	600	5.12
212	1.93	610	5.34
224	1.97	620	5.34
235	1.97	629	5.45
263	2.00	639	5.49
280	2.00	692	5.49
299	2.04	715	5.53
317	2.04	738	5.56
336	2.08	857	5.56
354	2.11	879	5.64
375	2.11	930	5.64
394	2.11	979	5.71
413	2.14	1025	5.71

Table A48. Thermogravimetric on Sr-N. This sample also contained Sr-C. 0.2235g. Heating rate 10.40°C/min.

T°C	% loss	T°C	% loss
15	0.0	515	0.75
25	0.0	525	0.85
40	0.0	535	0.91
53	0.05	544	0.93
72	0.11	554	0.94
83	0.11	564	1.02
93	0.13	574	1.03
105	0.14	580	1.22
127	0.13	593	1.32
139	0.14	597	1.41
149	0.14	604	1.54
160	0.13	613	1.66
182	0.14	619	1.79
194	0.14	630	1.91
205	0.14	641	2.02
216	0.16	652	2.16
226	0.17	662	2.29
249	0.16	673	2.35
259	0.16	683	2.43
281	0.19	693	2.49
291	0.20	704	2.49
303	0.22	716	2.52
313	0.25	728	2.55
323	0.30	741	2.52
333	0.31	752	2.55
343	0.30	763	2.59
353	0.33	774	2.60
392	0.33	786	2.62
410	0.36	800	2.65
420	0.34	811	2.67
430	0.41	846	2.67
440	0.41	859	2.68
449	0.47	884	2.73
459	0.49	898	2.77
468	0.53	930	2.77
477	0.52	948	2.79
486	0.60	978	2.84
496	0.67	991	2.84
505	0.72	1050	2.96

Table A49. Thermogravimetric on Sr-Q.
0.1035g. Heating rate 10.26°C/min.

T°C	% loss	T°C	% loss
10	0.0	356	6.91
20	0.0	367	7.20
30	0.0	376	7.44
45	0.0	387	7.68
53	0.20	396	8.16
64	0.30	405	8.41
85	0.92	416	8.65
95	1.21	425	8.74
108	1.50	435	8.84
119	1.79	445	8.94
132	2.03	455	9.03
144	2.27	484	9.32
155	2.56	495	9.47
166	2.80	505	9.47
189	3.24	515	9.56
197	3.53	525	9.61
208	3.67	557	9.76
217	4.01	567	9.81
235	4.40	576	9.90
245	4.69	608	10.05
255	4.93	650	10.05
273	5.36	683	10.24
284	5.60	724	10.24
293	5.80	769	10.39
302	5.94	815	10.43
311	6.04	890	10.54
718	6.28	973	10.63
327	6.52	985	10.64
337	6.67		

Table A50. Thermogravimetric on Ba-A
0.3515g. Heating rate 10.00°C/min.

T°C	% loss	T°C	% loss
20	0.0	536	1.12
40	0.0	557	1.28
58	0.0	568	1.42
69	0.06	578	1.68
83	0.12	589	1.82
95	0.16	599	1.91
107	0.17	610	2.08
118	0.20	621	2.18
119	0.21	631	2.33
139	0.23	641	2.43
150	0.24	651	2.55
158	0.26	662	2.62
167	0.27	673	2.67
193	0.30	683	2.72
212	0.31	694	2.79
222	0.33	706	2.83
240	0.34	750	2.87
250	0.36	760	2.93
267	0.38	772	2.94
284	0.41	782	2.96
302	0.43	793	2.97
321	0.46	805	2.99
327	0.48	816	3.02
336	0.50	827	3.03
344	0.51	839	3.04
353	0.53	851	3.06
364	0.54	865	3.09
373	0.60	877	3.10
407	0.63	889	3.09
435	0.65	902	3.12
495	0.68	913	3.12
464	0.71	924	3.14
473	0.74	935	3.12
480	0.77	947	3.14
491	0.81	959	3.12
501	0.88	970	3.12
510	0.91		
520	0.97		
527	1.08		

Table A51. Thermogravimetric on Ra-G
0.1980g. Heating rate. 9.500° C/min.

T° C	% loss	T° C	% loss
20	0.0	313	11.72
30	0.0	322	11.89
46	0.0	330	12.14
54	0.0	338	12.32
65	0.33	346	12.55
75	0.78	353	12.65
85	1.24	364	12.78
95	1.69	374	12.88
107	2.17	384	13.00
120	2.57	392	13.18
131	3.00	399	13.28
139	3.48	407	13.41
149	3.91	416	13.51
157	4.39	434	13.76
165	4.75	450	13.99
172	5.18	471	14.19
180	5.53	493	14.34
190	5.93	575	14.49
198	6.29	534	14.67
207	6.62	555	14.72
215	6.89	575	14.87
222	7.20	595	14.97
231	7.47	615	15.02
239	7.70	635	15.10
246	8.00	656	15.18
253	8.28	678	15.18
262	8.51	700	15.22
270	8.84	720	15.25
277	9.32	764	15.33
283	9.97	807	15.38
292	10.63	902	15.43
299	11.11	950	15.48
306	11.44		

Table A52. Themogravimetric on Ba-J
0.1597g. Heating rate 10.09°C/min.

T°C	% loss	T°C	% loss
20	0.0	324	6.92
33	0.0	333	7.07
40	0.0	343	7.23
52	0.16	351	7.42
58	0.50	362	7.54
67	0.81	370	7.72
76	1.10	387	8.08
86	1.47	396	8.17
96	1.85	405	8.36
106	1.97	416	8.45
117	2.54	425	8.51
139	3.04	445	8.70
150	3.38	455	8.73
160	3.60	475	8.86
170	3.88	485	8.89
180	4.23	495	8.98
190	4.48	575	9.08
201	4.70	535	9.20
211	4.95	555	9.27
221	5.20	585	9.34
230	5.38	614	9.42
240	5.57	673	9.61
250	5.70	754	9.67
259	5.89	825	9.74
269	6.04	889	9.86
279	6.23	935	9.92
298	6.51	983	9.67
306	6.67	1009	9.80
316	6.79		

Table A53. Thermogravimetric on Ba-K.
0.1197g. Heating rate 910.13°C/min.

T°C	% loss	T°C	% loss
20	0.0	378	4.97
30	0.0	388	5.05
54	0.0	405	5.30
65	0.13	414	5.39
76	0.21	423	5.51
85	0.58	431	5.64
95	0.83	440	5.68
109	1.09	449	5.76
120	1.25	459	5.97
132	1.46	483	6.10
145	1.55	492	6.18
156	1.71	501	6.22
168	1.88	513	6.27
179	2.21	523	6.35
200	2.38	535	6.43
209	2.51	555	6.52
220	2.67	565	6.56
226	2.88	575	6.56
235	3.05	586	6.64
243	3.22	610	6.64
253	3.34	620	6.68
262	3.47	651	6.68
272	3.59	661	6.72
288	3.72	682	6.77
291	3.84	693	6.81
299	3.97	713	6.85
307	4.09	724	6.93
315	4.18	737	6.89
323	4.26	771	6.85
333	4.43	793	7.02
343	4.51	815	6.93
351	4.64	912	7.02
359	4.80	970	7.02
369	4.85		

Table A54. Thermogravimetric on Ba-M.
0.2372g. Heating rate 9.28°C/min.

T°C	% loss	T°C	% loss
20	0.0	327	7.88
30	0.0	335	8.05
45	0.0	344	8.24
58	0.06	353	8.47
65	0.21	363	8.71
67	0.30	372	8.94
72	0.42	382	9.49
80	0.65	390	9.54
84	0.78	407	9.89
88	0.93	415	10.06
93	1.05	425	10.22
96	1.20	434	10.37
103	1.37	443	10.50
107	1.52	451	10.60
113	1.69	460	10.62
117	1.86	468	10.69
126	2.19	477	10.73
136	2.53	486	10.75
144	2.87	495	10.79
148	2.99	504	10.86
152	3.16	513	10.88
161	3.48	521	10.90
170	3.79	537	10.94
189	4.30	545	10.98
196	4.62	555	11.00
205	4.87	573	11.04
213	5.10	583	11.07
222	5.38	590	11.11
231	5.61	600	11.13
240	5.82	617	11.17
247	6.05	644	11.26
255	6.30	665	11.32
264	6.49	693	11.34
272	6.75	719	11.40
276	6.54	747	11.40
281	6.91	775	11.45
286	6.98	806	11.45
292	7.13	836	11.47
301	7.34	866	11.47
310	7.55	928	11.47
318	7.72	988	11.51
		1020	11.55